SYNTHESIS AND CHARACTERIZATIONS OF LAYERED COBALT OXIDES $ACoO_2$ (A=Na, Li, Pt, and Pd) FOR THERMOELECTRIC APPLICATIONS

Teză destinată obţinerii
titlului ştiinţific de doctor inginer
la
Universitatea "Politehnica" din Timişoara
în domeniul INGINERIA MATERIALOR
de către

Ing. Kiran Kumar Bokinala

Conducător ştiinţific: CS I dr. fiz. Ioan Grozescu
Referenţi ştiinţifici: Dr. Sylvie Hebert
Dr. Michael Pollet
Dr. Ing. Corneliu Marius Craciunescu

Ziua susţinerii tezei: 27.09.2012

Seriile Teze de doctorat ale UPT sunt:

1. Automatică
2. Chimie
3. Energetică
4. Ingineria Chimică
5. Inginerie Civilă
6. Inginerie Electrică
7. Inginerie Electronică şi Telecomunicaţii
8. Inginerie Industrială
9. Inginerie Mecanică
10. Ştiinţa Calculatoarelor
11. Ştiinţa şi Ingineria Materialelor
12. Ingineria sistemelor
13. Inginerie energetică
14. Calculatoare şi tehnologia informaţiei

Universitatea „Politehnica” din Timişoara a iniţiat seriile de mai sus în scopul diseminării expertizei, cunoştinţelor şi rezultatelor cercetărilor întreprinse în cadrul şcolii doctorale a universităţii. Seriile conţin, potrivit H.B.Ex.S Nr. 14 / 14.07.2006, tezele de doctorat susţinute în universitate începând cu 1 octombrie 2006.

România, 300159 Timişoara, Bd. Republicii 9,

tel. 0256 403823, fax. 0256 403221

e-mail: editura@edipol.upt.ro

DECLARATION

I hereby declare that the work represented in this project entitled "SYNTHESIS AND CHARACTARIZATIONS OF LAYERED COBALT OXIDES; $ACoO_2$ (A=Na, Li, Pt, and Pd) FOR THERMOELECTRIC APPLICATIONS" is based on the original work done by me under the guidance of Dr.Marinela Miclau from INCEMC-Timisoara, Romania and Dr. Michael Pollet from ICMCB-Bordeaux, France. This work is a part of SOPRANO; an EU project under FP7 people program , submitted for the Ph.D degree under the guidance of CSI Dr. Ioan Grozescu it has not been included in any other project submitted previously for the award of any degree.

Timisoara, September 2012 Signature of candidate

ACKNOWLEDGEMENTS

First of all I would like to thank my younger sister Kiran mayi Bokinala for her moral support, love and affections as well as fulfilling my duties and responsibilities at home during my absence, which made me to have peace of mind and to concentrate on my research work. I wish to express my deep and sincere gratitude to ***Dr. Marinela Miclau*** and ***Dr. Michael Pollet*** for introducing me to the area of materials for thermoelectric applications, their encouragement and guidance throughout the period of this investigation. I have been greatly benefited by their exceptional skills and analytical capabilities. I am heartily thankful to them. I wish to thank FP7 people program for the financial support. I wish to extend my thankfulness to **Dr. Ioan Grozescu** and **Dr.Sylvie Hebert** for their encouragement. I wish to express my sincere thanks to my colleagues from hydrothermal team from INCEMC-Timisoara, technical and office staff for spending their valuable time regarding my project. I am heartily thankful to analysis departments, from whom I did receive much patience and attention regarding my scientific work especially for **Dr.Ina Bucur,** Daniel Ursu and Eiric Lebraud for structural characterizations, **Dr.S.Paula** and B. Anillese for morphology studies, Latetia for elemental analysis (ICP), **Dr.Anana Maria** (FTIR), **Dr.Radhu banica** (UV-VIS), D.Rudolph for electrical and seebeck measurements, and **Dr.Michael Pollet** for Magnetic measurements. Without their help I might not have done those alone. I would like to extend my gratitude to all the members from INCEMC-Timisoara and group-1 from ICMCB-Bordeaux for their friendly nature and support regarding my project work, especially **Dr.Raul BUCUR**. I wish to acknowledge my colleagues Sanjay, Srinivas, Ivan, Livue and Radhu for their cooperation and encouragement. I wish to extend my sincere thanks to Dr.N. Harish kumar (IIT-Madras) for his encouragement throughout my career. I would like to express my sincere thanks to my best friends B.Neelasekhar (France), Ravichandra reddy (Swis), Elgar, Babu, Anji, Sk.M.Jillani, Rambabu and Anil (India) who always stands around for scientific as well as personnel discussions whenever I needed them.

Kiran kumar Bokinala

Layered cobalt oxizii de ACoO2 (A = Na, Li, Pt, Pd și) pentru aplicații termoelectrice

Teze de doctorat ale UPT, Seria 15, Nr. 4, Editura Politehnica, 2012, 112 pagini,60 figuri, 21 tabele.

ISSN: 2285-1720
ISSN-L: 2285-1720
ISBN: 978-606-554-531-1
Cuvinte cheie: Layered oxizi de cobalt, thermoelectricity, abordarea hidrotermală, chimice noi pentru inlocuiri bivalenți
Rezumat, Layered cobalt oxides $ACoO_2$ (A=Na, Li) were synthesized using soft hydrothermal method and structural properties were studied for $Na_{0.6}CoO_2$ and structural and magnetic properties were studied for $LiCoO_2$.The obtained polycrystalline $LiCoO_2$ shows good purity while the synthesis conditions are much lower compared to the available literature. Magnesium substituted polycrystalline samples of $Na_{0.7}CoO_2$ were obtained using binary oxide (CoMg)O as one of the precursors in solid state method and structural, magnetic and transport properties were studied. Mg substituted $ACoO_2$ (A=Pt,Pd) single crystals were obtained using metathetical reactions with binary oxide (CoMg)O as one of the precursors and high level Mg substitutions were achieved. The structural, magnetic, transport and absorption properties were studied for Mg substituted $PdCoO_2$ single crystals. Structural, magnetic and surface properties were studied for Mg substituted $PtCoO_2$ crystals.

Index

List of figures

List of tables

ABSTRACT

The aim of the present work is to synthesis and characterizes the layered cobalt oxides for thermoelectric applications. Work includes synthesis and characterizations of Mg substituted $ACoO_2$ (A-Na, Li, Pt, and Pd) compounds.

Delafossite cobalt oxides $PtCoO_2$ and $PdCoO_2$ exhibits metallic behavior and anisotropy in transport properties. The single crystals of hole (Mg) doped $PtCoO_2$ and $PdCoO_2$ were grown in metathetical reactions using a *new solid state chemical approach*, and succeeded to obtain the single crystals with higher level divalent substitutions which was a challenge in conventional methods. The physical properties of the Mg substituted $Pt(Pd)CoO_2$ single crystals have been studied for their Structural, magnetic, transport properties employing several techniques; X-ray diffraction, Magnetic Property Measurement System (MPMS), and Physical Property Measurement system (PPMS). The huge anisotropy in transport properties was obtained in ab-plane and c-axis directions; four orders in magnitude (10^4) in $Pd(CoMg)O_2$ single crystals.

The Phase diagram $Co\text{-}H_2O\text{-}NaOH$ was studied in subcritical and supercritical hydrothermal conditions by varying several parameters; temperature, molality of the solution, concentration of precursor, synthesis duration, and the concentration of hydrogen peroxide. The layered sodium cobalt $Na_{0.6}CoO_2$ was successfully synthesized using hydrothermal method for the *first time* and the synthesis conditions were much lower in compared to the previous literature using any other methods.

$LiCoO_2$ was synthesized using hydrothermal method and obtained the concaved cuboctohedrons at lower synthesis conditions. Several parameters; molality of solution, synthesis time and the concentration of $Co(OH)_2$ was varied and optimized the *lowest synthesis conditions* for obtaining concavedcuboctohedron shaped $LiCoO_2$ particles and structural, surface morphology and magnetic properties were studied by employing X-ray diffraction, Scanning Electron Microscopy, Inductive Coupled Plasma analysis, Electron paramagnetic Resonance spectroscopy, and SQUID magnetometer.

Mg substituted Na_xCoO_2 and $LiCoO_2$ were obtained using an alternate approach; using binary oxide as precursor in solid state reactions. The structural, magnetic, electrical, and thermoelectric properties were studied.

Chapter 1

Layered cobalt oxides: an introduction

1.1. Background

ABO_2 compounds are well studied oxides due to their wide range applications. Alkaline cobalt oxides like $LiCoO_2$ which has been using as cathode materials for Li-ion batteries [1-5], recently found that layer-structured Oxide $NaCo_2O_4$ was a highly effective thermoelectric material. The dimensionless figure of merit ZT of single crystal of $NaCo_2O_4$ was shown to exceed unity [6], which is a standard value for practical applications. After this discovery, several new layered cobalt oxides were synthesized and identified. The p-type materials have been found with max power (Tl /Sr/Co/O & Pb/Ca/Co/O) at room temperature. Na_xCoO_2 is the material having more potential for this purpose as has large thermopower, high electrical conductivity, and low thermal conductivity. Power factor (ZT) =1 T=1000K for single crystals and ZT~0.8 at T=1000K for poly crystalline. In fact, single crystalline γ-Na_xCoO_2 (x = 0.70) exhibits a metallic conduction with low resistivity of ρ=200 μ Ω cm as well as large thermo power of S=100 μVK $^{-1}$ at room temperature, yielding excellent TE power factor of $S^2/\rho = 5 *10^{-3}$ WK^{-1} m^{-2} [7-9]. These values observed at room temperature stand comparison with conventional thermoelectric materials composed of doped semiconductors.

Crystal structure consisting of alternating layers of Na ions and triangular CoO_2 planes is the embodiment of such a system. The charge on the CoO_2 planes is controlled by the degree of filling of the Na layer. Edge –shared distorted octahedra of oxygen ions form a two-dimensional triangle lattice. Co ion is at the centre of distorted octahedra to form a 2D triangle lattice. Na ion is in a prism site between CoO_2 blocks. An important feature is Na ions randomly occupy the regular site by 50% and Na content changes from 50% to 75%. Thermoelectric properties are realized at 75% of Na occupancy [10].

The valance of Co can be controlled by doping of Na atoms. For completely filled Na (x=1) $n^+=3.0$, E_f is at the top of the band so conductivity is very low. With decreasing x (Na content) n^+ will increase towards Co^{+4} and E_f will be in hybridized location, so good electronic conduction will appear. Large thermo power is accompanied in the region where n^+ is between 3.1 and 3.3 as

$$S = -(\partial \ln \sigma(E)/\partial E)_{E=Ef} \qquad 1.1.1$$

$\sigma(E)$ is proportional to density of states at E_F .

Thermo power in metals is given by Heike's formula:

$$S = \frac{k_B}{C} \log \frac{g_A}{g_B} \frac{P}{1-P} = s/C; \qquad 1.1.2$$

Where g_A, g_B are electronic degeneracy of electronic configuration of *A,B* ions, P is atomic content of *A* ion, C is charge difference between A,B ions and s is entropy per carrier. In the edge-sharing CoO_6 octahedra result from the superposition of triangular lattices of oxygen and cobalt. This opens up the possibility of geometric frustration of the interactions, between magnetic moments on cobalt sites. The

lattices of oxygen and cobalt. This opens up the possibility of geometric frustration of the interactions, between magnetic moments on cobalt sites. The crystalline field forces the Co into low spin state. The resultant spin of Co^{4+} (x=0) and Co^{3+} (x=1) are ½ and 0. And its behaviour changes from an electron-doped Mott insulator (x=1) to a hole doped band insulator (0<x<1). Bellow x=0.5 the material is paramagnetic with high conductivity. With increasing the x to 2/3 the material has metallic behaviour but the magnetic property is different than other metals. In general metals the alignment of spins in the direction of magnetic field goes to zero at low temperatures. But in Na_xCoO_2 the susceptible spin population is equal to the number of holes and stays even at low temperature. Such a phase - metallic-like in charge conduction and insulator-like in spin alignment - is called *'Curie-Weiss metal'*. For concentration (x=0.68) the material fallows curie-Weiss law. It shows *spin-density wave metal* behaviour at x=0.7. For x=0.5 , bellow 88k it shows anti ferromagnetic behaviour within the CoO_2 planes with alternating rows with ordered and non-ordered Co ions. In this "charge-ordered insulator" phase Na ions order with a very long range correlation, conformed with thermal conductivity and Hall resistance measurements, even at T» 300K [11].

The main practical problem of the traditional solid-state method is uncontrollable Na content in the structure and to get rid of Co_3O_4 impurities. Hydrothermal synthesis of these compounds might results higher purity as well as the lower synthesis parameters. There exists no report on single phase synthesis of Na_xCoO_2 using hydrothermal method. The $LiCoO_2$ has been studying for decades due to its practical applications to Li-ion batteries. It also forms in a layered type structure; CoO_6 octahedra with alternate layers of Li ions. The easier intercalation and de-intercalation of Li ion in the structure make the $LiCoO_2$ much useful in compared to any other oxide materials. It generally forms in two structures like O3 (R-3m and Fd3m) and P2 (P63/mmc). The HT-$LiCoO_2$ (R-3m) is mostly used cathode as a material. Several synthesis methods like solid state, combustion synthesis and sol-gel methods. These methods need high temperature as well higher synthesis durations and continuous flow of oxygen in case of solid state method.

Several reports have been reported synthesis of $LiCoO_2$ using hydrothermal method in both supercritical as well as subcritical hydrothermal conditions. In the available literature, it was used either higher concentrations of ionic mineralisers or higher concentrations of hydrogen peroxide (oxidant). A report also has made on obtaining concavedcuboctohedron shaped $LiCoO_2$ particles using hydrothermal method which cannot be obtained by other synthesis methods.

1.2. Structure of layered cobalt oxides

1.2.1. Structure of sodium cobalt oxides

Alkali-metal cobalt oxides with layered structure, $ACoO_2$ have attracted much interest not only in the physical aspect of their two-dimensional (2D) nature with triangular Co sub lattice but also in their potential for practical applications. $LiCoO_2$ has already been used as a cathode material for Li-Ion batteries [12-13]. The metallic conduction and high thermopower in $Na_{0.7}CoO_2$ attracted the scientific community to search for possible thermoelectric applications in oxide

materials with layered structures [6-7]. The crystal structure of Na_xCoO_2 consisting of alternating layers of Na ions and triangular CoO_2 planes, is the embodiment of such a system. The physical and transport properties are expected to be two-dimensional; anisotropy in c-axis to ab-plane. The charge on the CoO_2 planes is controlled by the degree of filling of the Na layer. The structure, magnetic and transport properties vary with Na content in the structure. It shows P2 (*P63/mmc),* P3 (*Pnmm*), O3 (*R-3m*) , P1 (*C2/m*) and OP4 (*P63/mmc*) [9-14]. The compounds with higher content of Na can be obtained by direct synthesis but for the lower content of Na compounds can be stabilised using de-intercalation[11]. The hydrated phase $Na_{0.3}CoO_2.1.3H_2O$ presents the superconductivity lower to 5K [8]. $Na_{0.5}CoO_2$ (P3) shows magnetic order and insulating behaviour at lower temperatures [18-19]. Also $Na_{0.7}CoO_2$ (P2) is a good candidate for the thermoelectric applications.

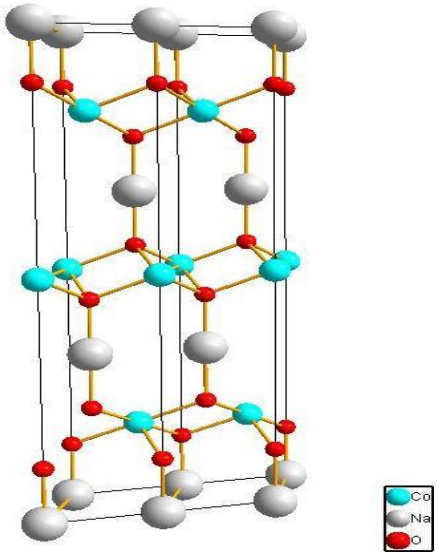

Figure 1.1. Crystal structure of Na_xCoO_2 (R3m)

Na_xCoO_2 is *hexagonal structure* with space *group P63/mm*. The nearest neighbour planes are rotated by 180 ^{0} giving two CoO_2 layers per unit cell. Rhombohedral phase with *R3m space group* offset in the hexagonal arrangement with cobalt ions at (0, 0, 0),(2/3, 1/3, 1/3) and (1/3, 2/3, 2/3) giving three CoO_2 layers per unit cell. The possible sites for Na are 2b (Na1) (0, 0, 1/4) and 2c (Na2) (2/3, 1/3, 1/4). The possible displacements of Na2 atoms are 6h (x/3, x, 1/4).
Hexagonal structure a=2.84126 Å and c=10.8144 Å [17].
Rhombohedral a=2.889 Å, c=15.6.09 Å. [20].
Superconducting phase a = 2.82374(10) Å, c= 19.6576(8) Å. [8].

1.2.2. Structure of lithium cobalt oxide

Lithium cobalt double oxide $LiCoO_2$ is well known for its high performance as cathode part of Li-ion batteries as it gives both high output voltage and high specific energy [21-25]. $LiCoO_2$ owes its efficiency to its layered structure which alternates Li and CoO_2 layers; in its thermodynamically stable form, it crystallizes with R-3m space group (O3-polytype [26]) with both direct solid state or hydrothermal synthesis methods [27]; other polytypes were also identified like O2- [28] and O4-polytypes [1] and for the Li deficient cases, O1- [2], O6- [3], and T2-polytypes [4] were observed which are consequences of orientation within the O-Co-O slabs.

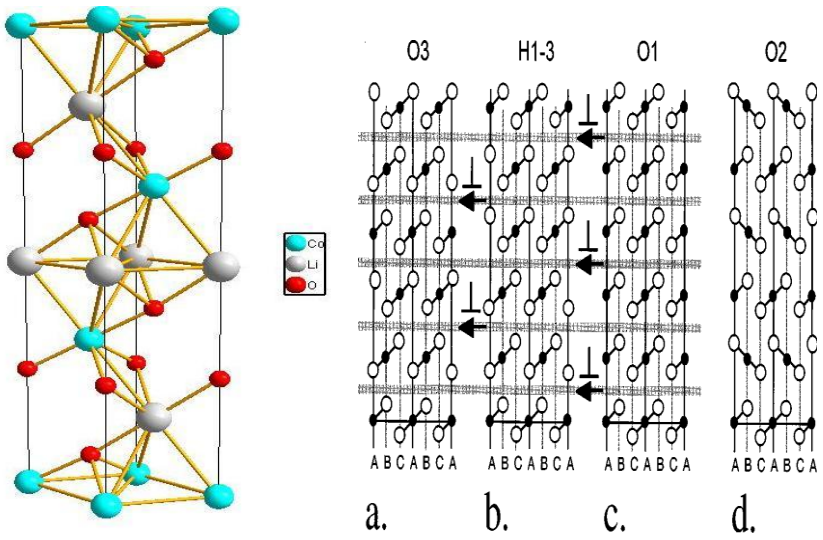

Figure 1.2.a. Crystal structure of $LiCoO_2$ (R-3m), b. Different polytypes due to dislocation in Li plane [29]

1.3. Magnetic and electrical properties of layered cobalt oxides

1.3.1. Overview of the magnetic and electrical properties of layered cobalt oxides

The electronic structure decides the characteristic behaviour of the material. The electronic states of the Cobalt in octahedra, 3d orbital splits into doubly degenerated (e_g –high energy) and triply (t_{2g} – low energy) degenerated levels. Due to rhombohedral distortion the low energy level again splits into doubly generated (e^1_g-low, itinerant) and non-degenerated (a_{1g} –high, localized) levels.

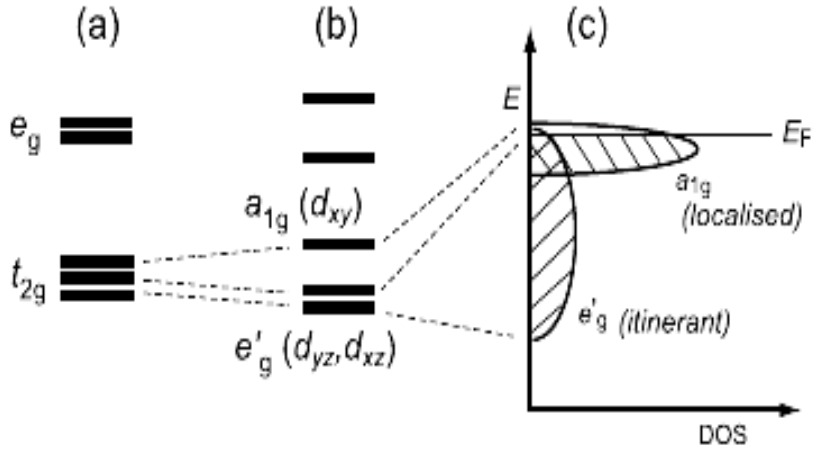

Figure 1.3. Splitting of 3d energy levels of Co ion and Density of states near E_F [35]

At the Fermi-level (E_f) is depended on the valance of Co^{n+} ions and it consists of superimposition of *itinerant* and *localized* levels. The valance of Co can be controlled by fill percent of Na atoms. For completely filled Na (x=1) n^+=3.0, E_f is at the top of the band so conductivity is very low. With decreasing x (Na content) n^+ will increase towards Co^{+4} and E_f will be in hybridised location so good electronic conduction will appear. Large thermo power is accompanied in the region where n^+ is between 3.1 and 3.3 as S= - $(\partial \ln \sigma(E)/\partial E)_{E=Ef}$ $\sigma(E)$ $\sigma(E)$ is proportional to density of states at E_F [30]. From this explanation it is clear that the valance of Co will vary with the substitution of Na. That changes the electronic structure correspondingly the electronic conductivity. Rhombohedral phase with Co^{+3} shows insulating properties where as hexagonal structure with partial Co^{+4} shows metallic behavior. Good thermoelectric properties are found to be in the intermediate valance state of Co^{n+} (+n=3.0--4.0). In γ-Na_xCoO_2 (x=0.7) the ratio of these valance states is given by Co^{3+}: Co^{4+} = 3:7.
The hexagonal phase shows p-type metallic behaviour. The resistivity is anisotropic, high values along c-axis direction.

1.3.2. Magnetic and electric properties of Na_xCoO_2

The resistivity is as low as 200 μΩ cm at 300K parallel to CoO_2 planes. It is the best conductivity among transition metal oxides. The thermo power is 100mV/K at 300 K

which is as large as degenerate semiconductors. The out-of-plane resistivity ρc is about 100 times larger than the in-plane resistivity, indicating quasi-two-dimensional electronic states as expected from the layered structure. The broad peak appeared near 200 K suggests that only the out-of-plane transport is incoherent above 200 K. This can happen when the mean free path is longer than the in-plane lattice parameter (0.3 nm), and shorter than the out-of-plane lattice parameter (1 nm). The temperature dependence is roughly linear in T, suggesting that it can be understood as the diffusive part of the thermopower of a metal. Thermal conductivity lies near 40-50 mW/cmK. Low lattice thermal conductivity to the disordered Na layer in which Na ions and vacancies make a solid solution. In fact, single crystalline γ-Na_xCoO_2 (x = 0.70) exhibits a metallic conduction with low resistivity of ρ=200 μ Ω cm as well as large thermo power of S=100 μVK^{-1} at room temperature, yielding excellent TE power factor of $S^2/\rho = 5 * 10^{-3} WK^{-1} m^{-2}$ [6]. In the edge-sharing CoO_6 octahedra result from the superposition of triangular lattices of oxygen and cobalt. This opens up the possibility of geometric frustration of the interactions, between magnetic moments on cobalt sites. The crystalline field forces the Co into low spin state.

The resultant spin of Co^{4+} (x=0) and Co^{3+} (x=1) are ½ and 0. And its behaviour changes from an electron-doped Mott insulator (x=1) to a hole-doped band insulator (0<x<1). [9].Bellow x=0.5 the material is paramagnetic with high conductivity. With increasing the x to 2/3 the material has metallic behaviour but the magnetic property is different than other metals. In general metals the alignment of spins in the direction of magnetic field goes to zero at low temperatures. But in Na_xCoO_2 the susceptible spin population is equal to the number of holes and stays even at low temperature.
Approximate Resistivity values for different compositions at room temperature (300K):

x=1	insulator
X=0.75	2 mΩ cm
X=0.65	4 mΩ cm
X=0.50	5 mΩ cm (insulating at low temperature)
X<0.5	metallic
X=0.31	o.36 mΩ cm (super conductor bellow 5K)

Table 1.1. Variation of electric properties with Na content in Na_xCoO_2

Such a phase - metallic-like in charge conduction and insulator-like in spin alignment - is called *'Curie-Weiss metal'.* For concentration (x=0.68) the material fallows curie-Weiss law. It shows *spin density wave metal* behaviour at x=0.7.For x=0.5 , bellow 88k it shows ant ferromagnetic behaviour within the CoO_2 planes with alternating rows with ordered and non-ordered Co ions. In this "charge-ordered insulator" phase Na ions order with a very long range correlation, conformed with thermal conductivity and Hall resistance measurements, even at T» 300K (fig 1.4).

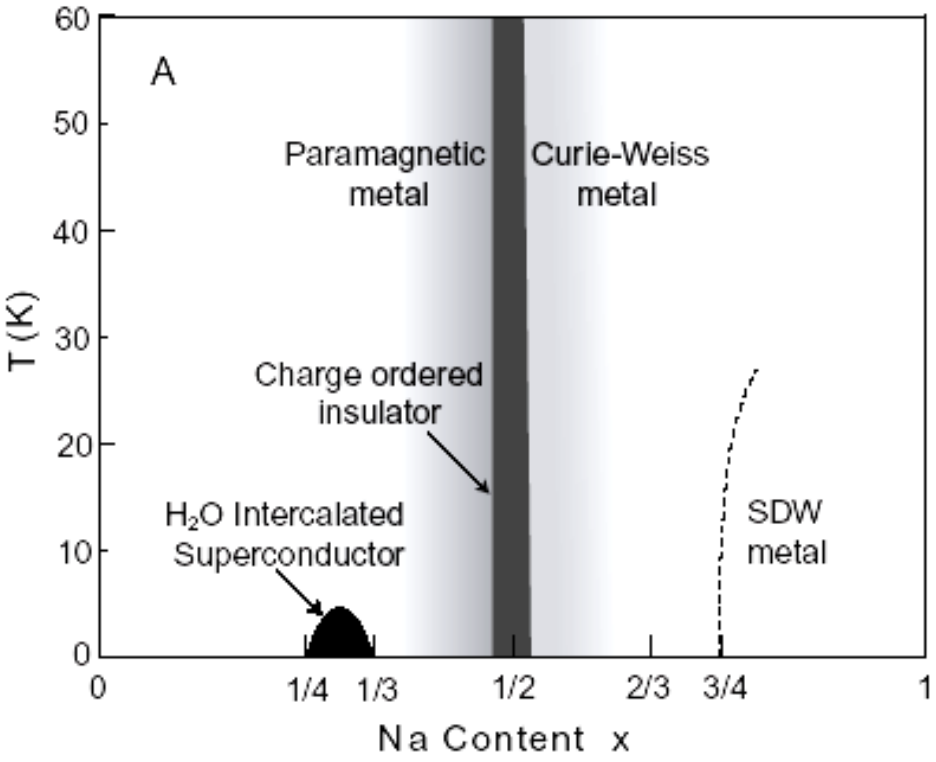

Figure 1.4. Variation of magnetic properties with Na content [11]

The change in susceptibility along ab-plane at T=0 k with Na content in the structure is given bellow table 1.2.

Localization approximation:

In the localized spin approximation there are three kinds of possible spin states for each cobalt ion, i.e. Co^{3+}: s=0, 1, and 2. Co^{4+}: s=1/2, 3/2, 5/2 respectively.

The magnetic moment was calculated using the formula

$\mu_{cal} = [X *4S(Co^{3+})(S(Co^{3+})+1) +(1-x)*4S(Co^{4+})(S(Co^{4+})+1)]^{1/2}$

1.3.1

Assuming that $[Co^{3+}]$: $[Co^{4+}]$ = X: 1-X

Superconductivity in Na_xCoO_2; yH_2O: At 0.25<x<0.33 the material has superconducting property in the presence of water at 5K. It is found that y=1.3, 0.3 is optimal concentration to obtain superconductivity. The distance between

succeeding CoO_2 layers increased dramatically from 10.9628(8) Å to 19.6207*(14) Å.* The effect of water molecule makes two effects. It enhances the 2D structure of CoO_2 layers and screening the strongly fluctuating electrostatic potential of Na ions from the charge carriers in the CoO_2 layers.

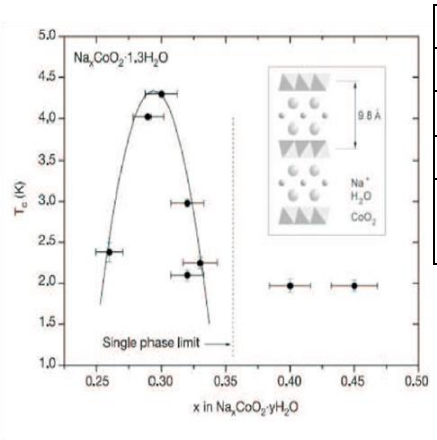

Fig.1.5. Effect of Na content in the structure on T_c.

x= 1	$1.2*10^{-3}$ emu/mole Oe
x= 0.75	$1.5*10^{-3}$ emu/mole Oe
X=0.68	$1.3*10^{-3}$ emu/mole Oe
X=0.5	$0.55*10^{-3}$ emu/mole Oe
X=0.31	$0.6*10^{-3}$ emu/mole Oe

Table.1.2. Variation of susceptibility with Na content

1.3.3. Magnetic properties of Li_xCoO_2

The magnetic behaviour of Li_xCoO_2 is shown in bellow figure 1.6. There exist two major differences between Na_xCoO_2 and Li_xCoO_2. The critical point *x*c, where the magnetic behaviour changes from Curie-Weiss behaviour to Pauli paramagnetic behaviour, is smaller in Li_xCoO_2 than Na_xCoO_2, *i.e.* *x*c = 0.35 ~ 0.40 and ≈ 0.5 in the former and the latter, respectively. Second, μ_{eff} is different in magnitude between Li_xCoO_2 and Na_xCoO_2. In the former, the magnitude of μ_{eff} (= 0.28 ~ 0.35 μ_B/Co^{4+}) is much smaller than the theoretical spin-only value of Co^{4+} (= 1.73 μB), while in the latter the μ_{eff} value is consistent with a spin-1/2 local-moment population equal to the Co^{4+} concentration. Since these two systems contain the triangular CoO_2 block in common, these differences are believed to originate from modifications in the crystal structure.

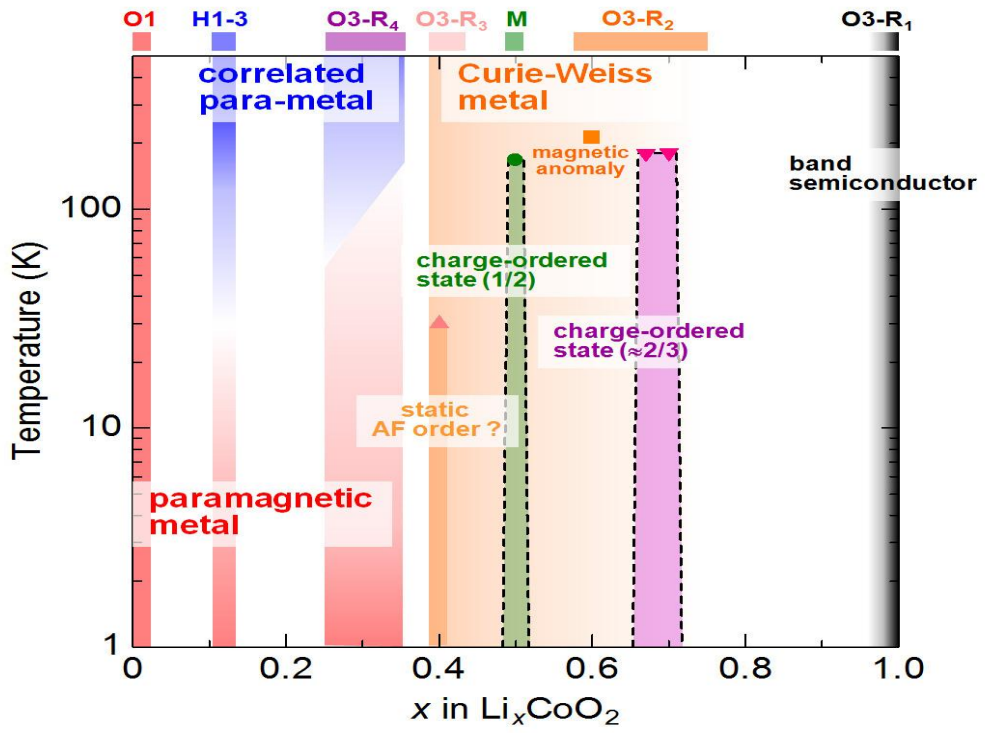

Figure.1.6. Magnetic behaviour of Li_xCoO_2 [31]

1.3.4. Thermoelectricity in layered sodium cobalt oxides

The thermopower is defined as a measure of an induced voltage with respect to the temperature gradient.

$S = \Delta V / \Delta T$ 1.3.3.1

When a thermal gradient is applied to a solid, it will be accompanied by an electric field in the opposite direction.

The electric field generated by thermal gradient can be written as

$E = S\nu\tau$ 1.3.3.2

where, S is thermo power, v is carrier concentration and t is relaxation time.

For three dimensional systems we can write

$$vS= -\frac{\tau}{6}\frac{dv}{dT}^{2}(\nabla T) \qquad 1.3.3.3$$

Mean velocity is given by the following formula

V_E=-eEt/m 1.3.3.4

In thermoelectric material the thermal and electrical flow is in opposite direction with same velocity $V_E = v_S$

S= C_v/3ne 1.3.3.5

$$C_v = \frac{\pi^2}{2}\frac{k_B}{E_f}T * nk_B \quad \text{(for semiconductors)} \qquad 1.3.3.6$$

$$S= -1.42\ \frac{k_B}{E_f}T\ * 10^{-4}\ \text{volt/K}$$

Thermopower in metals

According to Heike's formula $S= \frac{k_B}{C}\log\frac{g_A}{g_B}\frac{P}{1-P}$ = s/C 1.3.3.7

Where g_A, g_B are electronic degeneracy of electronic configuration of *A, B* ions.
P is atomic content of *A* ion, C is charge difference between A, B ions and S is entropy per carrier.

In layer cobalt oxide, Co^{3+} has low spin state and entropy is zero. The hole in t_{2g} state has 6 fold degeneracy. The entropy for the single hole is given as $k_B$log6. The maximum thermopower at higher temperatures is expected to be $k_B$log6 /e. At room temperature, Na_xCoO_2 (x=0.7) shows 100 μV/K [10] which is just 2/3 of the high temperature limit ($k_B$log6). For non stoichiometric $Na_xCoO_{2+\delta}$ the values of thermo power are given in bellow table 1.3.

$LiCoO_2$ is widely used as cathode part of materials in Li-ion batteries. It gives high output voltage and high specific energy. The evolution of open circuit voltage as a derivative of Li-content is shown in figure1.7.

X=55	50 μV/K
X=55	50 μV/K
X=65	75 μV/K
X=75	115 μV/K

Table 1.3. Thermopower variation with Na content in non stoichiometric samples

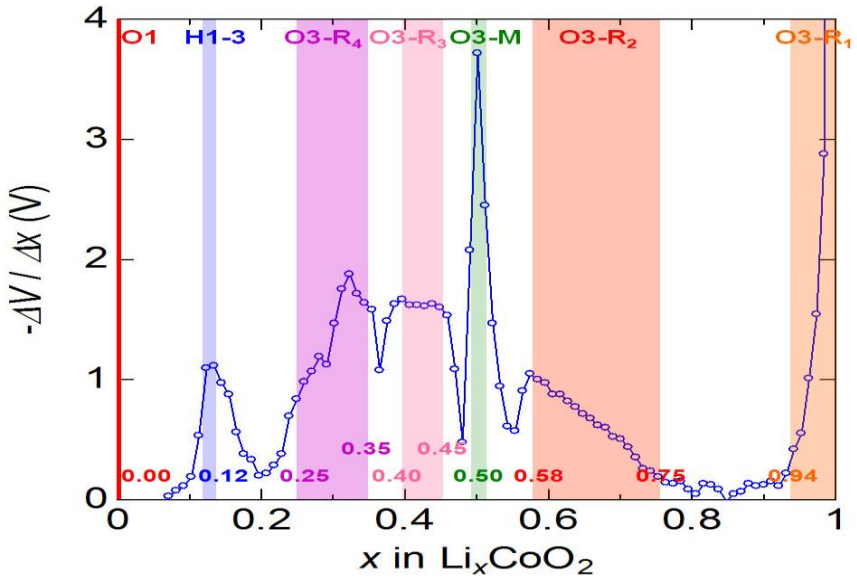

Fig.1.7. Thermoelectric properties of Li_xCoO_2, where dV= open circuit voltage and x=Li content [31].

1.3.5. Substitution effects in Na_xCoO_2

Na_xCoO_2 is a transition metal oxide and is attractive for chemical substitution studies for both cation and anions. Na and Co can be replaced by various elements. Both electroni spin state of cobalt and the carrier concentration are tuneable with substitutions. The low level substitutions at Na site with several elements have been reported.

Calcium doped $Na_{0.7}CoO_2$

Ca is the most suitable element for Na substitution as the size of Ca^{2+} is nearly equal to Na^+. Change in CoO_2 planes caused by decreasing Co valance V_{co} with Ca content doped into vacant Na sites. V_{co} is successfully decreased to 3.16 in $Na_{0.7}Ca_{o.o7}$ CoO_2 without increasing resistivity. Spin state transition was observed at 400K [32]. γ-Na_xCoO_2 x=0.75 (V_{co}=3.25) is found to enter into a commensurate spin density wave (C-SDW) state bellow 22K. While x=0.9 (V_{co}=3.1) into incommensurate spin-density wave(IC-SDW) bellow 19K. So Ca doped Na_xCoO_2 samples are expected to have transition from a paramagnetic state to SDW state at low temperature and is observed [33].

Ni substituted $Na_{0.9}CoO_2$

Ni substituted $Na_{0.9}CoO_2$ shows drastically changes in electrical resistivity, thermoelectric power and thermal conductivity values are shown in table 1.4
Effect of Ni substitution

Property	$Na_{0.9}CoO_2$	$Na_{0.9}Co_{0.99}Ni_{0.01}O_2$
Resistivity(mΩ cm)	8	3.5
Thermo power (μV/K)	120	140
Thermal conductivity (W/mK)	21.12	14.70
Fig of merit (ZT)	0.0026	0.01

Table 1.4. Effect of Ni substitution [25]

Increasing in thermopower is due to increase in spin-entropy caused by the substitution of Ni. Thermal conductivity was reduced by increasing phonon scattering by Ni. [32].

Pb substituted samples

Pb substituted $Na_{0.5}CoO_2$ and $Na_{0.95}CoO_2$ show increase of ZT and exceeds unity [33]. The substitution of alkaline –earth metals shows the carriers as holes [34-35]. While the substitution of Co site with Mn, shows metal insulator transition around 35K [36]. The high level substitution of Mn at Co-site results increase of magnetic fluctuations at cobalt site [37].

1.4. Synthesis methods of layered cobalt oxides

1.4.1. Conventional synthesis methods for layered cobalt oxides Na_xCoO_2

The solid state method is widely used to synthesize layered cobalt oxides. In conventional solid state method, the powders of Na_2CO_3 and Co_3O_4 uses as precursors with thermal treatment at 850^0C for 12 to 24h in continuous O_2 flow [38-39]. The compounds with Na<0.6 obtain by de-intercalation of Na-ions using I_2 or Br_2 solutions. The intercalation Na can be archived by immersing Na_xCoO_2 (x>0.7) [40-42] in the oxidizing agents like Br_2 or I_2 or NO_2BF_2 or CH_3CN for several days. Electro chemical process also can be used to intercalate the Na ions, both intercalation and de-intercalation can be achieved at room temperature. In this method, the parent material was used as cathode part of electrochemical cell [43-46]. The γ-Na_xCoO_2 nano tubes were synthesized by the urea-based sol-gel route [47] with the assistance of supporting templates using anodized aluminium oxide (AAO) membranes having a pore size ranging from 40-350 nm. The sol used in the fabrication of nano tubes was prepared by dissolving metal nitrates in a molar ratio of $NaNO_3$: $Co(NO_3)_3{\cdot}6H_2O$ = 1 : 1 (0.05-mol each) in 50 ml of deionised water. Urea (0.133 mol) was then added in a molar ratio of Co: urea = 3: 8 and heated to 60- 80ºC on a hot plate until the sol was formed. The AAO membranes were dipped into the sol for 10 min.

The AAO membrane was taken out and filled with the hot sol gradually using vacuum immersion techniques for a period of 2 h. The filled AAO membrane was then dried on a hot plate at 65ºC for 30 min, followed by cleaning its surface using anhydrous alcohol to remove residual gel. The resulting filled AAO membrane was then heated to 600ºC at a heating rate of 1ºC/min and held for 10 min, followed by heating to 650ºC at a heating rate of 1ºC/min and held for 4 h. The reaction temperature was purposely to be kept under 700ºC since AAO membrane after being heated above 700ºC would persistently remain in the final product even if treated with alkaline NaOH solution. The desired phase can be obtained by heating the filled membranes at as low as 650°C. Note that polycrystalline γ-$Na_{0.7}CoO_2$ powders were normally synthesized in a preheated furnace at 800°C [47].

$LiCoO_2$

Among the several synthesis methods already proposed to produce $LiCoO_2$, all present at least one of the following weaknesses: high temperature synthesis, multiple steps, long preparation time, long synthesis times, specific care, limited yield and/or presence of impurities in the final product. For standard solid state synthesis method for instance, the synthesis temperature of the initial mixture of Li_2CO_3 and Co_3O_4 reaches 850^0C [48]

and Co_3O_4 impurities are present [44]. For sol-gel synthesis $Co(NO_3)_3.6H_2O$ and $LiNO_3$ as metal oxides sources, absolute alcohol reagent as a solvent, and citric acid as a chelating agent are used to optimise the mixture prior to synthesise the compound at high temperature [48].More recently a microwave assisted synthesis with double-containment was reported [49]. In the above synthesis methods the problem should be summarised as follows; the control of stoichiometry of Na, cobalt impurities in the final product and the oxygen stoichiometry. The hydrothermal method was assumed to keep good oxygen stoichiometry and the cationic impurities can be tuneable.

1.4.2. Hydrothermal synthesis of layered cobalt oxides

The term *hydrothermal* is purely of geological origin. It was first used by the British geologist, Sir Roderick Murchison (1792–1871), to describe the action of water at elevated temperature and pressure in bringing about changes in the earth's crust, and leading to the formation of various rocks and minerals. The first successful commercial application of hydrothermal technology began with mineral extraction or ore beneficiation in the previous century. The use of sodium hydroxide to leach bauxite was invented in 1892 by Karl Josef Bayer (1871–1908) as a process for obtaining pure aluminium hydroxide which can be converted to pure Al_2O_3 suitable for processing to metal. Even today, over 90 million tons of bauxite ore is treated annually by this process. Similarly, limonite, wolframite, cassiterite, laterites, a host of uranium ores, sulphides of gold, copper, nickel, zinc, arsenic, antimony, and so on, are treated by this process to extract the metal. The principle involved is quite simple, very effective, and inexpensive, as shown below, for example [50].

$$Al(OH)_3 + OH^- \rightarrow [AlO(OH)_2]^- + H_2O \qquad 1.4.2.1$$

$$AlOOH + OH^- \rightarrow [AlO(OH)_2]^- \qquad 1.4.2.2$$

Further importance of the hydrothermal technique for the synthesis of inorganic compounds in a commercial way was realized soon after the synthesis of large single crystals of quartz by Nacken (1946) and zeolites by Barrer (1948) during late 1930s and 1940s, respectively. The term *hydrothermal* usually refers to any heterogeneous reaction in the presence of aqueous solvents or mineralizers under high pressure and temperature conditions to dissolve and recrystallize (recover) materials that are relatively insoluble under ordinary conditions. Morey and Niggli (1913) defined hydrothermal synthesis as "…in the hydrothermal method the components are subjected to the action of water, at temperatures generally near though often considerably above the critical temperature of water (~370°C) in closed bombs, and therefore, under the corresponding high pressures developed by such solutions [55].

Under hydrothermal conditions, the reactants which are otherwise difficult to dissolve go into solution as complexes under the action of mineralizers or solvents, hence, one can expect the conditions of chemical transport reactions. Therefore, some workers even define hydrothermal reactions as special cases of chemical transport reactions. Owing to the specific physical properties, particularly the high salvation power, high compressibility, and mass transport of these solvents, one can also expect the occurrence of different types of reactions like:
i. Synthesis of new phases or stabilization of new complexes.
ii. Crystal growth of several inorganic compounds.
iii. Preparation of finely divided materials and micro crystallites with well-defined size and morphology for specific applications.
iv. Leaching of ores in metal extraction.

Polycrystalline samples using hydrothermal synthesis

Oxides form one of the largest groups of inorganic compounds both in nature and in the laboratory. The hydrothermal technique is one of the most popular techniques for growing these high-temperature oxides, complex oxides and low-temperature modifications of the oxides. The work on the hydrothermal synthesis of oxides began during the 19th century with quartz [32] Followed by this, large-scale research activity began during the 1890 s, on corundum and other related high temperature oxides. [39,51] today, we find a large number of oxides obtained by the hydrothermal method: TiO_2, ZrO_2, HfO_2, Cu_2O, BeO, Bi_2O_3, In_2O_3, Al_2O_3, ZnO, Fe_2O_3, to mention a few, and a great variety of mixed oxides. Some of these carry great significance as synthetic gemstones, and some as technological materials. Here, we describe the hydrothermal growth of selected oxides of both gemstone and technological grades. In hydrothermal synthesis for powdered materials, it isn't used temperature gradient like in single crystal growth case. The pressure inside the autoclave can be varied in accordance with the filling percentage of the autoclaves [50]. The main characteristics of hydrothermal synthesis could be included by the following rules:

1. The reaction depends on temperature, pressure, molaity of the solution, solubility of the precursors and the synthesis time.
2. The solubility of the precursors is one of the main factors in hydrothermal synthesis so generally hydroxides are used as precursors.
3. Gibbs free energy is the most important factor for the reaction in hydrothermal synthesis. As the temperature increases, the Gibbs free energy of the water increases, but at certain temperature Gibbs free energy decreases with increasing the molaity. We need to arrange the proper conditions; temperature, molaity, concentration of the solution and pressure.

The pressure applied in hydrothermal synthesis is from the system not from external; the filling percent and the temperature are the factors that decide the pressure in accordance with P-T diagram of water (fig 1.8). Using hydrothermal synthesis we can obtain the powder form of the materials micro and nano sized materials.

Classified	Action	Application
1. Transfer Medium	Transfer of kinetic energy, Heat and pressure abrasion,	Erosion, Machining
2. Adsorbate	Adsorption/Desorption at the surface	Dispersion, Surface Diffusion, Catalyst, Crystallization, Sintering, Ion Exchange, etc.
3. Solvent	Dissolution/Precipitation	Synthesis, Growth, Purification, Extraction, Modification, Degradation, Etching, Corrosion, etc.
4. Reactant	Reaction	Formation/Decomposition (hydrates,hydroxides,oxides) corrosion, etc.

Table 1.4.a. Action of Hydrothermal Fluid (High-Temperature–High- Pressure Aqueous Solution/Vapour) on Solid State Materials [50]

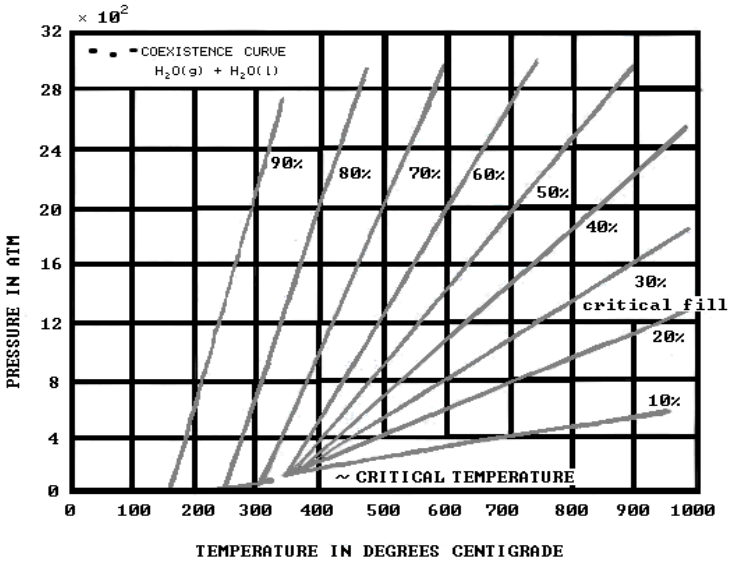

Figure 1.8. Pressure vs temperature vs filling percentage of an autoclave-for diagram for water [50]

Na_xCoO_2

The layered sodium cobalt oxide wasn't obtained using hydrothermal method. There exists no literature to obtain Na_xCoO_2 using hydrothermal method.

$LiCoO_2$

The hydrothermal synthesis method has already been extensively used to synthesise a wide range of oxide materials [52-55]; it was shown to be advantageous as it requires lower synthesis parameters, it is less expensive and it leads to the good oxygen stoichiometry. The problem of the impurities can be easily overcome by varying the ratios of precursors: In the specific case of $LiCoO_2$, cobalt impurities can be avoided by increasing the Li to Co ratio. So far, $LiCoO_2$ has been prepared by hydrothermal subcritical as well as in supercritical conditions with 50% concentrations of hydrogen peroxide as an oxidant [56-57]. In fact, it is challenging to find synthesis conditions which allow to reduce the concentration of hydrogen peroxide and to tune the size grains. In order to optimize the synthesis conditions of $LiCoO_2$ using hydrothermal method, we studied the influence of the precursors' concentration, the molaity of the solution and the synthesis temperature on the resultant phase as well as the influence of the reaction time on the surface morphology.

Formation mechanism of concavedcuboctohedron shaped $LiCoO_2$

In the previous study by H.Chen et al [54], used Co $(NO_3)_2$, Co $(OH)_2$ and LiOH are the precursors and KOH as mineralizing agent. They suggested that the origin of these shapes comes from the interaction between nano crystals of CoO with Li-ions.The nano sized CoO pits into all the directions along [*l* 0 0] and due to the high Li-ion density in the solution Co^{2+} ion will exchange with Li^+ in {1 1 1} planes making the neighbouring Co-ion to Co^{3+} which is more stable for cobalt this mechanisms they named as *oxidation-ion-exchange*. These alternating Co^{3+} and Li^+ layers favour to form $LiCoO_2$. Each cuboctohedrons consists of four equivalent hexagonal plates of $LiCoO_2$ with 70.5° inclined to each other. These plates will grow along [100], [010] and [110] directions. The three important factors are: 1. the ability of CoO to form $LiCoO_2$ by ion exchange on its surface and to expose the stable faces. 2. Slight variations in stoichiometry of the Li*x*CoO2 phase at the twin boundaries, allows 4 twins with rhombohedral symmetry to grow with minimal stress at the interfaces. 3. The symmetry of the parent lattice will control the morphology and the type of twin's formed. When Co $(OH)_2$ is used as the precursor the Co^{2+} in the solution $(Co(OH)_4^{2-})$ is oxidised to Co^{3+} and forms the $LiCoO_2$. The growth is along $[001]_H$, $[010]_H$, and $[110]_H$ directions.

1.5. Characterization methods of layered cobalt oxides

1.5.1. Structural characterization

X-ray diffraction: Diffraction can occur when electromagnetic radiation interacts with a periodic structure, whose repeat distance is about the same as the wavelength of the radiation. X-rays have wavelengths about angstroms which is in the range of typical inter atomic distances in crystalline solids. Therefore, X-rays can be diffracted from the repeating patterns of atoms that are characteristic of crystalline materials. Diffraction data has historically provided information regarding the structures of crystalline solids. Since the relative atomic positions of atoms can be determined, X-ray diffraction provided important evidence and indirect proof of the periodic arrangement of atoms in a crystalline solid. The symmetry of the diffraction patterns corresponds to the symmetry of the atomic packing. X-ray radiation directed at the solid provides the simplest way to determine the interatomic spacing that exists. The intensity of the diffracted beams also depends on the arrangement and atomic number of the atoms in the repeating motif, called the unit cell. X-ray powder diffraction is based on the Braggs law of diffraction, which is given by

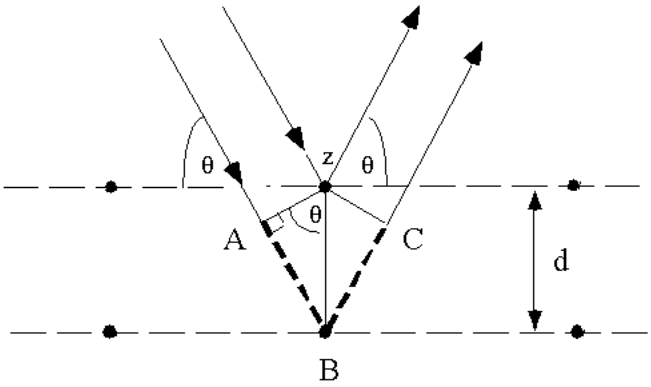

Figure 1.9. Braggs diffraction [64]

$$2d \sin\theta = n\lambda \qquad 1.5.1$$

Where d is the inter-planar spacing, θ is the angle of diffraction, n is the order of diffraction and λ is the wavelength of the X-ray used. Cu K_α radiation was used in the setup. From XRD data (2Θ Vs intensity), we can find crystal structure and lattice constant of the sample used.

Few applications of XRD

XRD is a non-destructive technique

• To identify crystalline phases and orientation

- To determine structural properties:
  Lattice parameters (10-4Å), strain, grain size, expitaxy, phase composition,
  Preferred orientation (Laue) order-disorder transformation, thermal expansion
- To measure thickness of thin films and multi-layers*
- To determine atomic arrangement

Significance of Peak Shape in XRD

1. Peak position
2. Peak width
3. Peak intensity

Structure refinement using FULL PROOF

Is software used to analyze the XRD patterns of the crystals that work on the basis of Rietveld refinement method. In single crystals using relatively large crystals of the material we can obtain the perfect data to measure the structure parameters, but in powder materials are in the form of very small crystallites. Dta will overlap thereby preventing the proper determination of the structure. The "Rietveld Method" creates an effective separation of these overlapping data.

The Rietveld method uses a least squares approach to refine a theoretical line profile until it matches the measured profile. The introduction of this technique was a significant step forward in the diffraction analysis of powder samples as, unlike other techniques at that time; it was able to deal reliably with strongly overlapping reflections. The Rietveld method refines user-selected parameters to minimize the difference between an experimental pattern (observed data) and a model based on the hypothesized crystal structure and instrumental parameters. The numerical intensity value Yi at each of several thousand equal steps with respect to 2θ, as we are using the constant wavelength.

The quantity minimized in the least-squares refinement is residual

$$\chi^2 = \sum_{i=1}^{n} w_i \{y_i - y_{ci}(\beta)\}^2 \qquad 1.5.2$$

Where y_i is the observed intensity at the ith position, Y_{ci} is the calculated intensity at ith step and $W_i = 1/Y_i$

For the minimum error $\frac{\partial \chi^2}{\partial \beta} = 0$ 1.5.3

A Taylor expansion of Y_i around Yci allows the application of an iterative process. The shifts to be applied to the parameters at each cycle for improving χ^2 are obtained by solving a linear system of equations

$$A\delta_\beta = b \qquad 1.5.4$$

$$A_{kl} = \sum_i w_i \frac{\partial y(\beta 0)}{\partial \beta k} \frac{\partial y(\beta 0)}{\partial \beta i} \qquad 1.5.5$$

$$b_k = \sum_i w_i (y_i - y_k) \frac{\partial y(\beta 0)}{\partial \beta k} \qquad 1.5.6$$

The shifts of the parameters obtained by solving the normal equations are added to the starting parameters giving rise to *a* new set

$$\beta_i = \beta_0 + \delta_{\beta 0} \qquad 1.5.7$$

and we will start these as new starting parameters, repeat the cycle until a convergence criterion is satisfied The variance of the adjusted parameters are calculated by the expression

The least squares procedure provides the value of the parameters constituting the local minimum closest to the starting point.

$\sigma^2 (\beta_k) = (A^{-1})_{kk} \chi^2_v$ 1.5.8

$\chi^2_v = \frac{\chi^2}{N-P+C}$ 1.5.9

N is the number of observation (number of Y_i) P is the number of parameters and C is the number of constrains applied.

Peak shape: In the collected XRD data, It was effected by the incident beam, experimental arrangements, the sample size and shape we can refined. If this distribution is assumed then the contribution of a given reflection to the profile y_i at position $2\theta_i$ is

$Y_I = I_k \exp [-4\ln (\frac{2}{H_k^2}) (2\theta_i - 2\theta_k)^2]$ 1.5.10

Where H_k is FWHM at 2theta value $2\theta_k$ and I_k is the calculated intensity.

As an example XRD pattern of Na_xCoO_2 refined with FULLPROF program is shown in figure 1.10.

1.5.2. Elemental/compositional/ Surface morphology

Energy Dispersive X-ray analysis (EDAX) uses to determine the elemental composition with higher weighed elements. Inductive Coupled Plasma (ICP) also to determine the elemental analysis. The later method is more precise in comparison to earlier. In ICP method, the required material should be decomposed in either water or by addition of HCl/HNO_3 for non-soluble compounds and the concentration of each element will be determined separately. The Scanning Electron Microscopy uses the study of surface morphology of the grains. The size and the shape of the compound can be determined using SEM.

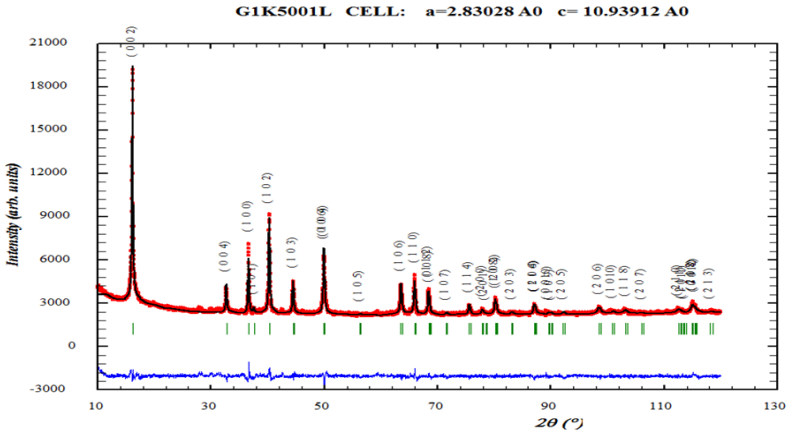

Figure 1.10. XRD pattern of Na_xCoO_2 refined with FULLPROF program

1.5.3. Seebeck measurements using PPMS

The Seebeck coefficient is a thermoelectric measure of the magnitude of voltage produced by a temperature gradient across a material. If the temperature difference is between two points is small, the Seebeck coefficient approximated by:

$S = \Delta V/\Delta T$ 1.5.3.1

While a thermal gradient can be generated by heating either end of the sample. Thermometers (usually thermocouples or resistive sensors) attached at two points along the length of the sample designate the temperatures Th and Tc. The temperature difference between these two points is

$\Delta T = T_h - T_c$ 1.5.3.2

Corresponding to this temperature difference, there will be an induced thermoelectric voltage

$\Delta V_{true} = V_h - V_c$ 1.5.3.3

Depending on the type of a dominant carrier (either electron or hole), the voltage ΔVtrue will be either positive or negative. As already noted, the Seebeck voltage is measured with the aid of thin niobium wires that are inserted into the small holes together with the junctions of the K-type thermocouple.

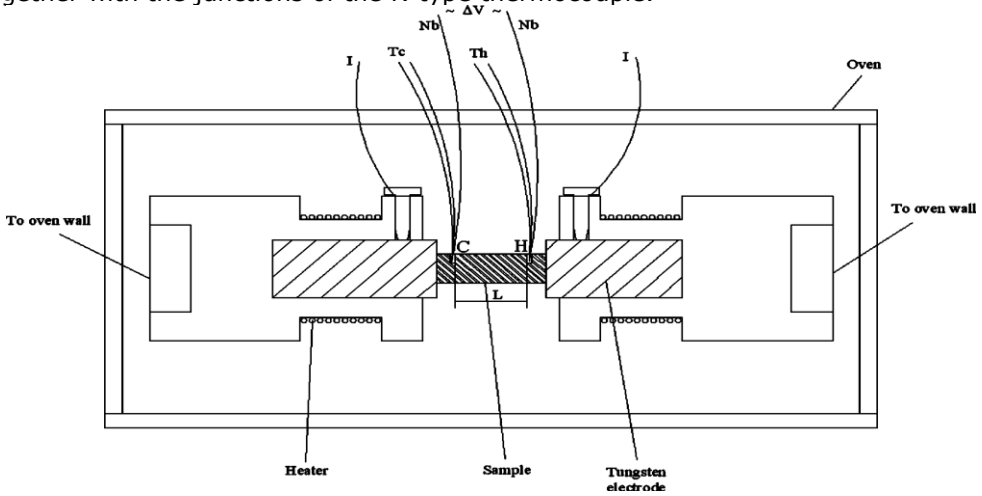

Figure 1.11. Schematic representation of seebeck measurement [62]

Thus, both the voltage differences ΔVtrue and the temperature difference ΔT are measured between the same two points *H* and *C*. The voltage detected at the terminals of the nano voltmeter. The accuracy of the temperature gradient measurement is estimated to be within ±0.2%, the accuracy of the voltage gradient measurement is estimated to be within ±0.1%. After taking all these errors into account, the total error of the Seebeck coefficient is estimated to be within ±0.3%.

1.5.4. Transport properties using four–point Probe method

The purpose of the four-point probe is to measure the resistivity of any semiconductor material. It can measure either bulk or thin film specimen, each of which consists of a different expression. The four probe setup consists of four equally spaced contacts to the sample. A high constant current source is used to supply current through the outer two contacts; a voltmeter measures the voltage across the inner two contacts to determine the sample resistivity. Typical probe spacing s ~ 1 mm.

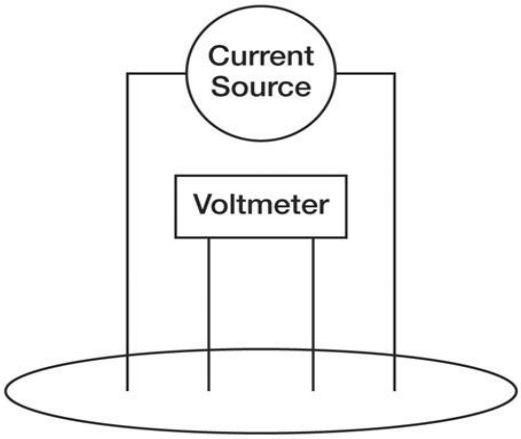

Figure 1.12. Arrangement of four-point probes for resistivity measurement [63]

Bulk Sample: Assume that the metal tip is infinitesimal and samples are semi-infinite in lateral dimension.

For bulk samples where the sample Thickness t >>s, the probe spacing, we assume a spherical protrusion of current emanating from the outer probe contacts The differential resistance is :

$$\Delta R = \rho\left(\frac{dx}{dA}\right) \qquad 1.5.4.1$$

We carry out the integration between the inner probe tips (where the voltage is Measured):

$$R = \int_{X1}^{X2} \rho \frac{dx}{2\pi x^2} = \frac{1}{2s}\frac{\rho}{2\pi} \qquad 1.5.4.2$$

Where probe spacing is uniformly s. Due to the superposition of current at the outer two tips,

$$R = V/2xI. \qquad 1.5.4.3$$

Thus, we arrive at the expression for bulk receptivity:

$$\rho = 2\Pi s\left(\frac{V}{I}\right) \qquad 1.5.4.4$$

1.5.5. Magnetic characterizations using SQUID-MPMS

Superconducting QUantum Interference Devices (SQUIDs) are sensitive probes that can detect small Changes in the magnetic field. They take advantage of two important properties of superconductors, quantization and the Josephson Effect. The SQUIDS can detect even very smaller fields down to 10^{-15} T. The most widely distributed commercial SQUID system is Quantum Design's Magnetic Property Measurement System (MPMS). The essential feature is the use of a gradiometer to measure the magnetic properties of a sample inserted into one of its pickup loops via a vertical tube with room-temperature access. The temperature of the sample can be varied from about 2 to 400 K, and the magnetic field can be varied from zero to 7 T. The system can be used to measure both the intrinsic magnetic moment of a sample in zero magnetic fields and the magnetic susceptibility by applying a magnetic field. The original system operated in liquid helium, but a version equipped with a cry cooler is now available: the latter is an excellent example of a turnkey system where the operator does not need to be aware that it contains a superconducting device. The detailed on MPMS functioning is discussed in chapter 2.

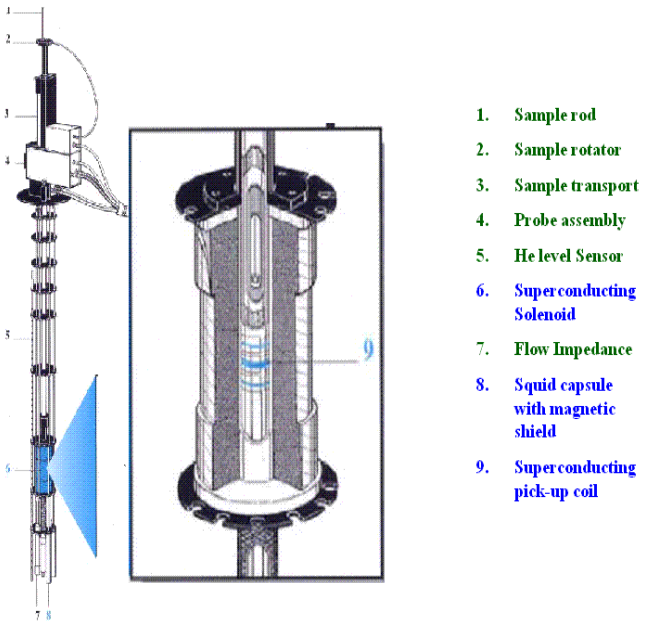

Figure 1.13. Schematic diagram of MPMS [59]

1.6. Challenges in hydrothermal synthesis of layered cobalt oxides compounds

Several cobalt oxides with Co^{2+} or Co^{3+}; CoO, Co_3O_4, $LiCoO_2$, $CuCoO_2$ etc have been successfully synthesised by hydrothermal method. Synthesis of binary oxides in hydrothermal synthesis is quit easier but for ternary compounds, where the phase diagram might complex for some compounds. In case of Na_xCoO_2, the two species of CoO and Co_3O_4 are more stable due to lower formation energies for Co^{2+} and Co^{3+}. The mixed valence of Cobalt in Na_xCoO_2 makes the narrow possibility of stabilizing the phase at lower temperature. In the previous study of Co-H_2O system from 25^0C-150^0C, shows the narrow windows for stabilizing Co^{3+} (CoOOH) at low temperatures [64].

Na_xCoO_2: Several synthesis parameters like temperature, pressure, molaity of the solution, concentrations of the precursors, and the synthesis time will affect the resultant phases. To find the exact suitable combinations of the above factors, it is necessary to study the effect of each parameter on the resultant phase for obtaining single phase materials. The hydrogen peroxide may contribute to oxidizing the cobalt partially to Co^{4+} thus may provide the opportunity for stabilising the Na_xCoO_2 phase at lower temperature. With these basic assumptions, we focused to study the phase diagram C-NaOH-H_2O, and to stabilise the Na_xCoO_2 at low temperatures using hydrothermal method. The complete details of the study of the phase diagram and the synthesis of Na_xCoO_2 is discussed in chapter 3.

$LiCoO_2$: The molaity of the solution, synthesis time, pressure, and the cooling rate are the factors that cause changes in morphology of the obtained materials using hydrothermal methods. Each of alkaline mineralisers like NaOH, LiOH, and KOH affects differently on the solubility as well as the morphology of the particles. To optimise the molaity as well as the synthesis times regarding to find out the lower synthesis parameters for obtain concaved cuboctohedrons, one might have to study the phase diagram. We varied the LiOH, NaOH, and the combination of these two, for obtain the concaved cuboctohedrons with lower mineralising agents. The complete details will be discussed in chapter 4. Several successful attempts have been made to obtain $LiCoO_2$ using hydrothermal method. Either higher concentrations of mineralisers like KOH or higher concentrations of oxidizing agent (H_2O_2) or supercritical hydrothermal conditions were used to stabilise the single phase $LiCoO_2$. The present study focussed to obtain $LiCoO_2$ at lower concentrations of ionic mineralisers as well as lower concentrations of hydrogen peroxide. The desert rose as well as concavedcuboctohedrons were obtained at very lower concentrations of mineralisers as well as hydrogen peroxide. During this study, the effect of concentration of precursor $Co(OH)_2$, synthesis duration and the molaity of ionic mineralisers were studied. Alkaline layered cobalt oxides show much interest regarding several practical applications and also in the aspect of fundamental studies. These materials show strong correlation effects and unusual physical properties. The bi-dimensional nature in structure gives huge anisotropy in physical properties. In Na_xCoO_2, a small change in Na content changes the structural thus the physical properties. It forms in 4 different strictures thus the physical properties changes from insulating to metallic, and superconductor at low temperatures with water intercalation. The A layer acts a s a key role to change the valence as well as carrier concentration in CoO_2 plane. The structure allows a wide range of

substitutions both in A-layer as well as Co-site in the structure thus allows tuning the physical properties. The intercalation and de-intercalation of A-cation made these materials much popular as cathode materials for ionic batteries. Several compounds of $ACoO_2$ have been made by several synthesis methods and with possible substitutions to improve the physical properties. Besides having these properties, the difficulties arise to stabilise some of these phases as well as substitutions. For examples like get rid of Co_3O_4 impurities.

Chapter 2

Introduction to metallic delafossite cobalt oxides $ACoO_2$ (A=Pt and Pd)

2.1. Background

The delafossite compounds, having ABO_2 chemical structure were named in honor of the French crystallographer Gabriel Delafosse (1795-1878). The first most identified compound was $CuFeO_2$ [65] several wide range of compounds were categorised later with A=Pt, Pd, Ag and Cu, B=transition metals, rare earth and p-block. The crystal structure was assigned to R-3m by R.D.Shannon and his group [66-68]. The delafossite compounds show wide range of applications like Optical Transparent Conducting Oxides (TCO) [69-70], catalyst for exhaust gas purifications and thermoelectric applications. The transport properties show wide range of electrical properties, from p-type conducting [75], n-type conducting [74], and metallic [76].
The delafossite compounds with A-cation having d^{10} configuration have filled valance band thus exhibits p-type semiconducting behaviour. This p-type semiconducting property comes from either the ionized A-vacancies. In Cu based delafossite compounds, it isn't observed a strong dependence of conductivity on Cu vacancies. But in Ag based delafossite compounds the conductivity varies with respect to the Ag vacancies (Ag_xCoO_2). The delafossite compounds with A-cation having d^9 configuration of the monovalent Pd(Pt)-ion creates an unfilled orbital and causes the metallic behaviour at room temperature, where the metallic property of these compounds comes from the metallic bonding of Pd(Pt) ions.
This bi-dimentional structure results anisotropy in physical properties. The charge and spin of B-layer can be controlled by substitution of non-equivalent elements at B-site. The wide range of A-site and B-site substitutions are possible in these compounds, thus the different applications. The metallic delafossite compounds $PdCoO_2$ and $PtCoO_2$ are much attracted due to their metallic conductivity and anisotropy. These oxide materials show comparable conducting behaviour to that of metals. The previous studies show that the substitution of di-valence element on Co-site can improve the thermoelectric properties of these metallic delafossite cobalt oxides.

2.2. Structure of delafossite-type oxides

The crystal structure of ABO_2 consisting of alternating layers of A- ions and triangular BO_2 planes. The edge –shared distorted octahedra of oxygen ions form a two-dimensional triangle lattice. The Co-ion is at the centre of distorted octahedra to form a 2D triangle lattice. Depending on the orientation of each layer in stacking the delafossite can form several polytypes like 3R (*R-3m*) [67], 2H (*P63/mmc)* [71], and recently formed D4 (*P63/mmc)* [72].

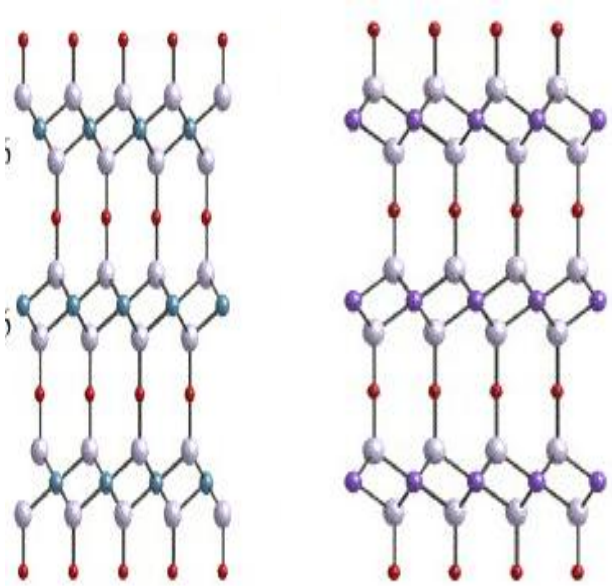

Figure 2.1 Delafossite with 3R structure (R-3m) and 2H(P63/mmc) phases.[122]

By stacking the double layers with alternating A-layers oriented 180^0 relative to each other; the hexagonal 2H type is formed. This structure has *P63/mmc* space group symmetry. If the double layers are stacked with the A-layers oriented the same direction relative to one another but offset from each other in a three layer sequence, the rhombohedral 3R type is formed. This structure has space group symmetry of *R-3m* (Fig 2.1) in D4 –phase, the alternate phases of D3 and D2 stack together like shown in figure 2.4.
The radius of B-ion has strong effect on the a-axis while the O-A-O bond length affects the c-axis. As the B-cation radius increases, the B-O distance increases while O-O distances unchanged so the changes in B ionic radius has strong effect on a-axis and the c-axis has the lower impact .

The octahedral coordination of B-cation site in delafossite structure allows the wide range of cation size; from ~0.5 Å to ~1 Å. This allows the substitution of a charge compensated pair into the site with overall charge of +3 at B-site such as 1:1 ratios of 2+/4+ ($AgCo_{0.5}Sn_{0.5}O_2$, $CuCo_{0.5}Ti_{0.5}O_2$, $CuCu_{0.5}Ti_{0.5}O_2$, $CuNi_{0.5}Ti_{0.5}O_2$,and $CuNi_{0.5}Sn_{0.5}O_2$) , 1+/5+(no stable compounds reported with a mixture of 1+/5+ cations), 2:1 ratios of 2+/5+ ($CuNi_{2/3}Sb_{1/3}O_2$) and 3+/3+ ($CuGa_{1-x}Fe_xO_2$, $CuGa_{1-x}In_xO_2$, and $CuLa_{0.5}Y_{0.5}O_2$). The larger A-cation results higher values of a-lattice parameter (Figure 2.2).

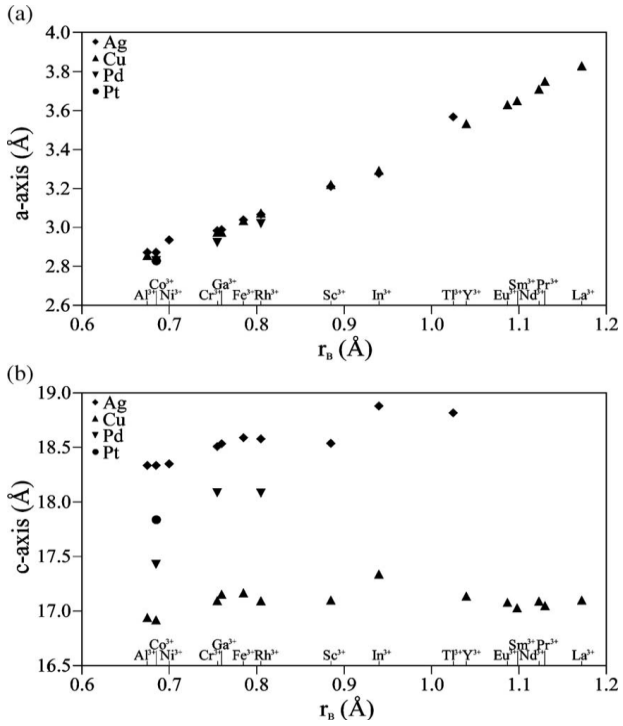

Figure 2.2.The effect of radius of B-ion on a-axis and c-axis in delafossite compounds [76].

The phase diagram (Fig 2.2) shows the generalized phase formations of ABO_2 compounds based on the ionic radii of A and B ions. The structural dependence on radii of A and B-cations is shown in figure 2.3., which represents several kinds of ABO_2 compounds.

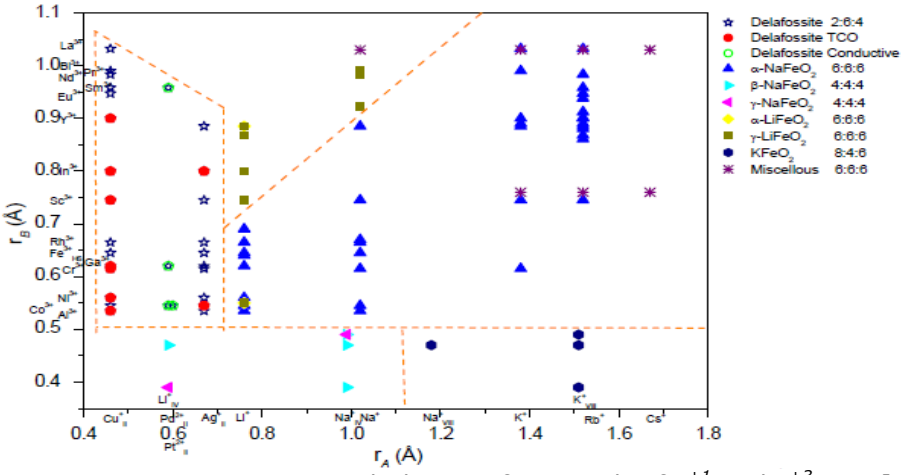

Figure 2.3. Structure map with the set of ionic radii of A^{+1} and B^{+3} ions [76]

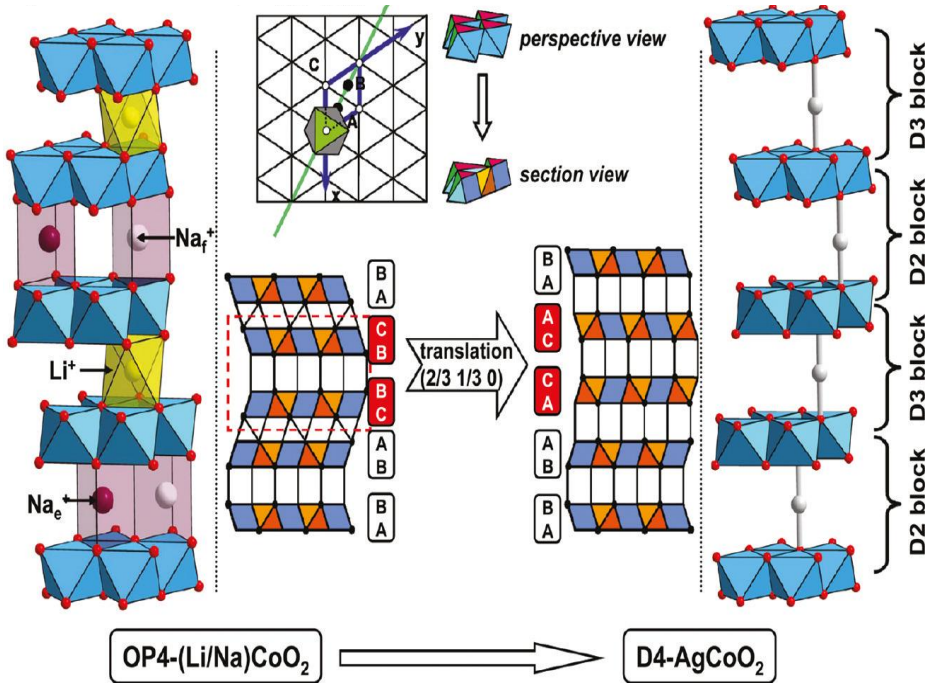

Figure 2.4. New polytype of delafossite $AgCoO_2$; D4(P63/mimic) [101]

2.3. Properties of delafossite type oxides

$AgMO_2$: The silver delafossites $AgAlO_2$, $AgScO_2$, $AgGaO_2$, and $AgInO_2$ have larger band gaps and lower visible light absorption. The visible colors of different Ag delafossite compounds are ; white ($AgAlO_2$), light gray ($AgScO_2$), olive green ($AgGaO_2$), and bright orange ($AgInO_2$) shows an increase of band gap from Al to Ga [99]. The $AgCoO_2$ shows p-type conducting behavior and the heterojunction with n-type ZnO has been made [100]. The new poly type of delafossite structure;D4 phase also obtained and show better transport properties than 2H and 3R [101]. The new poly type of delafossite structured phase also obtained and show better transport properties than 2H and 3R [101]. These compounds were obtained using ion-exchange method. 3R(R-3m) phase was obtained using $LiCoO_2$, 2H (P63/mimic) phase using P2-$Na_{0.7}CoO_2$, and D4 (P63/mimic) phase using P4-$Li_xNa_yCoO_2$ [101]. It was observed in their study that the resistivity and the seebeck coefficient are 2H < 3R < D4 [101].

$CuMO_2$: It has been observed that most of the p-type semiconducting delafossite materials are Cu-based. Copper based delafossites are well studied regarding their applications to TCOs. $CuAlO_2$, $CuInO_2$, and $CuCrO_2$, these compounds show semiconducting behaviour.Amongst various Cu-based delafossite materials, CuAlO2

is the first and most important material in this group. Although this material is known to exist for nearly 50 years [76] and back in 1984, its p-type conductivity was first reported by Benko and Koffyberg [85], but Kawazoe et al. [79] first prepared it in transparent thin film form for possible application in p-TCO technology. The structural properties of this material were extensively studied by Ishiguro et al. [79–82]. Other p-TCO thin films belonging to this group are copper gallium oxide ($CuGaO_2$) and copper indium oxide ($CuInO_2$) [83–85]. The lattice parameters of these materials were reported in various papers [79-82]. Properties of $CuCoO_2$ has previously been prepared by hydrothermal [107] and solution-based [103] techniques, as well as thermal decomposition of copper–cobalt hydroxyl salts [104], and ion-exchange between CuCl and $LiCoO_2$ [105]. $CuCoO_2$ with 3R (R-3m) with lattice parameters of a = 2.8494(2) Å and c = 16.926(1) Å shows an electrical resistivity of 5Ωm at 300K and room temperature seebeck coefficient of −175μV/K [105]. The band gap is found to be much lower, about 0.4eV. There have been many discussions in the literature about the influence of the size and electronic structure of the trivalent metal cation on conductivity [88-91]. It is expected that the Cu–Cu distances should play a part in any conductivity, with holes expected to hop from Cu to Cu [91]. The Cu–Cu distance is determined by the size of the M ion, which suggests that the conductivity will increase as the size of the M ion decreases. In fact this seems to be true for $CuBO_2$, which has the smallest Cu–Cu distance of all delafossites, and is reported to have the highest nondoped conductivity [92].It was observed that undoped $CuAlO_2$ has been reported to have a higher conductivity than both undoped $CuScO_2$ and $CuYO_2$ [93]. the lack of Cu–O–Cu linkages as seen in Cu2O. In the delafossite structure there are only Cu–O–M–O–Cu linkages. The authors suggest that the higher conductivities observed for $CuCrO_2$ and $CuFeO_2$ may be due to favorable mixing with the 3d states on the M cation in the Cu–O–M–O–Cu linkages [96]. As the size of the trivalent ion increases, it has been postulated that the ability to dope the material also increases [94]. A theoretical investigation of $CuMO_2$ (M = Al, Cr, Y, Sc) it was proposed that the Cr 3d states appear in the valence band of $CuCrO_2$ and mix with the O 2p, with this increased covalence in the system leading to increased hole mobility [90]. This analysis has been supported by calculations on the p-type chemistry of CuAlO2 and $CuCrO_2$ [95-96]. This shows that the thermodynamic transition levels for the copper vacancy in $CuCrO_2$ are much shallower than for $CuAlO_2$, which is primarily mediated by the increased covalence of the Cr d states with the Cu and O states in the valence band of $CuCrO_2$. $CuCrO_2$ is a semiconductor which exhibits a complicated arrangement of Cr magnetic moments. Actually, these moments form a non-collinear Heisenberg antiferromagnet on a triangular lattice, arranged with a 120◦ structure in the *ac* plane, with a moment of 3.1 +/- 0.2 μB [33].These studies also highlight the vital role of the trivalent cation in any p-type conductivity. In over all the p-type conductivities in Cu-based delafossites remain too low for high performance TCO applications [97].

The lower hole mobilities in p-type delafossites relative to Cu_2O may be caused by
Properties of Pd/PtCoO$_2$: The delafossite compounds with A-cation having d^9 configuration of the monovalent Pd(Pt)-ion creates an unfilled orbital and causes the

metallic behaviour at room temperature, where the metallic property of these compounds comes from the metallic bonding within A ions.

These materials have strong anisotropic behaviour; the resistivity along c-axis shows T-linear behaviour whereas perpendicular to c-axis shows T^2-dependence. The high metallic property is due to the metallic bonded Pd-plane where the Fermi level exists in half filled 4d orbital. The Pd-ion goes mono valent ($4d^9$) whereas Co is trivalent [107]. The metallic behaviour parallel to c-axis is due to spread of Pd metallic bond over c-axis. Such a metallic bonds can be found in $YBa_2Cu_3O_x$[107].The magnetic properties follow Curie-Weiss like dependence with temperature.

The longer crystals can be obtained by metathetical method for 30h of synthesis time using $PdCl_2$ and CoO are the precursors in a vacuum closed quartz tube. The lattice constants are found to be a=2.8317 Å° and c=17.740 Å [86].In $PdCoO_2$ the Co is in a distorted octahedral site coordinated with six oxygen atoms. The edge shared octahedra form a CoO_6 layer extended to the c-plane. The Pd is in two fold linear states coordinated with two oxygen atoms. The structure is constructed with edge linked CoO_6 octahedra connected by O-Pd-O dumbbells.

The first structural refinement for $PtCoO_2$ and $PtCoO_2$ was done by C.T.Prewitt et all[67], the reflections represents the delafossite structure with R-3m space group. By analogy with the known delafossite phases, one would expect monovalent Pd and trivalent Co in PdCoO2. However, because monovalent Pd had never been observed in an oxide and because platinum cobalt oxide apparently exhibits varying stoichiometry, the formulation $Pd^{+1}Co^{+3}O_2$ seemed suspect. For example, one might imagine $Pd_{0.8}Co_{0.8}O_2$ since Pd is normally divalent and Co^{2+} is not uncommon. This is the first compound monovalent Pd is reported in an oxide compound. However, it must be emphasized that this is only a *formal* valence state. The palladium compounds, as well as $PtCoO_2$, exhibit high electrical conductivity due to monovalent state of Pd. The initial evidence for $Pd^{+1}Co^{+3}O_2$ is the very weak non-Curie-Weiss, paramagnetic acceptability. The monovalent palladium sub lattice, with delocalized electrons giving rise to a high metallic conductivity, would normally be expected to contribute only a temperature-independent term, while low-spin, trivalent cobalt would be diamagnetic. The weak, temperature-dependent term is most likely due to a small paramagnetic impurity. For example, a 1% Co impurity would account reasonably well for the observed behavior. In the case of $PtCoO_2$; the platinum system is the only one of the known delafossite systems in which wide variations of stoichiometry can occur. In this system, the stoichiometry that does pertain seems to be dependent on synthesis conditions, perhaps on applied pressure. Metathetical reactions at ambient pressures tended to give the larger variations in stoichiometry.

2.4. Synthesis methods for metallic delafossite cobalt oxides $ACoO_2$ (A=Pt and Pd)

Solid state method: The polycrystalline delafossite compounds were used to prepare using solid state synthesis method in which both cationic precursors were oxides. These materials need higher pressures to obtain using traditional solid state method. The details are given bellow.
$PdCoO_2$: In solid state method the powders of PdO and CoO were uses ad precursors, the precursors were vacuum sealed in Platinum tubes and the thermal treatment was carried out at 800^0C at 3K bars of pressure.
$PdO + CoO \rightarrow PdCoO_2$ [67]
$PtCoO_2$: For obtaining $PtCoO_2$, PtO_2 and Co_3O_4 were used as precursors. The mixed precursors were sealed in gold tubes with 3kbars of pressure and the thermal treatment was kept at 700-950^0C.
$3PtO_2 + Co_3O_4 \rightarrow 3PtCoO_2 + 2O_2$ [66]

Hydrothermal synthesis: In hydrothermal synthesis method, the metallic delafossites were obtained using thin walled platinum or gold tubes as autoclaves with an applied pressure of 300atm while the thermal treatment was around 500-700^0C using PtO_2 and Co_3O_4 as precursors. In case of $PtCoO_2$, 20% of HCl was used get the single crystals. The absence of HCl results polycrystalline sample. The addition of 10-15 wt% of MnO_2 can cause to change the morphology of crystals from hexagonal to elongated rhombohedra[66]. *Drawbacks in the above methods are:* both hydrothermal as well as solid state methods requires high pressures, solid state methods results only polycrystalline samples, and the substitutions in ternary oxides using hydrothermal method is a difficult task.
A single crystal, also called monocrystal, is a crystalline solid in which the crystal lattice of the entire sample is continuous and unbroken to the edges of the sample, with no grain boundaries. Grain boundaries have a lot of significant effects on the mechanical, physical and electrical properties of materials. Therefore, single crystals are demanded in many fields, such as microelectronics and optoelectronics, as well as structural and high temperature materials.
Single crystals of several alkaline lamellar cobalt oxides like Na_xCoO_2 [119], $LiCoO_2$ [120], as well as delafossite compounds like $CuCrO_2$ [128] have been reported with better properties. The single crystals of metallic delafossites $PtCoO_2$ and $PdCoO_2$ have been obtained using hydrothermal (2.3.2.) as well as metathetical reactions (2.3.2), in which metathetical reactions are the easier as well as efficient way to obtain the single crystals.

Metathetical synthesis of $PtCoO_2$ and $PdCoO_2$: In metathetical reaction more than one element exchanges the part in reactions. In this reaction polycrystalline as well as single crystals can be obtained.
$PdCoO_2$: For obtaining $PdCoO_2$ single crystals in metathetical reactions $PdCl_2$ and CoO (OR Co_3O_4) were used as precursors. The mixed precursors were vacuum sealed in a quartz tube and thermally treated at 700^0C for 40h of synthesis duration.
$PdCl_2 + 2CoO \rightarrow PdCoO_2 + CoCl_2$
or

$Pd + PdCl_2 + Co_3O_4 \rightarrow 2PdCoO_2 + CoCl_2$
$PtCoO_2$: For obtaining $PtCoO_2$ single crystals in metathetical reactions $PtCl_2$ and CoO (or Co_3O_4) were used as precursors. The mixed precursors were vacuum sealed in a quartz tube and thermally treated at 700^0C for 40h of synthesis duration.
$PtCl_2 + 2CoO \rightarrow PtCoO_2 + CoCl_2$

$(1+n)\ PtCl_2 + (1-(n/3))\ Co_3O_4 + (4n/3)\ CoO \rightarrow Pt_{1+n}Co_{2-(2n/3)}O_4 + (1+n)\ CoCl_2$ [66]
Where n=0.6 to 0.8.
The crystal size depends on the reaction time as well as cooling temperature. The crystals obtained using metathetical reactions were about 0.8 mm *0.8 mm * 0.1mm ^{3} [107]. The by-products as well as the precursor that remained can be leached out using hot ethanol and water.

2.5. Magnetic and electrical properties of $PtCoO_2$ and $PdCoO_2$

The $PdCoO_2$ is classified as s-d conductor. From the magnetic susceptibility measurements it was confirmed that Co to be in trivalent 1s state and from Pd 3p XPS spectrum shows monovalent state of Pd. The metallic conductivity comes from the metallic bonds in the Pd plane. Overlapping of s-d hybridized orbital Pd monovalent state forms a half filled conduction band [106]. The purely dependence of high electrical conductivity on Pd 3d orbital is concluded by photoemission study by T.Higuchi et al [107].The thermoelectric power of $PdCoO_2$ shows increases with increasing temperature until 200K after that it is constant until 350K and decreases above this temperature. The values at 100K and 400K are given as 2-4μV/K, which are comparable with the transition metals [109]. Because of the structure has layered triangular lattice which can cause magnetic spin frustration trigger the spin glass like magnetic behaviour. The effect of defects injection on magnetic properties of polycrystalline $Pd_{0.72}Co_{0.68}O_2$ has been studied by Hirotaka.et.all [107]. The magnetic properties of the sample show a deviation of FC from ZFC a 55K indicating anti-ferromagnetic transition. The well-defined peak at T_g=4.5K indicating a *spin glass* like transition [107]. The specific heat of the $Pd_{0.72}Co_{0.68}O_2$ is measured form 1.8-300K. The second order anomaly is found around 50K. This transition indicating the existence of magnetic ions which are generated by lattice defects in $Pd_{0.72}Co_{0.68}O_2$. But there is no clear indication in the specific heat at T_g suggesting the existence of spin glass phases. Manganese substituted For non stoichiometric $PdCoO_2$ shows spin-glass behaviour bellow 20K [117]. The susceptibility measurements with temperature shows a significant hysteresis below about 60 K and broad cusp around 16 K in the directions perpendicular or parallel to the *c*-axis. These behaviors became more conspicuous with decreasing the applied magnetic field.

It was found that Mn ions replaced Co ions and the valence state was 3+ in high spin state. Pd $(Co_{0.96}Mn_{0.04})O_2$ displayed only the Curie–Weiss temperature dependence of magnetic susceptibility below 5 K. On the other hand, Pd $(Co_{0.89}Mn_{0.11})O_2$ showed a large anisotropic hysteresis and dull cusp around 16 K in the temperature dependence of magnetization in a low magnetic field, and showed the residual magnetization in the magnetization curve at 5 K. The solid solutions $(PtPd)CoO_2$ were studied by M.Tanaka et al [107].The temperature dependence of susceptibility show Curie-Weiss behavior.
Kyoo kim and his group studied the Fermi surface of the $PdCoO_2$ [110].They found that the Fermi Surface (FS) in delafossite $PdCoO_2$ originate from surface states as well as bulk states, The bulk states at E_F corresponds to Pd $4d_{3Z}2_{-r}2$- Pd 5s hybrid states (ψ_{d-s}) which are responsible for the high in-plane conductivity in $PdCoO_2$ and for CoO_2 FS arises from Co t_{2g} –O 2p states. Due to the localized nature of surface states the Spin-Orbit (SO) interaction and the exchange interaction turn out to be Important to describe surface electronic structure near E_F for the CoO_2 and Pd terminated cases. The polarization-dependent soft x-ray absorption spectroscopy study [111] and Angle-Resolved Photoemission Spectroscopy study [112] shows that Co is trivalent and Pd is monovalent in $PdCoO_2$. The $PtCoO_2$ shows paramagnetic behaviour just as other metallic delofossite cobalt oxide, $PdCoO_2$. Even the solid solution of $PtPdCoO_2$ shows paramagnetic behaviour in susceptibility measurements [107].

2.6. Thermoelectric properties of metallic delafossite cobalt oxides $ACoO_2$ (A=Pt and Pd)

The materials $PdCoO_2$ and $PtCoO_2$ show good metallic behaviour in a-b direction but poor metallic property along c-axis. The $PtCoO_2$ is close to Ioffe-Regel limit along c-axis. At room temperature. Tanaka et al [108] found that the in plane resistivity is ρ (260K) =4.7μΩ cm and ρ (260K) / ρ (16K) = 8. Hiroshi TAKATSU reported crystals with that ρ (300K) /ρ (1.6K) =400 and they are able to observe quantum oscillations [113]. The strong quasi two-dimensionality of the electronic states is reflected by the Fermi surface depicted. Apart from the very small bending parallel to the *c* direction, it gives rise to completely in-plane Fermi velocities and explains the strong anisotropy in electric conductivity.
Khuong P. Ong et al [116] calculated the band structure calculations of $PtCoO_2$. The Fermi surface is a single large electron cylinder centered on the Γ-Z line and with a hexagonal shape that is rotated 30^0 with respect to the zone, similar to the Pd compound. This nearly 2D surface shows apparent nesting between the flat, concave faces of the hexagons. Nonetheless, no charge density or spin density wave instabilities are seen experimentally. This is presumably a consequence of the high band velocity. The corners of the Fermi surface are along the Γ-F direction. This is similar to PdCoO2. In both compounds the Fermi surface contains one electron (1/2 the zone). Within the Boltzmann theory the transport parameters at low T can be expressed as integrals over the Fermi surface of band structure quantities and scattering rates, while at finite T, the formulas are the same, but involve integrals with Fermi distributions.

These simplify greatly if one makes the constant scattering time approximation. Within this approximation, the scattering rate is assumed to be independent of momentum and energy. This does not, however, involve any assumption about doping level or T dependence. The very large values of the thermopower in the c-axis direction would be consistent with practical thermoelectric applications, especially for the Pt compound, although Pt is very expensive. In the present materials it is expected that the thermal conductivity will be anisotropic because there should be a strong electronic contribution in-plane but not in the c-axis direction, assuming that the Wiedemann- Franz relation holds. Low temperature thermopower is given by Mott formula

$$S(T) = (\pi^2 K^2 T/3e)\ (d\ln(\sigma_{xx})/dE) \qquad 2.5.1$$

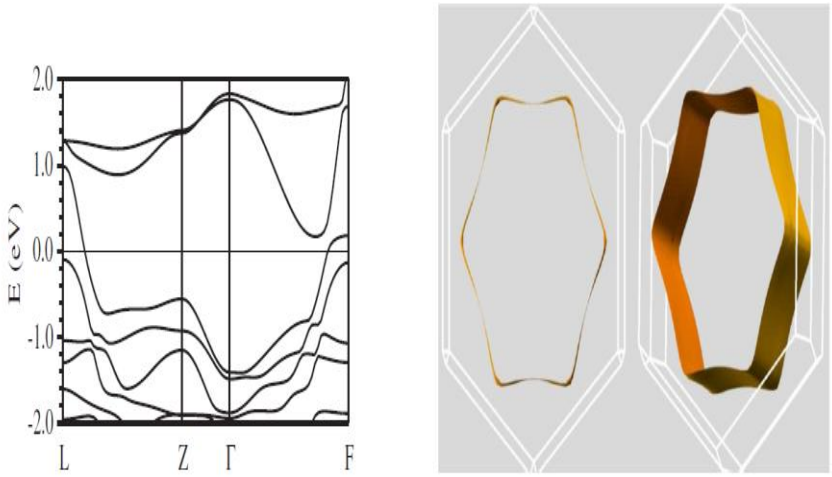

Figure 2.5. Calculated band structure (at 0eV) and Fermi surface of $PtCoO_2$ compound [116].

The strong anisotropy of PdCoO2 and PtCoO2 comes from band structure effects. S(T) is related to the logarithmic derivative of the conductivity. This anisotropy is exceedingly low for the actual chemical potential. It increases strongly above E_F. The plot is reminiscent of that conductivity of a conventional semiconductor as a function of doping level. Here the chemical potential is pinned in the gap by the fact that the material is actually a high carrier density metal and not a semiconductor. In any case, the origin of this behavior of the conductivity is seen in the band structure. Figure 2.5.5 shows the Fermi surface for a 100 meV increase in the Fermi level.

These may be interesting materials from the point of view of correlated electron behavior. The crystal structure can be described as metallic Pd/Pt sheets with a Pd/Pt distance of 2.83 A °, separated by CoO_2 sheets.
This CoO_2 structure is effectively insulating at the band structure level, leading to the conductivity anisotropy. The same structure CoO2 sheets occur in Na_xCoO_2, which has remarkable physical properties. Naively, one may suppose that the insulating CoO_2 should be strongly correlated with local moment magnetism driven by the Coulomb repulsion. This is not the case based on experiment, which points to band insulating behavior, and low spin Co. A correlated state may be nearby and could manifest itself in transport. We note that Boltzmann theory is very robust for coherent transport. It accurately describes the in-plane thermopower of Na_xCoO_2 at room temperature and above even though the material is near magnetism and possibly influenced by a quantum critical point.

Roles of high frequency phonons: The effect of high frequency phonon on transport properties was studied using Raman and IR spectroscopy [54]. The existence of these high-frequency optical phonon modes can account for the temperature dependence of the specific heat, which is indeed not saturated to the classical Dulong and Petit value even at 250 K. Moreover, the influence of high frequency phonons is needed to explain the origin of non-linear temperature dependence of the electrical resistivity. Thus, high frequency optical phonon modes play important roles in the physical properties of $PdCoO_2$. The very high in-plane conductivities are strongly anisotropic and can be explained in terms of the Pd/Pt dominated electronic structure near E_F. The large thermo power in c-axis direction would be very much useful practical applications. The thermal conductivity of these materials is expected to be anisotropic as there should be a strong electronic contribution in in-plane and lesser in c-axis direction [114].

2.7. Elemental and surface analysis methods
Electron probe micro-analyzer (EPMA)

An electron probe micro-analyzer is a micro beam instrument used primarily for the **in situ** non-destructive chemical analysis of minute solid samples. EPMA is also informally called an **electron microprobe**. It is fundamentally the same as an SEM, with the added capability of chemical analysis. The primary importance of an EPMA is the ability to acquire precise, quantitative elemental analyses at very small "spot" sizes (as little as 1-2 microns), primarily by wavelength-dispersive spectroscopy (WDS). The spatial scale of analysis, combined with the ability to create detailed images of the sample, makes it possible to analyze geological materials **in situ** and to resolve complex chemical variation within single phases (in geology, mostly glasses and minerals). The electron optics of an SEM or EPMA allow much higher resolution images to be obtained than can be seen using visible-light optics, so features that are irresolvable under a light microscope can be readily imaged to study detailed micro textures or provide the fine-scale context of an individual spot analysis. A variety of detectors can be used for:

- Imaging modes such as secondary-electron imaging (SEI), back-scattered electron imaging (BSE), and cathode luminescence imaging (CL),
- Acquiring 2D element maps,
- Acquiring compositional information by energy-dispersive spectroscopy (EDS) and wavelength-dispersive spectroscopy (WDS),
- Analyzing crystal-lattice preferred orientations (EBSD).

Fundamental Principles of Electron probe micro-analyzer (EPMA)

An electron microprobe operates under the principle that if a solid material is bombarded by an accelerated and focused electron beam, the incident electron beam has sufficient energy to liberate both matter and energy from the sample. These electron-sample interactions mainly liberate heat, but they also yield both derivative electrons and x-rays. Of most common interest in the analysis of geological materials are secondary and back-scattered electrons, which are useful for imaging a surface or obtaining an average composition of the material. X-ray generation is produced by inelastic collisions of the incident electrons with electrons in the inner shells of atoms in the sample; when an inner-shell electron is ejected from its orbit, leaving a vacancy, a higher-shell electron falls into this vacancy and must shed some energy (as an X-ray) to do so. These quantized x-rays are characteristic of the element. EPMA analysis is considered to be "non-destructive"; that is, x-rays generated by electron interactions do not lead to volume loss of the sample, so it is possible to re-analyze the same materials more than one time.

X-ray Photoelectron Spectroscopy (XPS)

XPS was developed in the mid 1960s by K. Siegbahn and his research group. K. Siegbahn was awarded the Nobel Prize for Physics in 1981 for his work in XPS. The phenomenon is based on the photoelectric effect outlined by Einstein in 1905 where the concept of the photon was used to describe the ejection of electrons from a surface when photons impinge upon it. For XPS, Al Kalpha (1486.6eV) or Mg Kalpha (1253.6eV) are often the photon energies of choice. Other X-ray lines can also be chosen such as Ti Kalpha (2040eV). The XPS technique is highly surface specific due to the short range of the photoelectrons that are excited from the solid. The energy of the photoelectrons leaving the sample are determined using a Concentric Hemispherical Analyser (CHA) and this gives a spectrum with a series of photoelectron peaks. The binding energy of the peaks are characteristic of each element. The peak areas can be used (with appropriate sensitivity factors) to determine the composition of the materials surface. The shape of each peak and the binding energy can be slightly altered by the chemical state of the emitting atom. Hence XPS can provide chemical bonding information as well. XPS is not sensitive to hydrogen or helium, but can detect all other elements. XPS must be carried out in UHV conditions.

2.8. Interests and issues in $PtCoO_2$ and $PdCoO_2$

The metallic delafossite compounds shows interesting aspects like metallic conductivity and anisotropy in physical properties. The metallic behaviour comes from the Pd-Pd bonding in ab-plane, so the anisotropy in physical properties results. PdCoO2 will approach the Ioffe-Regel limit only at high T, but PtCoO2 may show a crossover in the c-axis direction near room temperature. a crossover in the c-axis direction near room temperature. The thermo powers of these materials are predicted to be very unusual, with very large values along c and small metallic values of opposite sign in-plane. While the unusual transport arises from a detail of the band structures it is chemically robust since both the Pt and Pd compounds have similar behavior. Depending on the thermal conductivity the c-axis direction may have high thermoelectric ZT. The substitution of divalent element at Co-site can suppress the conductivity thus to improve the thermoelectric power in these metallic delafossites. The substitution of Mg at Co-site has been studied by Masashi Hasegawa et al [115], using metathetical reactions with individual precursors for each cations. The optimal value of Mg substitution was 1.8 %. These crystals show curie-Weiss behavior in susceptibility measurements. The transport measurements weren't reported with any substitutions. It might be challenging to substitute higher concentrations of Mg at Co-site as well to obtain the larger dimensions of the crystals, so that to measure the transport measurements. The higher level Mg can be substituted by taking (CoMg)O solid solution as the precursor in metathetical reactions.

Chapter 3

Synthesis and characterization of layered sodium cobalt oxides

3.1. Hydrothermal synthesis of Na_xCoO_2

As discussed in chapter 1, the oxide materials prepared using hydrothermal method show good oxygen stoichiomety and the tenable impurity, we used $Co(OH)_2$ and NaOH as the precursors to obtain Na_xCoO_2 using hydrothermal method. In order to to obtain the required phase we studied the stability diagram; Na-Co-H_2O in soft hydrothermal conditions.

The stability diagram for Na-Co-H_2O system has been builded and studied for obtaining the layered sodium cobalt oxide materials by hydrothermal synthesis. In the same time, the well-known dates of Co–H_2O system have been extended at 250ºC in basic solution. The study of the stability diagram for Na-Co-H_2O system open the possibility to obtain Na_xCoO_2 phase using soft hydrothermal method. The proposed hydrothermal synthesis has the advantage of simplicity, inexpensiveness, time saving and mild operating conditions**.**

Precursors: Precursor used in hydrothermal conditions are $Co(OH)_2$ and NaOH. The $Co(OH)_2$ has very less solubility product $K_{sp}=1.0*10^{-15}$. Crystal structure is rhombohedra, and the solubility in water is 320 µg/100 mL. For NaOH, the solubility in water is 1260 g/ l at 20^0C. The precursor NaOH also can be used as ionic mineralizer; to increase the solubility of $Co(OH)_2$ as the solubility of cobalt hydroxide is very less.

Autoclaves: For subcritical conditions, autoclaves with Teflon liners and steel covers used until 250^0C. Bellow figure 3.1 shows the autoclaves used for subcritical conditions.

Figure 3.1. Teflon liners and steel covers used as autoclaves (a) subcritical, and (b). supercritical conditions

General procedure: The solution was prepared with measured amounts of precursors and distilled water. The autoclaves used at low temperatures; until 250^{0}C is Teflon liners with steel covers. The filling percentage kept at 85% with the solution so the pressure expected to be bellow 50 bar in soft hydrothermal conditions. In supercritical and higher temperatures than 300^{0}C we used steel made autoclaves. The autoclaves kept in the furnace with 10^{0}C/Hr as temperature gradient while heating in subcritical conditions and maintained the same in supercritical conditions. The samples were cleaned several times to get rid of byproducts.

3.1.1. Experiments using equimolar ratios of precursors

Initial experiments were carried out with the stoichiometric quantities for 1gm of $Na_{0.7}CoO_2$. The starting temperature was 180^{0}C and the reaction time kept for 24hr. The precursor didn't dissolved at 180^{0}C and 200^{0}C, but a partial dissolved at 250^{0}C and complete dissolve at 300^{0}C and above. The phases observed at 300^{0}C were Co_3O_4 and CoO, and at 375^{0}C was CoO.

Precursors		Processing condistions					XRD results
NaOH gm	$Co(OH)_2$ gm	Temp (^{0}C)	filled %	Pressure (bars)	Time Hrs	NaOH/ H_2O_2	Observed phases
0.3741	0.8665	180	70	<50	24	-	$Co(OH)_2$
		200	80	<50	48	-	$Co(OH)_2$
		250	75	50	24	-	$CoO/Co(OH)_2$
		300	75	50	24	-	Co_3O_4/CoO
		375	75	300	24	-	CoO

Table 3.1. Experiments using stoichiometric quantities of the precursors; $Co(OH)_2$ and NaOH

It was observed no phases of Na_XCoO_2 in this temperature range with the stiochiometric quantities of the precursors, where the concentration of $Co(OH)_2$ was above 140 mmol/L.These experiments carried out with stoichiometric quantities for 1gm of $Na_{0.7}CoO_2$; it observed that the solubility of precursor is playing an important role. Therefore, we changed concentration of $Co(OH)_2$ to 13mmol/l. For 150^0C , the variation of the molaity of NaOH solution didn't affect the solubility of $Co(OH)_2$ and the change of Co valence didn't observed. Increasing the molaity of NaOH also didn't affect the precursor phase. From the solubility information for $Co(OH)_2$, we started to work with the 13mmol/l of the solution. Lower concentration of cobalt hydroxide expected to increase the solubility.

3.1.2. Stability diagram of $Co(OH)_2$-NaOH-H_2O system

The stability diagram for Na-Co-H_2O system with with NaOH, $Co(OH)_2$ as precursors and also NaOH as a mineralizer was built using XRD patterns. The results are summarized in the figure 3.1.1.

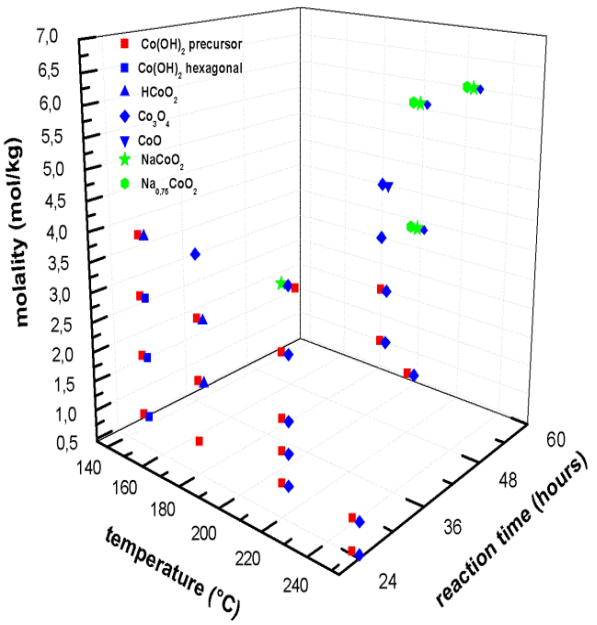

Figure 3.1.1. The stability diagram for Na-Co-H_2O system with 13mmol/l$Co(OH)_2$ as precursors and NaOH as a precursor and mineralizer.

The study of the stability diagram for Na-Co-H_2O system emphasizes the influence of the concentration mineralizer, the temperature, the reaction time and $Co(OH)_2$ concentration in the formation of desired phase, Na_xCoO_2 phase.

The role of the NaOH in the synthesis Na_xCoO2 phase is to increase the solubility of the metal complexes by increasing the hydroxide concentration and also one of precursors of desired phase. Whatever the NaOH amount, at 180°C, no Na_xCoO_2 phase was found. It was observed only the partially evolution of $Co(OH)_2$ precursor (space group: P-3*m*1; JCPDS 01-074-1057) to $Co(OH)_2$ hexagonal, (JCPDS 00-001-0357) for the low temperature and NaOH concentration. At 150°C and 4m NaOH, $Co(OH)_2$ hexagonal, as an intermediate phase, dissapers and it is replaced by CoOOH.

The transformation of $Co(OH)_2$ precursor continues with the increasing the NaOH molaity and temperature, CoOOH was found that crystallizes in the three layered polytype ($3R_1$) and became the majoritary for 180°C and 3m NaOH. The similar results were observed for other cobalt oxyhydroxide samples prepared by air oxidation as well as hydrogen peroxide oxidation, the cobalt oxyhydroxide obtained by different routes lead to $3R_1$ polytype only .The next step of $Co(OH)_2$ evolution was the appearance of mixture between Co^{2+} and Co^{3+} ions, Co_3O_4 phase. It can be observed that Co_3O_4 phase remains stable at 220°C and low molaity NaOH.
The above evolution of $Co(OH)_2$ can be summarized by the follow reactions:

$$Co(OH)_2+0.25O_2 \rightarrow CoOOH+0.5H_2O \quad (3.1.1)$$

$$3CoOOH \rightarrow Co_3O_4+1.5H_2O+0.25O_2 \quad (3.1.2)$$

The stability diagram for Na-Co-H_2O system has shown that Na_xCoO_2 phase is built if the temperatures vary between 220°C and 250°C and respectively, the NaOH molaity from 4m to 6m. It can be observed that Na_xCoO_2 phase is a multiphase mixture which consists of $Na_{0.75}CoO_2$ and $NaCoO_2$ phases (Figure 3.1.1). In order to find the optimal synthesis conditions of Na_xCoO_2 pure phase and to remove completely Co_3O_4 stable phase, only $Co(OH)_2$ concentration was decreased to 10 mmol/l and respectively, 6.5 mmol/l, the temperature and NaOH molaity were kept 220°C and respectively, 4m NaOH. Whatever time reaction (24, 48 and 60 h) and $Co(OH)_2$ concentration, the multiphase mixture which consists of $Na_{0.75}CoO_2$, $NaCoO_2$, Co_3O_4 and Na_2O phases remain (Figure 3.1.2).

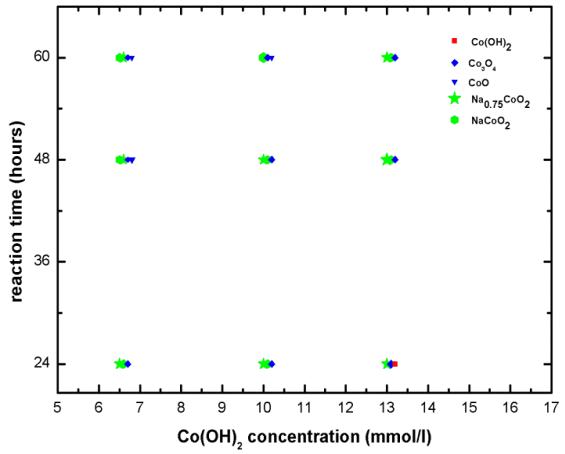

3.1.2. The stability diagram for Na-Co-H2O system with Co(OH)2 as precursors and 4m NaOH as a precursor and mineralizer at 220°C.

A reducing of Co_3O_4 phase was observed increasing the time reaction, but it was accompanied by CoO phase. The same behavior was observed at 250°C where all phases mentioned above remain stable (Figure 3.1.3).

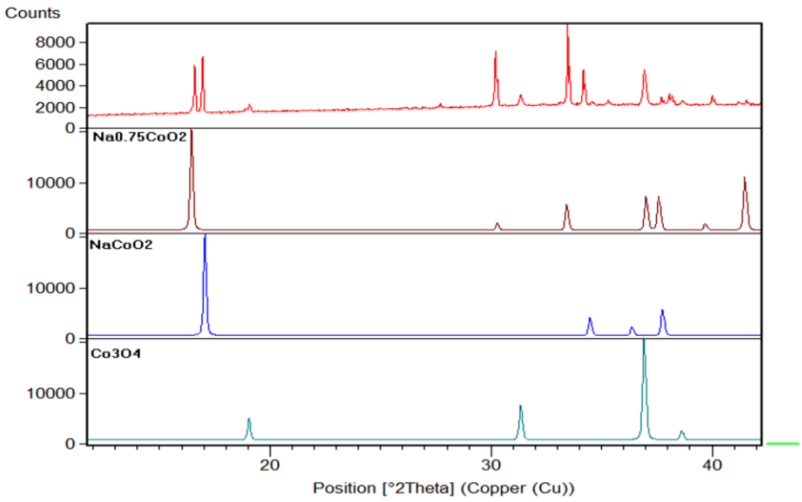

Figure 3.1.3. Room temperature X-ray diffraction patterns of the sample obtained at 250°C, 4m NaOH, 10 mmol/l Co(OH)2 and 24 h.

hydrated layered cobalt oxide $Na_{0.342}(H_3O)_{0.238}CoO_2(H_2O)_{1.19}$, with space group $P6_3/mmc$ is establish. This phase is very interesting because superconducting properties (Figure 3.1.4).

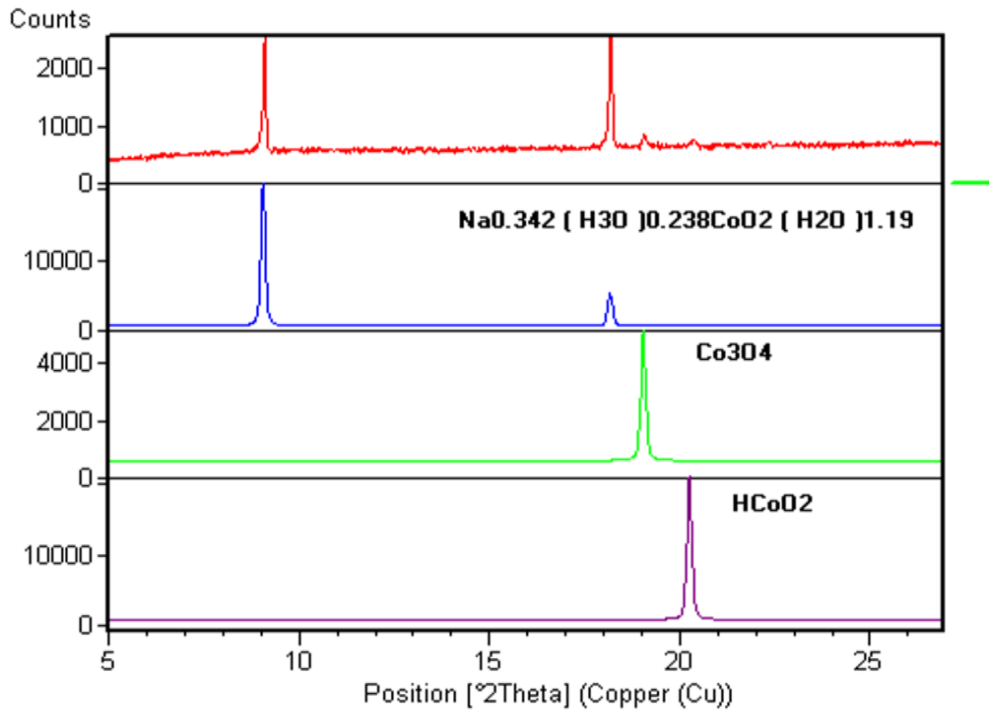

Figure 3.1.4. Room temperature X-ray diffraction patterns of the sample obtained at 220°C, 4m NaOH, 13 mmol/l Co(OH)2 and 48 h in during of cleaning process.

When Na_2O phase are removed completely, Na_xCoO_2 phase dissapears and the X-ray pattern is shown only Co_3O_4 phase (Figure 3.1.5). A possible explanation could be that non-complexed Co(III) ions are unstable oxidiser in water and thus Na_xCoO_2 still remains a instable phase.

The results indicate that the hydrothermal method is useful for preparing layered sodium cobalt oxide and low synthesis conditions determined from the stability diagram for Co-Na-H_2O system open the possibility to obtain Na_xCoO_2 pure stable phase by one step hydrothermal method.

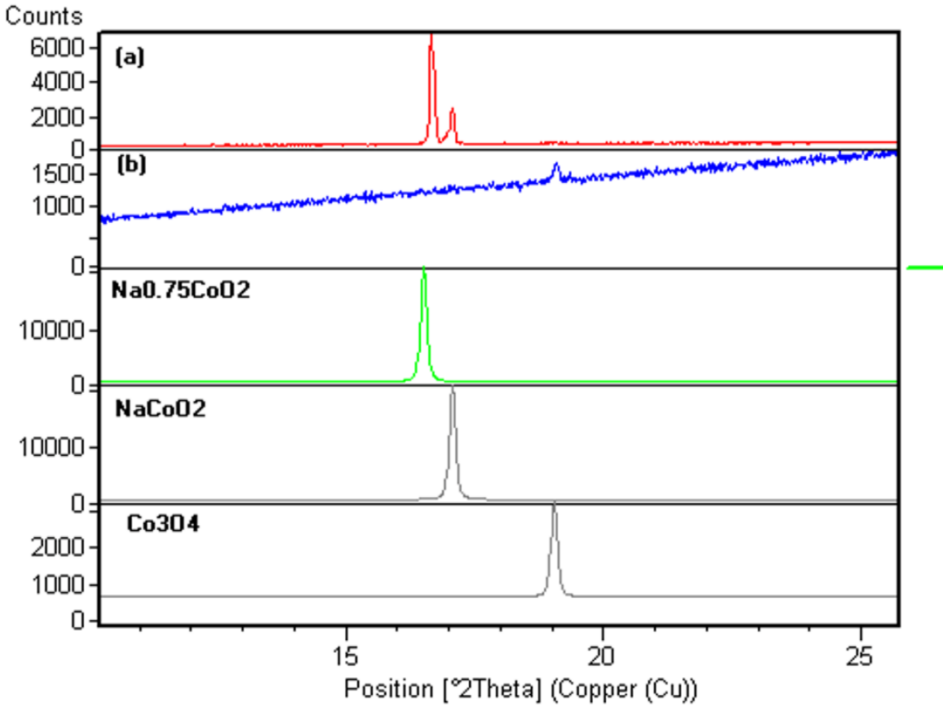

Figure 3.1.5. Room temperature X-ray diffraction patterns of sample obtained at 220°C, 4m NaOH, 10 mmol/l Co(OH)2 and 24 h (a) before cleaning process and (b) after cleaning process.

3.1.3. Study of thermodynamic parameters

From the experimental results with higher concentrations of Co $(OH)_2$ which resulting the precursor itself, the concentration of Co $(OH)_2$ was kept at 13 m mol//l (1mg of the sample instead 1g). The temperatures worked are 150^0C, 180^0C, 220^0C, 250^0C, 300^0C and 375^0C. The NaOH molaity is from 1m to 4m until 250^0C and 2.5m for the above temperatures. Addition of hydrogen peroxide was at 180^0C to 250^0C. All these results shows different phases of Cobalt at different conditions; concentration of Co $(OH)_2$, molaity of NaOH, Temperature and the synthesis time. We tried to correlate the experimental results with calculated thermodynamic parameters.

Increase in temperature as well as molaity of the solution expected to increase the solubility of cobalt hydroxide. The change in Gibbs free energy of the precursor as well

as solution causes forming of different phases at different conditions, temperature and molaity. The Gibbs free energy of solid-state material given by

$$\Delta G_{T,} = \Delta H_{T,} - T\Delta S_T \quad 3.1.3$$

$$\Delta H_{T,reaction} = \left(\sum_1 \Delta H_{T,reaction} * n_i \right)_{prod} - \left(\sum_1 \Delta H_{T,reaction} * n_i \right)_{prec} \quad 3.1.4$$

$$\Delta S_{T,reaction} = \left(\sum_1 \Delta S_{T,reaction} * n_i \right)_{prod} - \left(\sum_1 \Delta S_{T,reaction} * n_i \right)_{prec} \quad 3.1.5$$

Where
ΔH= change in enthalpy,
ΔG = Gibbs free energy,
ΔS = change in entropy,
C_p = heat capacity.

$$C_p = a + bT + cT^{-2}, \quad 3.1.6$$

The heat capacity of the solution changes as

$$C_p(solution) = C_{p,water} - \sum_{J=1}^{J=5} \sum_{I=0}^{I=5} aij\ \Gamma^I m^J \quad 3.1.7$$

$\Gamma = \frac{T}{T0}$, m= molaity of the solution. aij are the coefficients [18].
Rearranging the equations for the entire reaction, the above parameters rewritten as

$$\Delta G_{T,reaction} = \Delta H_{T,reaction} - T\Delta S_{T,reaction}$$

$$\Delta H_{T,reaction} = \left(\sum_1 \Delta H_{T,reaction} * n_i \right)_{prod} - \left(\sum_1 \Delta H_{T,reaction} * n_i \right)_{prec} \quad 3.1.8$$

$$\Delta H_{T,reaction} = \Delta H_{298} + \int_{298}^{T} \Delta C_P \, dT \quad 3.1.9$$

$$\Delta S_{T,reaction} = \Delta S_{298} + \int_{298}^{T} \frac{\Delta Cp}{T} \, dT \quad 3.1.10$$

Thermodynamic parameters of precursors and possible products: Even though all the parameters are available for only room temperatures, we used standard thermodynamic equations to calculate and approximate the thermodynamic parameters at higher temperatures.

Using these standard parameters at 298.15K and the standard thermodynamic formulae (1), (2), (3) and (4), the parameters at higher temperatures approximated.
Thermodynamic parameters at 298.15 K given as [61]

Compound	ΔG(*kJ/mol*)	ΔS *(J/mol.K)*	C_p *(J/mol.K)*		
			A	B	C
$Co(OH)_2$	−454.4	79.5	82.39	4.846×10^{-2}	2.1×10^{4}
Co_3O_4	−774.0	102.5	136.65	2.753×10^{-2}	-2.289×10^{6}
CoO	−214.2	52.97	55.1	-4.6×10^{-3}	-1.67×10^{5}
CoOOH	−349.5	66.98	172.24	-2.369×10^{-1}	7.11×10^{5}

Table 3.1.2. Thermodynamic parameters for precursors and expected products at 298.15

The variation of heat capacity of the water and the solution with NaOH is approximated for lower temperature and lower molaity by Alexey A. Alexandrov [62] and it is given by

$$C_p(\text{solution}) = Cp,\text{water} - \sum_{j=1}^{j=5}\sum_{i=0}^{i=5} aij\ \Gamma^i m^j \qquad 3.1.11$$

Where $\Gamma = \frac{T}{T0}$ m= molaity of the solution. aij are the coefficients [62]

The complexity of the NaOH soluton is that the heat capacity of the water increases with an increase in temperature but at any given temperature heat capacity decreases with increase in the molaity. We need to design the system of solutions that can provide the Gibbs free energy for $Co^{>3+}$ state. So it is necessary to study the system of Co-NaOH-H_2O. We used the available thermodynamic data at room temperature and fundamental formulae to estimate the thermodynamic parameters at higher temperatures for precursors.

Thermodynamic parameters for precursors:

species	*T* (^0K)	*-ΔG (kJ/mol)*	*-ΔH (kJ/mol)*	*ΔS(J/mol.K)*	C_P *(J/mol.K)*	
$Co(OH)_2$ (S)	298	454.4	430.709	79.5	97.067	
	423	466.724	417.833	115.582	103.005	
	453	470.352	414.520	123.250	104.444	
	493	475.563	409.967	133.055	106.367	
	523	479.746	406.451	140.143	107.811	
$H_2O(l)$	423	317.307	276.193	97.1970	77.896	-
					73.8348	1m
					69.073	2m
					63.752	3m
					57.266	4m
	453	320.369	273.576	103.2976	79.705	-
					74.705	1m
					67.053	2m
					63.680	3m
					60.170	4m
	493	324.789	269.193	111.4672	82.536	-
					75.442	1m
					68.39	2m
					61.841	3m
					55.372	4m
	523	328.366	266.833	117.6548	84.878	-
					77.272	1m
					69.594	2m
					61.432	3m
					52.131	4m

Table 3.1.3. Calculated thermodynamic parameters for precursors

Thermodynamic parameters for possible products:

species	*T* (*^{0}K*)	*-ΔG (kJ/mol)*	*-ΔH (kJ/mol)*	*ΔS (J/mol.K)*	*C_P (J/mol.K)*
Co_3O_4 (S)	298	774	743.455	102.5	119.078
	423	789.953	726.517	149.96	135.502
	453	794.682	722.070	160.29	137.966
	493	801.481	715.998	173.39	140.804
	523	806.934	711.352	182.75	142.679
CoO (s)	298	214.2	198.419	52.97	51.848
	423	222.035	191.895	71.252	52.190
	453	224.229	190.328	74.837	52.2024
	493	227.325	188.191	79.379	52.451
	523	229.726	186.700	82.267	52.0836
CoOOH (s)	298	349.5	329.539	66.98	109.65
	423	359.634	320.039	93.604	76.0049
	453	362.258	318.939	95.628	68.3919
	493	365.668	318.157	96.371	58.3736
	523	368.094	318.078	95.634	50.9406

Table 3.1.4. Calculated thermodynamic parameters for possible products

From these experimental results, it is clear that less solubility of Co $(OH)_2$ (320 µg/100ml in water at 20^{0}C) don't allow the initiation of the desired phase with Co^{3+} valence of cobalt for the low temperature (up to 250^{0}C).
In the following experiments, the concentration of $Co(OH)_2$ was 13 mmol/, the value given by the solubility product.

It should be noted that the values much differ from the experimental results, it might be due to contributions of pressure as well as the duration of synthesis time which we didn't took in calculations.

3.1.4. Hydrothermal synthesis of Na_xCoO_2

Addition of hydrogen peroxide expected to provide more oxygen in the system. Concentrations of hydrogen peroxide with 3%, 5% and 10% were used. We added the peroxide to those conditions where cobalt oxide phases appeared with sodium hydroxide solution itself. Addition of hydrogen peroxide is too complicated; the way of adding the hydrogen peroxide changing the resultant phases. For the practical restriction, we worked with the maximum concentration of H_2O_2 at 10%. For the higher molaity, 4m of NaOH at the temperature 180^{0}C and above the results shows $Co^{>2+}$. We added the peroxide for 4m of NaOH at 180^{0}C and above temperatures.

The addition of hydrogen peroxide for higher molalities shows the attractive results. Even though it expected to have more oxygen content with the addition of hydrogen peroxide, it was too difficult to justify the percentage as we lose the oxygen during the addition itself. We require the closed system to keep the all content of oxygen. For the lake of required equipment, we added the peroxide directly.
The four molaity of NaOH solution shows the $Co^{>2+}$ state so we added the hydrogen peroxide for those conditions.

It observed that the phases of Na_xCoO_2 appeared for 3% and 5% concentrations of hydrogen peroxide. For 3% and 5% concentrations of hydrogen peroxide CoOOH and Na_xCoO_2 came as minority phases for the given conditions. Further step we increased the temperature to 220^0C as we observed pure CoO_4 ($Co^{>2+}$ state). For the experiments at 220^0C with 4m of NaOH solution hydrogen peroxide is added at different ratios, 3% and 5%. Synthesis time kept at 60h and cobalt hydroxide concentration at 13 mmol / l. The results show surprising phases than previous conditions. For 3% of hydrogen peroxide, there were no considerable changes, but for 5% the phases of $Na_{0.7}CoO_2$ observed with minority phases of Co_3O_4. The addition hydrogen provides an excess content of oxygen in the system.

We restricted to 5% because of experimental limitations; the pressure inside the autoclave in the presence of H_2O_2 is unknown. It was expect to have high pressure so we restricted to 5%H_2O_2. Further step we increased the temperature to 250^0C. The results without hydrogen peroxide at 250^0C show the Co_3O_4 phases even for the lower molalities of NaOH. The results at 250^0C show no effect on the resultant phases.
We varied different ratios of precursors but the resultant is Co_3O_4 for 24hrs of synthesis time. For 250^0C and 13 mmol/l of $Co(OH)_2$, the Co_3O_4 is resulting for broad range of NaOH : $Co(OH)_2$ The phases of Na_xCoO_2 observed for 220^0C with 4m of NaOH solution and increasing the temperature is destroying the phases of Na_xCoO_2. We continued to optimize the conditions for single phase of Na_xCoO_2 at 220^0C.

The appearance of minority peaks of $NaCoO_2$ phase at 180^0C in 4m of NaOH solution with 5%H_2O_2 is attractive results because it is the lowest temperature, which allows obtaining the phases of Na_xCoO_2 compare with other material synthesis methods.
Increasing of the temperature to 220^0C in solution, which consists of 4m NaOH solution and 5% H_2O, determines the formation of $Na_{0.7}CoO_2$ phases.

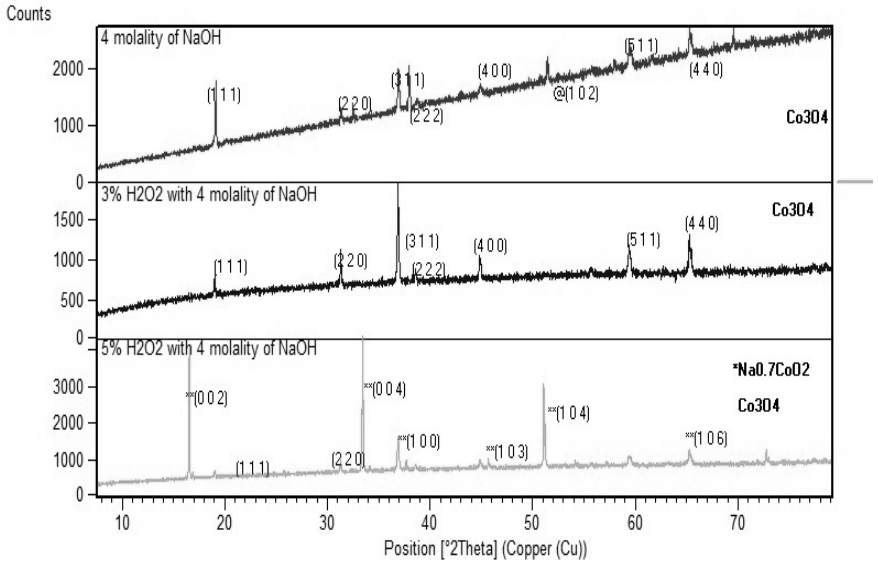

Figure 3.1.5. The X-ray patterns of the obtained samples. The effect of hydrogen peroxide at 3% and 5% concentrations after 60h at 220^{0}C

Majority phases of layered sodium cobalt oxides synthesized at lowest temperature 220^{0}C (3.1.6.).

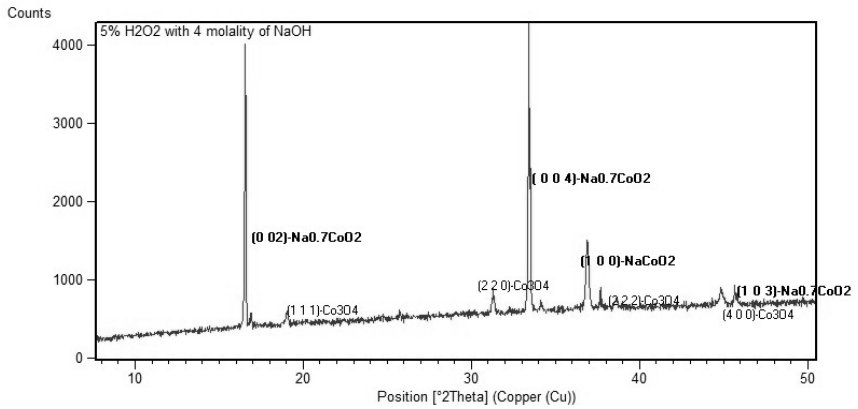

Figure 3.1.6. X-ray pattern of the sample prepared at 220^{0}C in 4m of NaOH solution and 5% of hydrogen peroxide.

Addition of hydrogen peroxide increased the valance of cobalt from 2.66 (Co_3O_4) to +3.30 ($Na_{0.7}CoO_2$). The uses of hydrogen peroxide expected to have or add more available oxygen content for the reaction. The phase of layered sodium cobalt oxide β-$Na\sim_{0.6.}CoO_2$ (NCO) is observed at the temperature 220^0C with 4m of NaOH solution, 5% of H_2O_2 (oxidizing agent-O.A) and 60h of synthesis time. After observing the β-$Na\sim_{0.6}CoO_2$ phase we tried to optimize the parameters that effect the formation of NCO.

3.1.4.1. The effect of temperature

We kept the rest of the parameters fixed and varied the temperature from 180^0C to 250^0C. An increase or decrease of temperature to ± 220^0C resulting Co_3O_4.It is observed that the temperature that favors the formation of NCO is around 220°C.The XRD patters of the synthesized samples were shown in figure 3.1.7.

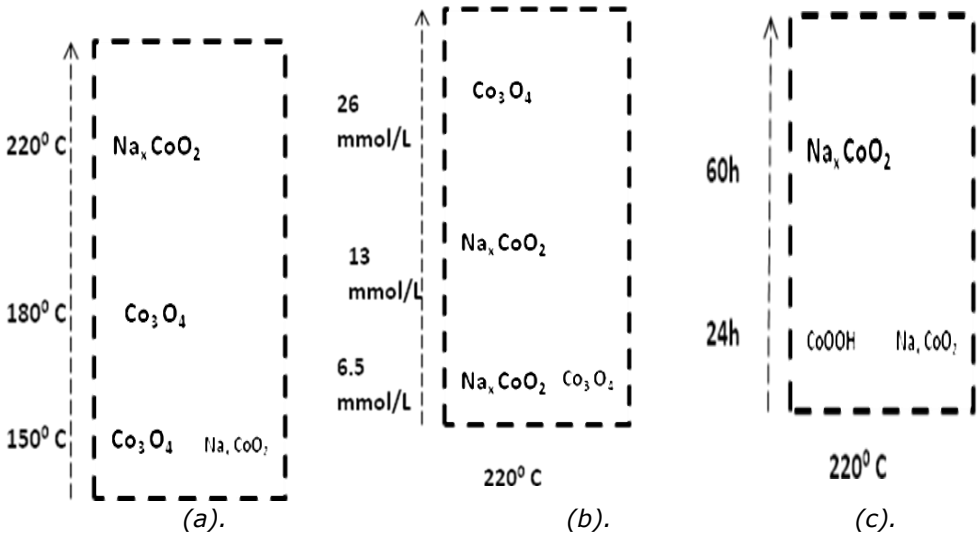

Figure 3.1.7.(a). Effect of temperature, (b). Effect of concentration of precursor, and (d).Effect of synthesis time; rest of the parameters kept same; $Co(OH)_2$-13mmol/L, H_2O_2-5%

At 180°C, only a part of the cobalt is partly oxidized and there were no traces of NCO. At 220°C, the cobalt is nearly fully oxidized and incorporated in NCO. Some traces of Co_3O_4 were present. At 250°C, only Co_3O_4 remains.

This shows that the temperature window for obtaining NCO is very small, that optimal value might be close to 220°C. The presence of Co_3O_4 at 220°C indicates that this temperature is already a bit too high and either NCO has already begun to decompose or CoOOH was already reduced to Co_3O_4. Such observation would tend to show that CoOOH, with trivalent cobalt, could be an intermediate of NCO.

3.1.4.2. The effect of concentration and purity of $Co(OH)_2$

Another important factor that effects the reaction is concentration of the precursor $Co(OH)_2$ which has very less solubility in the water. In our initial study, the β-$Na_{\sim 0.6}CoO_2$ phases were observed for concentration of $Co(OH)_2$ at 13 mmol/L. Tooptimize the concentration of $Co(OH)_2$ for obtaining NCO, we varied the concentration of $Co(OH)_2$ from 6.5 mmol/L to 26 mmol/L. The change in the concentration of $Co(OH)_2$ from 13mmol/L to 26mmol/L, is effecting the resultant phase and resulting Co_3O_4 but for 6.5 mmol/L of $Co(OH)_2$ the phase of NCO itself is remaining. We didn't worked with lower concentration than 6.5 mmol/L as the amount of the sample is very less and it is very difficult even to recover it from the solution of 4m of NaOH which needs to wash several times to get rid of sodium oxide by products. For the concentration of 6.5mmol/L and 13mmol/L, the cobalt is nearly fully oxidized and incorporated to form NCO phase. Some traces of Co_3O_4 were observed. But for 26mmol/L concentration of $Co(OH)_2$ the cobalt is oxidized to Co_3O_4, this indicates that the amount of peroxide is not sufficient to oxidize the cobalt in the system. Addition of peroxide at higher concentrations is expected to oxidize the entire cobalt, but increasing the concentration of peroxide will induce higher pressure and destroys the autoclave.

3.1.4.3. The effect of synthesis time

The effect of synthesis time is experimented at 24h and 60h to check the effect on the resultant phase while rest of the parameters kept same. The experimental details were given in table 2. For 24h, a minority phase of CoOOH is remaining, indicating that CoOOH is an intermediate phase during the process of obtaining NCO. For 60h, only NCO phase is resulting indicating that synthesis times also an important parameter for obtaining NCO phase.

Some selected crucial experiments for stabilizing Na_xCoO_2 using hydrothermal method at the specified conditions are shown in table 3.1.5

.

Temperature (^{0}C)	$Co(OH)_2$ mmol/L	NaOH molaity	$\%H_2O_2$	Time Hr	Resultant phases
180	13	4	5	60	Co_3O_4
220	13	4	5	12	CoOOH, Na_xCoO_2
220	13	4	5	24	Na_xCoO_2, CoOOH
220	13	4	5	60	Na_xCoO_2 /Co_3O_4
220	26	4	5	60	Co_3O_4
220	6.5	4	5	60	Na_xCoO_2 /Co_3O_4
250	13	4	5	60	Co_3O_4

Table 3.1.5. Experimental conditions and resultant phases for obtaining NCO

The temperature, concentration of $Co(OH)_2$ and synthesis time were effecting the NCO phases. These effective parameters were optimized to T=220°C.t=60h, $Co(OH)_2$ for the range of concentrations [6.5-13mmol/L].
The samples prepared at 220^{0}C with different synthesis times 24 h and 60h show c-axis aligned phase with CoOOH minority phase for 24h synthesis time. The observed minority phase of CoOOH for 24h synthesis time indicates the intermediate formation phase CoOOH that vanishes for 60h of synthesis time.
The reactions can written as

$$2\ Co(OH)_2 + NaOH + H_2O_2 \xrightarrow{220\ deg} 2\ HCoO_2 + Na^+ + OH^- + 2\ H_2O \qquad 3.1.12$$

$$HCoO_2 + Na^+ + OH^- \xrightarrow{60h} NaCoO_2 + H_2O \qquad 3.1.13$$

The total reaction is

$$2\ Co(OH)_2 + 2\ NaOH + H_2O_2 + H_2O \xrightarrow[60h]{220\ deg} 2\ NaCoO_2 + 5\ H_2O \qquad 3.1.14$$

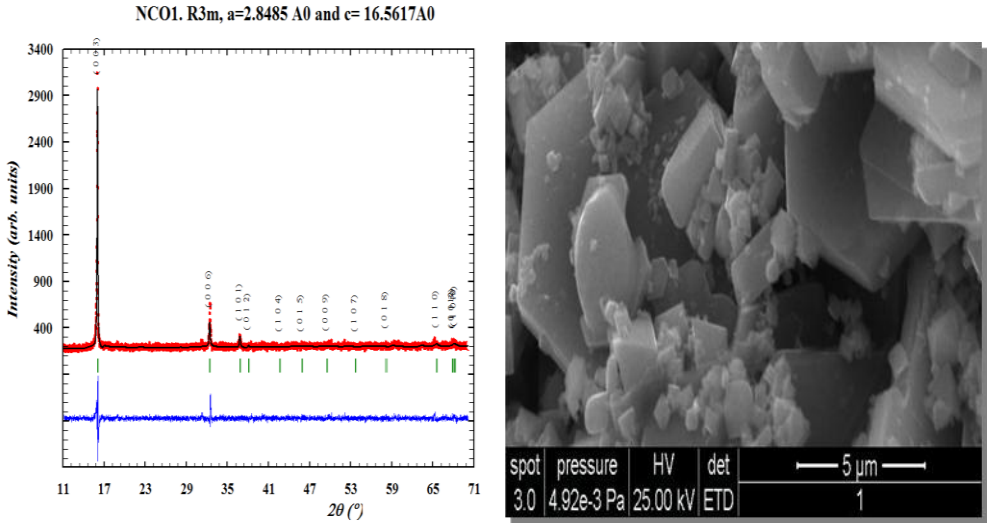

Figure 3.1.8. (a). X-ray pattern of $Na_{0.6}CoO_2$ (b) .SEM image show hexagonal plate like particles.

The obtained $Na_{0.6}CoO_2$ show R3m space group with lattice parameters a= 2.8485Å and c=16.5617Å.

3.1.4.4. Study of structural and surface properties

The obtained samples were well crystallized in hexagonal shape plates which were observed in SEM. The SEM images of the samples obtained by above conditions were shown in figures 3.1.9 and figure 3.1.10 Experimental conditions: Temperature 220°C, time=60h, OA=5% and molaity of NaOH is 4m. Figure (3.1.9). Using $Co(OH)_2$ 95% purity of and Figure (3.1.10) 99.99% purity.

The NCO samples obtained with lower purity (95%) of the precursor $Co(OH)_2$ shows the larger grain size than the NCO obtained with high purity of the precursor. It is indicating that the impurities were contributing to get the larger grain size by creating the non-homogeneous medium in the solution. It may be useful to use lower purity of precursor for obtaining the NCO crystals by hydrothermal synthesis as the grain obtained with impure precursor is 2 times larger than the NCO grain obtained with high purity precursor while rest of the parameters kept same.

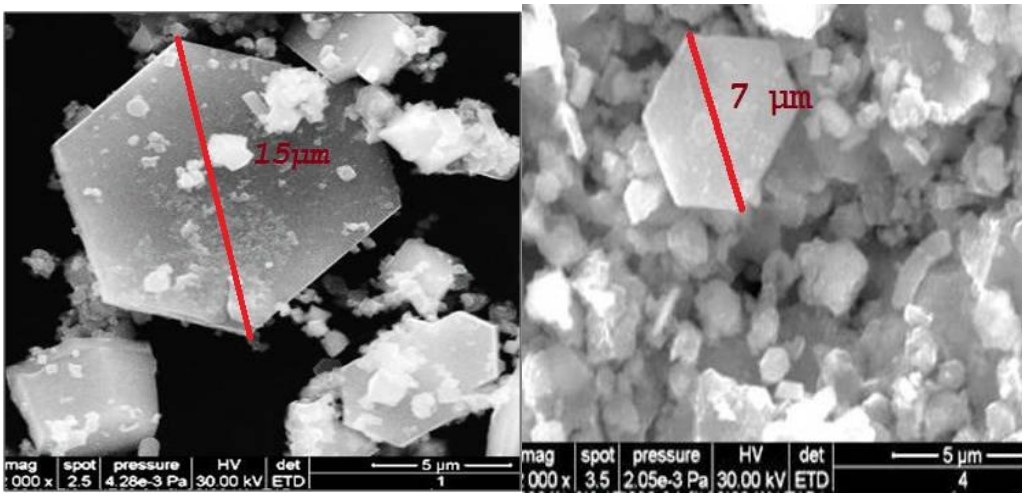

Figure 3.1.9 *Figure 5.1.10*
SEM images of the synthesized β-Na~$_{0.6}$CoO$_2$ samples

3.1.4.5. The effect of higher concentrations of H_2O_2

For the lower concentrations of H_2O_2, 3-5% , it was observed that the oxidizing agent is playing an important role along with the cleaning process. In order to check the effect of higher concentrations of H_2O_2, we restrict to 30% fill factor of the Teflon autoclave to avoid higher pressures those can destroy the autoclaves. The concentration of the $Co(OH)_2$ was kept at 10 mmol/L, temperature at 220^{0}C, The experimental results are shown in table 3.1.3.3. The profile matching for the single phase $Na_{0.6}CoO_2$ obtained using 20% peroxide, 4m of NaOH solution, 10 mmol/L of $Co(OH)_2$ for 24h synthesis duration is shown in figure 3.1.11.

Temp (^{0}C)	Autoclave fill/H_2O_2 (%)	NaOH	Synthesis duration	Product
220	10% peroxide	3m	24h	$Na_{0.6}CoO_2$ /Co_3O_4/CoOOH
220	20% peroxide	4m	60h	$Na_{0.6}$CoO2/ CoOOH/Co3O4
220	20% peroxide	4m	24h	$Na_{0.6}CoO_2$
220	20% peroxide	4m	1 week	$Na_{0.6}CoO_2$ /$Na_{0.75}CoO_2$

Table 3.1.3.3. Resultant phases using higher concentrations of peroxide; $Co(OH)_2$-13mmol/L and fill factor is 30%.

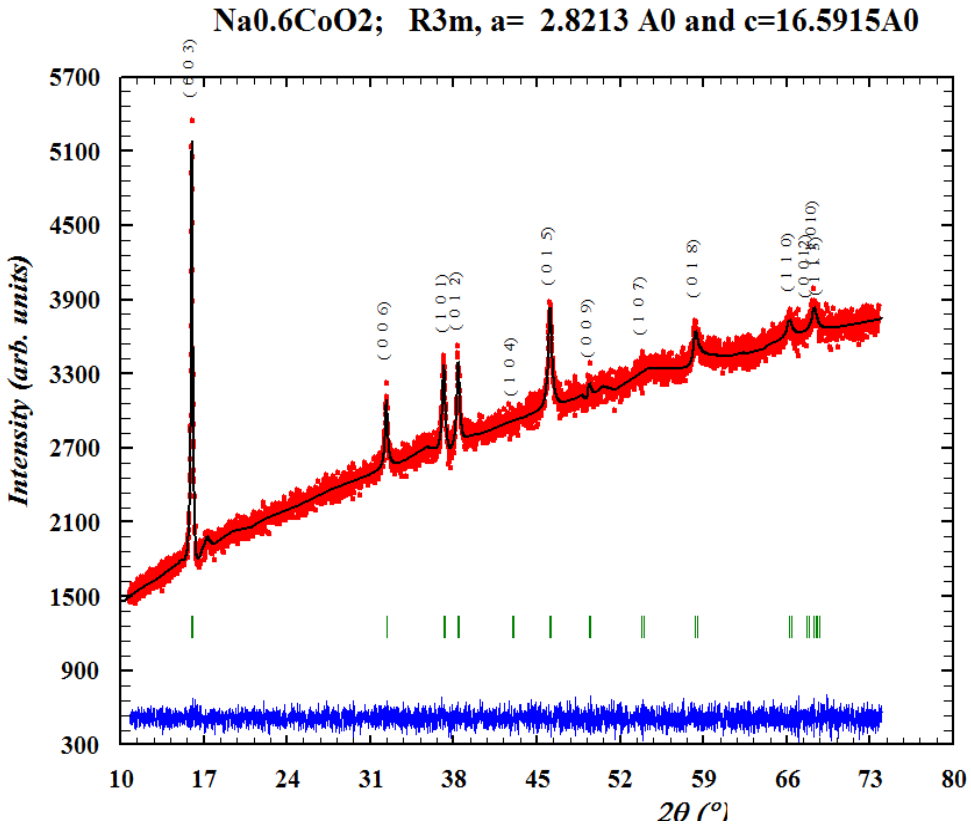

Figure 3.1.11. Profile matching for $Na_{0.6}CoO_2$ (R3m)

The profile matching results shows that the $Na_{0.6}CoO_2$ was crystallised with R3m space group with lattice parameters a= 2.8312 Å, and c= 16.5915 Å.

3.1.4.6. Structural stability of the obtained phases with temperature

The high temperature XRD was performed upto 600^{0}C. As the temperature increases to
300^{0}C appearance of an extra peak was observed. As the temperature increases further
to 450^{0}C, the initial phase was completely destroyed and the pattern was fitting with R-3m space group.

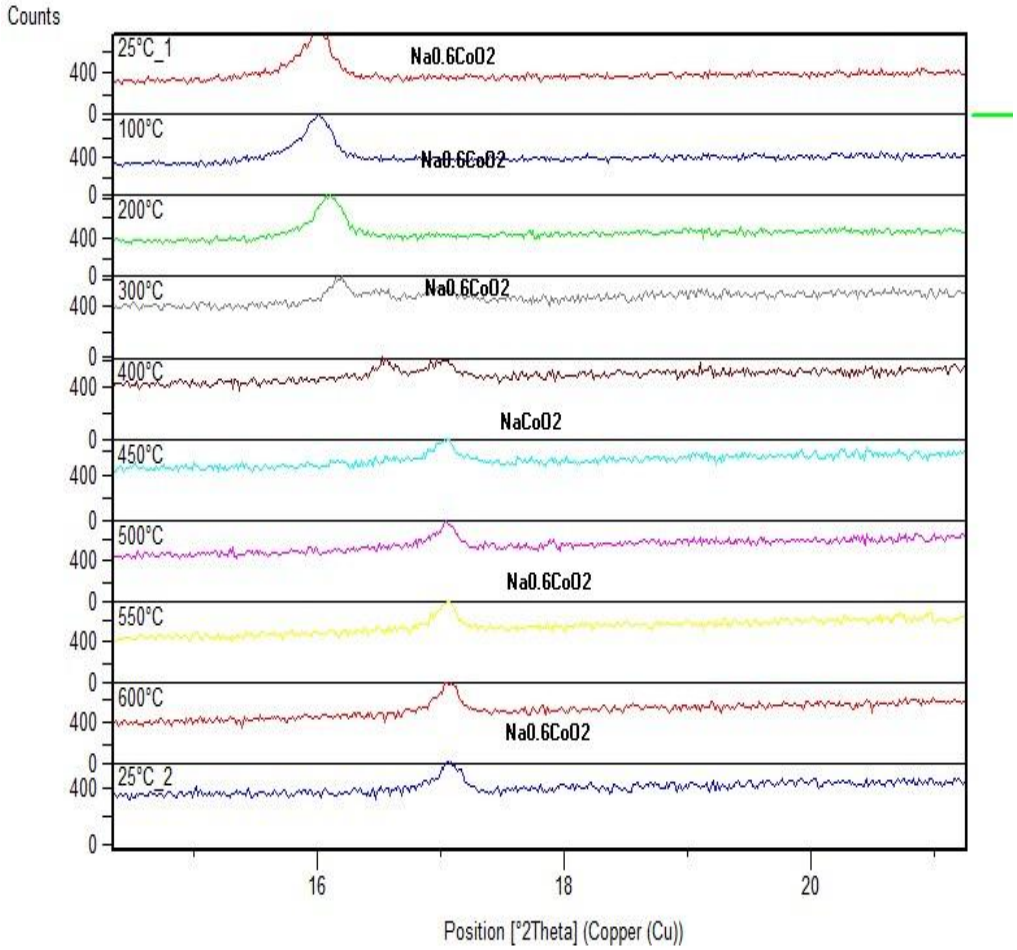

Figure 3.1.12. High-temperature X-ray diffraction patterns for $Na_{0.6}CoO_2$ (R3m)

It can be seen that around 300^{0}C the material start to change its space group and the process completes around 450^{0}C. It should be noted that no traces of Co_3O_4 was observed during and after the phase transformation.

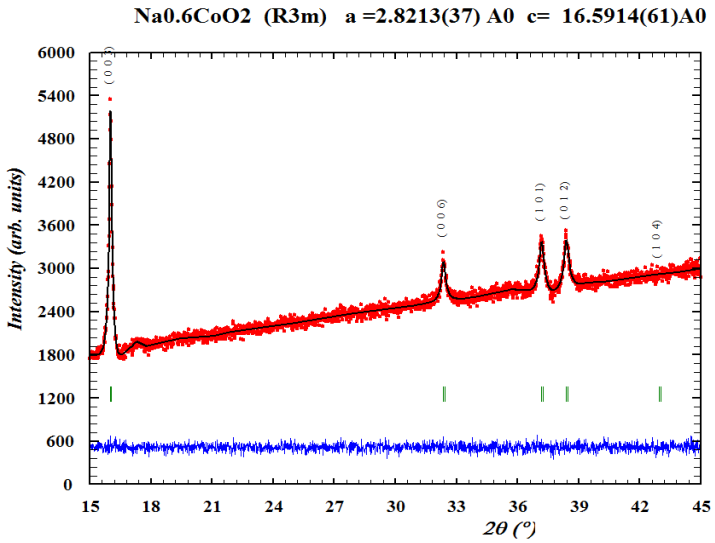

Figure 3.1.13. XRD patterns at 25^{0}C, before the thermal treatment (R3m)

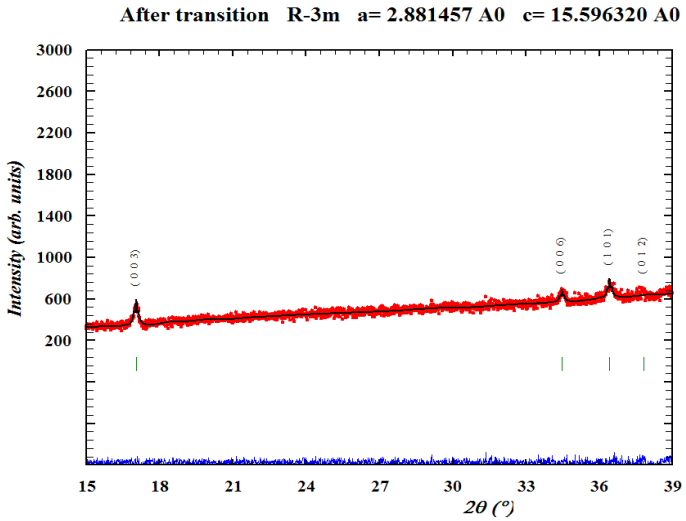

Figure 3.1.14. XRD patterns at 25^{0}C, after the thermal treatment (R-3m)

The phase transition from *R3m* to *R-3m* was observed in HTK study of the compound Na0.6CoO2, It should be noted that we need to conform the transition using reflections from higher angles.

Structural stability of β-$Na\sim_{0.7}CoO_2$ is studied using high temperature XRD system, the sample is mounted on the platinum strip and the temperature region studied is 25^0C to 840^0C. Non reaction of the sample with the platinum strip is insured before the experiment. The experiment is carried out in the vacuum chamber. The structure is stable until 500^0C and the minority phase of Co_3O_4 occurred at 600^0C. The phases of $Na\sim_{0.7}CoO_2$ were destroyed above 500^0C resulting Na_2O and Co_3O_4. The high temperature results were shown in figure 3.1.15.

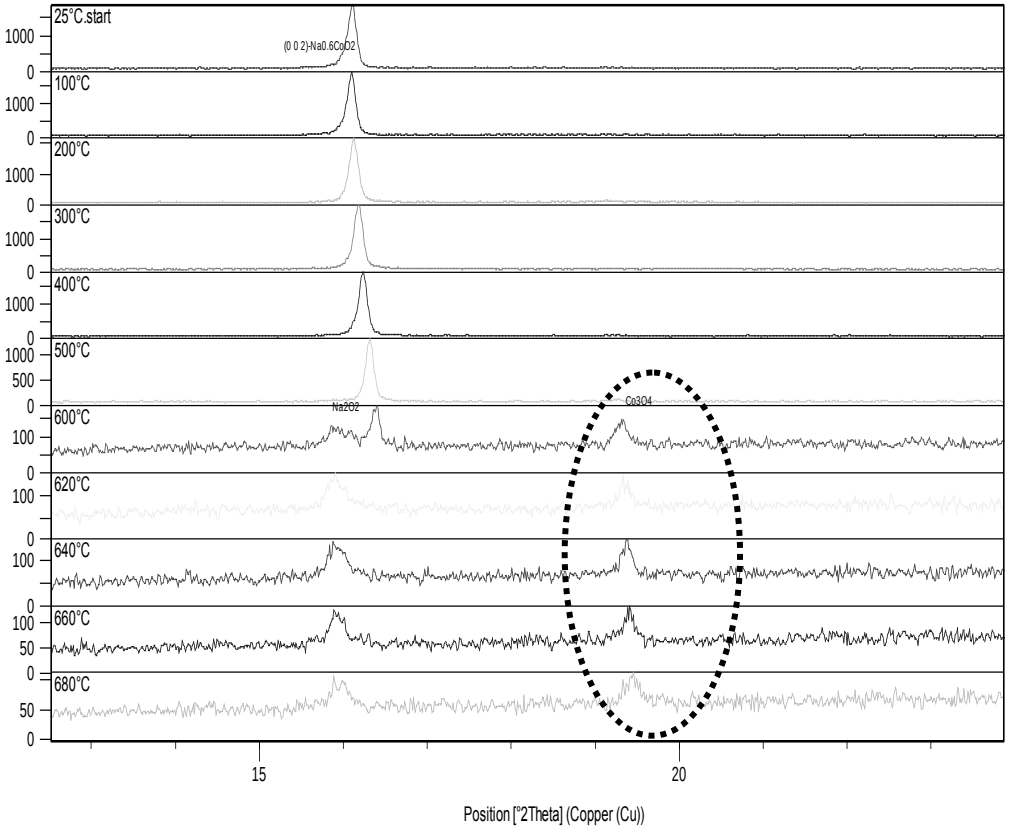

Figure 3.1.15. The HT-XRD patterns of the NCO at different temperatures; from 25°C to 680°C; dashed inset shows appearance of Co_3O_4 at 500^0C

The shift of (0 0 3) peak with increasing the temperature is observed until 500^0C, it represents the loss of Na-ions in the structure. After 600^0C the compound is completely decomposed. We need to do TGA and DSC to find the precise temperature of decomposes and the phase transforms of this material.

The same HT-XRD is performed with the sample prepared with 13 mmol/L of $Co(OH)_2$. The samples show no difference. The sample decomposes to Na_2O_2 and Co_3O_4 above 500^0C.

This discrepancy in high temperature transition shows that the Na content differs in both the synthesis approaches. Further investigation needed on the process for the conclusions.

3.2. Solid state synthesis of Mg-doped Na_xCoO_2

3.2.1. Experimental conditions

Polycrystalline samples of $Na_x(CoMg)O_2$ were synthesized using Na_2CO_3 and $Co_{1-x}Mg_xO$ were the starting materials in conventional solid state reactions, 5% excess of Na_2CO_3 was taken in due to the volatility of Na at higher temperatures. The precursors were well grinded and thermally treated at 900^0C for 24h with continuous flow of oxygen and subsequently pelletized and sintered at 900^0C during 24h in oxygen atmosphere. The powder X-ray diffraction was performed using PANalytical X'Pert Pro powder diffractometer using Cu-Kα radiation as incident beam. The patterns were refined using FOOLPROOF programme. Inductive Coupled Plasma Absorption Electron Spectroscopy (ICP-AES) analysis was performed for chemical composition analysis, Susceptibility measurements were carried out using Superconducting Quantum Interface Device (SQUID) magnetometer in the temperature range from 5 to 300K. The transport properties; (Direct current) DC electrical resistivity and seebeck measurements were performed using Physical Property Measurement System (PPMS) in the temperature range from 2 to 300K.
The expected reaction is

$$(0.7/2)Na_2CO_3+Co_{1-x}Mg_xO \rightarrow Na_{0.7}Co_{1-x}Mg_xO_2 \qquad 3.2.1$$

3.2.2. Study of structural properties

The powder X-ray diffraction patterns of the synthesized NCO with different content of Mg substitution were shown in bellow figure 3.2.1.

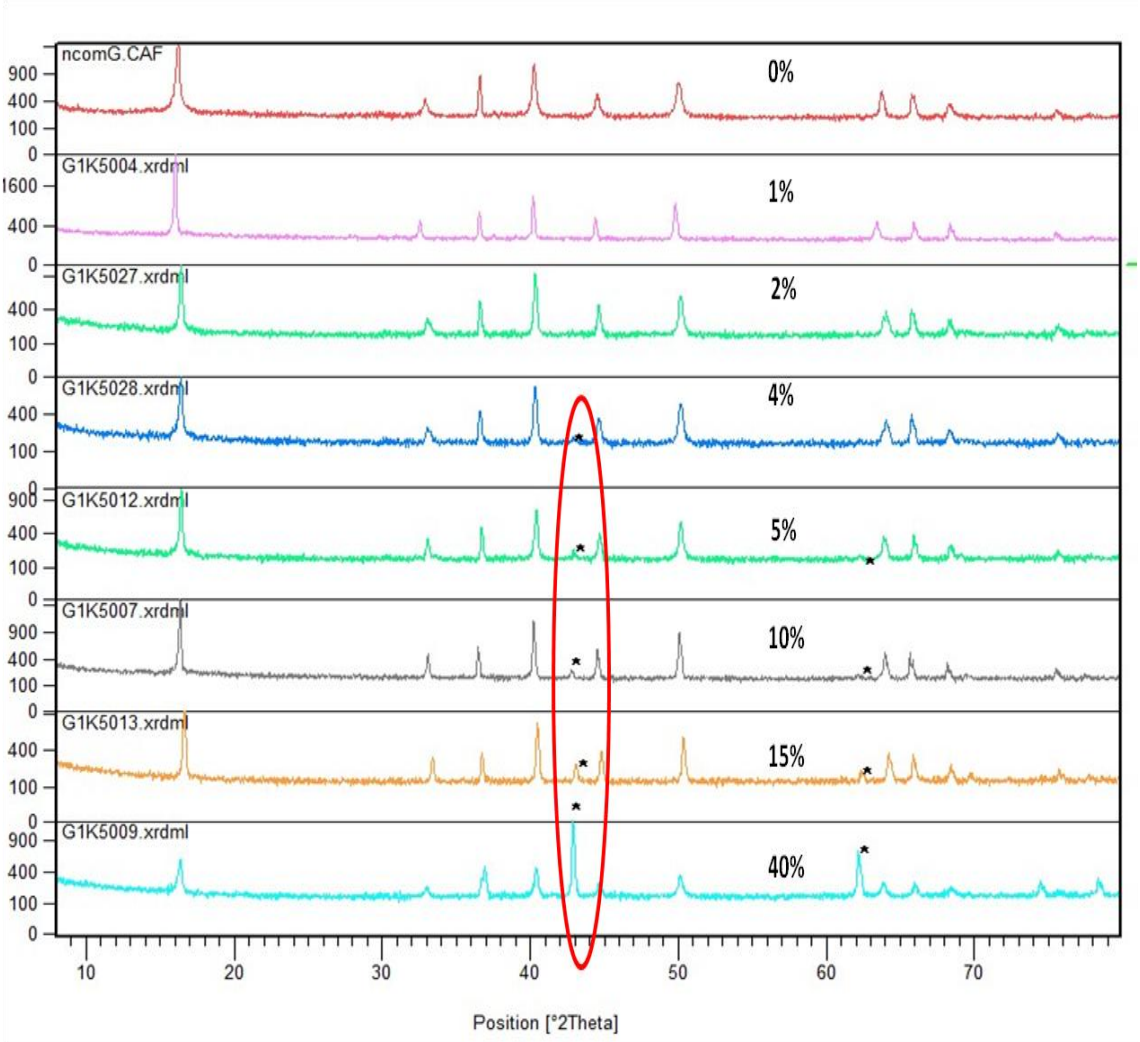

Figure 3.2.1. X-ray diffraction patters of $Na_X(CoMg)O_2$; inset in red mark indicates the MgO impurity.

All the sample show P2 poly type phase with P63/mimic space group. The impurity phase of MgO was observed at 4% of nominal Mg rate and increases further increment in nominal Mg substitution rate. The lattice parameters show increment with increase of Mg content. The lattice parameters obtained from refinement are shown in bellow table 3.2.1.

Mg (%)	a(Å)	c(Å)
0	2.824036	10.814
1	2.82791	10.9622
2	2.83034	10.8163
4	2.8338	10.8147
5	2.8438	10.9557

Table 3.2.1. Lattice parameters of $Na_X(CoMg)O_2$ solid solutions

The ICP measurements show approximate values of Mg content that respect to nominal substitution rate.

3.2.3. Study of magnetic properties

The susceptibility measurements show Curie-Weiss behavior. The variation of susceptibility and the Curie-Weiss fit are shown in bellow figure 3.2.2.
The parameters; Curie-constant (c) and Curie-Weiss temperature (θ) are derived by using $\chi = \chi_0 + C/(T-\theta)$, χ_0-temperature independent term. An excess spin contribution for the samples S2 and S6 is due to impurity (precursor) which cannt be detected from Powder X-ray diffraction.

The increase of Curie-constant was expected due to the fact that the cobalt will go to 4+ oxidation state with divalent Mg substitution in Cobalt 3+ (Low-Spin) state.
The increment of Co^{4+} will increase the conductivity in ab-plane. The impact of assumed low-spin state of Cobalt (s1/2=0.375) was clearly observed from magnetic measurements.

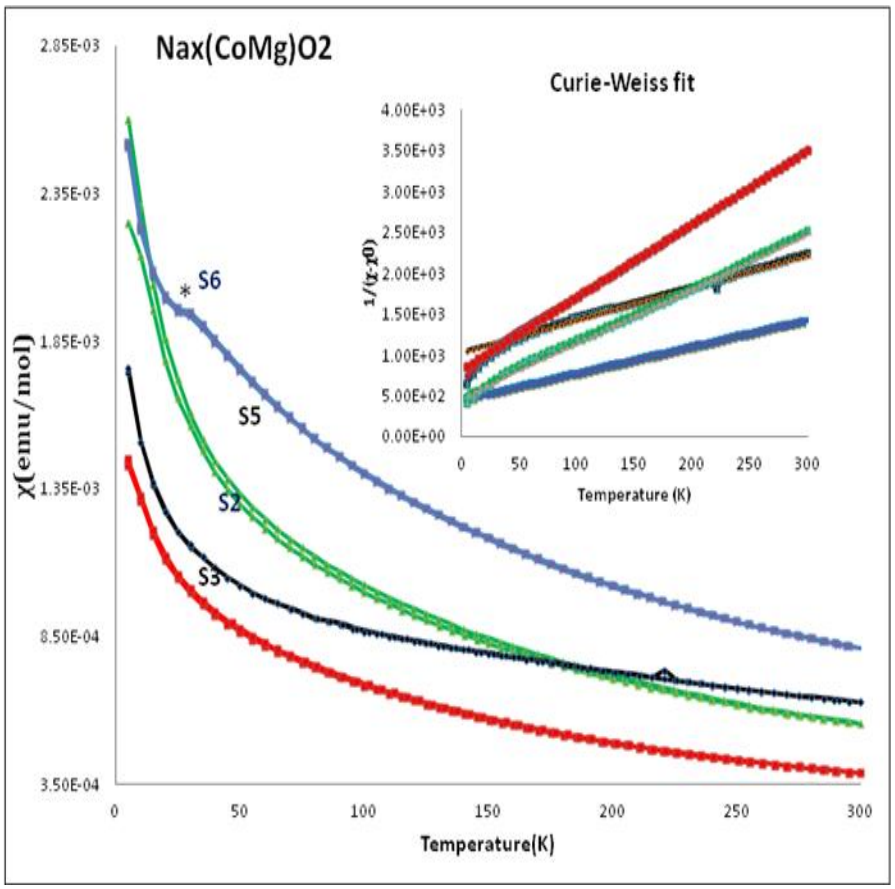

Figure 3.2.2. Susceptibility measurements of $Na_X(CoMg)O_2$; inset, Curie-Weiss fit.

	χ(emu/mol)	Theta (K)	c	spin1/2
S2	1.81E-04	-259.742	0.251496	67.00
S3	1.05E-04	-90.7585	0.111561	30.00
S5	1.59E-04	-73.6418	0.149957	40.00
S6	1.08E-04	-135.769	0.306066	82.00

Table 3.2.2. Derived physical parameters from Curie-Weiss fit of $Na_X(CoMg)O_2$ solid solutions

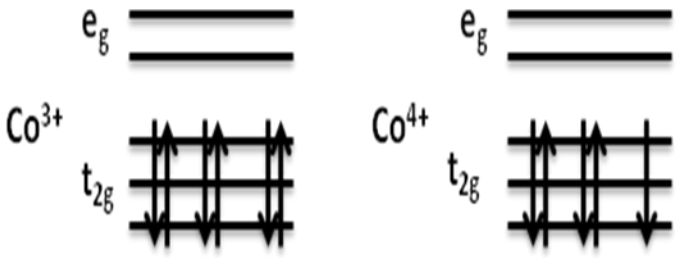

Figure 3.2.3. Cobalt oxidation states in Na_xCoMgO_2 ; 3, 4+ (LS)

3.2.4. Study of transport properties

The temperature dependence DC electrical resistivity measurements are shown in figure 3.2.4.

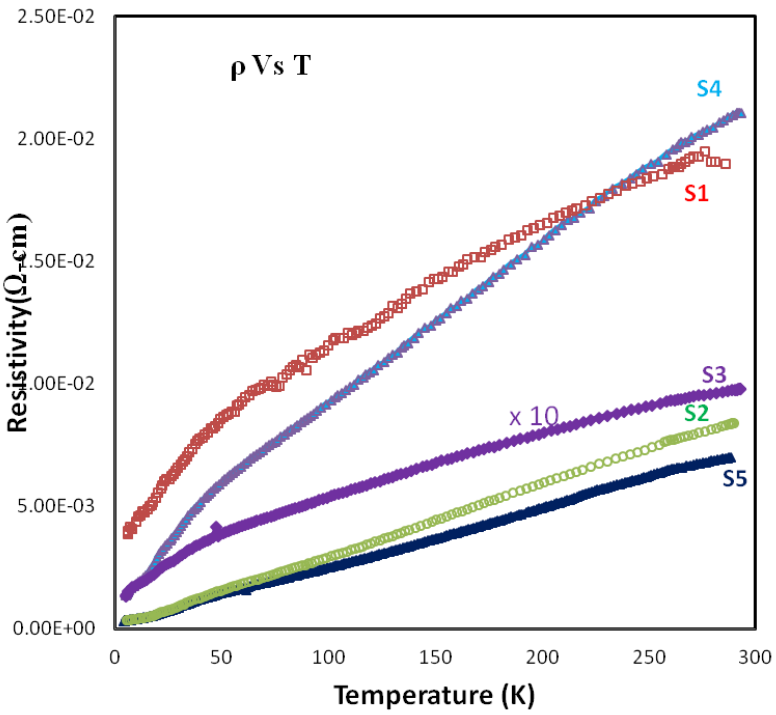

Figure 3.2.4. Resistivity measurements of the Mg substituted Na_xCoO_2 samples

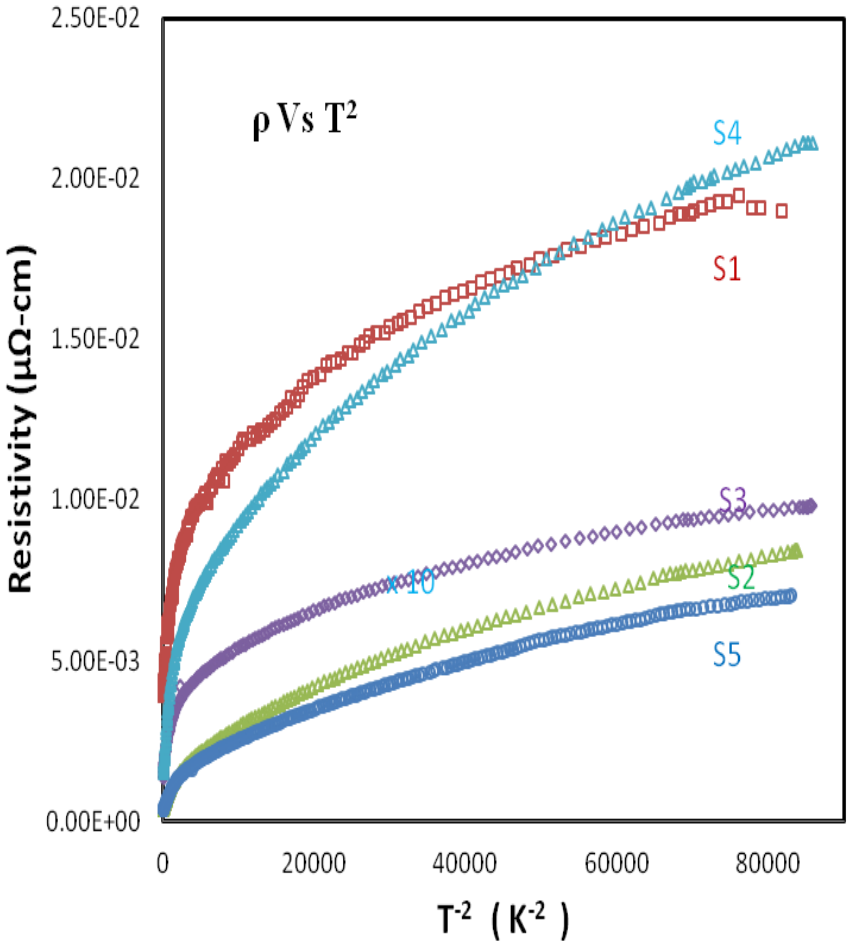

Figure 3.2.5. The fit in T, and T^2 laws of resistivity.

All the samples show metallic behaviour; slope of ρ vs T is positive. The linear variation of resistivity with temperature indicates the strong electron correlations in the material. At lower temperatures bellow to 30K, shows T^2 dependence of resistance which is due to electron-electron scattering at low temperatures.

The temperature independent resistivity ρ0 which dependence on extrinsic parameters and the proportional constant A that represents the characteristic electron interactions, were derived using the linear fits as shown in Figure 3.2.5. The randomness in the values might me due to variation in Na content which alters the Co^{4+} percentage in the structure as well as the impurity (MgO) in S4 and S5 samples. It should be noted that the pellets used were cold pressed; only the trend has to be considered not the values.

	$\rho(T)=\rho 0+AT$	$\rho(T)=\rho 0+AT^2$ (bellow 35K)
S1	$0.007 + 50 \times 10^{-6} \times T$	$0.0042 + 3 \times 10^{-6} \times T^2$
S2	$0.0003 + 30 \times 10^{-6} \times T$	$0.0004 + 0.6 \times 10^{-6} \times T^2$
S3	$0.003 + 20 \times 10^{-6} \times T$	$0.0018 + 1 \times 10^{-6} \times T^2$
S4	$0.003 + 60 \times 10^{-6} \times T$	$0.0017 + 3 \times 10^{-6} \times T^2$
S5	$0.0002 + 20 \times 10^{-6} \times T$	$0.0004 + 0.6 \times 10^{-6} \times T^2$

Table.3.2.4. Derived values from linear and square law fits of resistance with temperature

3.2.5. Study of Seebeck measurements

The variation of thermopower in the temperature region 2K to 300K is show in figure 4 (a). The Seebeck value increases with increasing the temperature. The spin entropy contribution to the thermopower obtained by subtracting the thermo power values of $K_{0.6}CoO_2$ (figure 4(b)). This approximation has revealed in a previous report [36], which results the good correlation between theoretical and experimental values of spin entropy contribution to the thermopower.

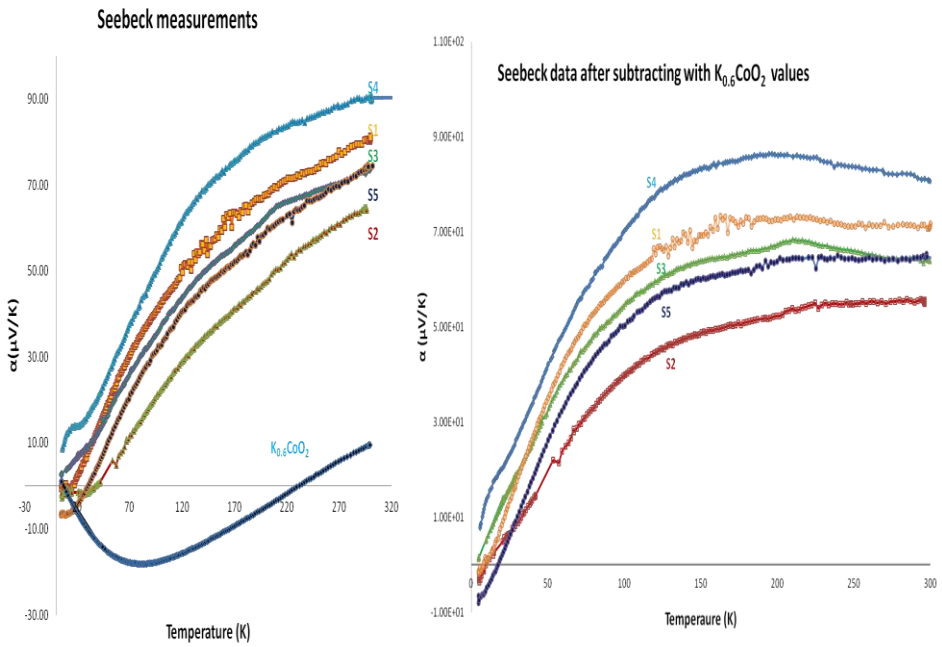

Figure 3.2.6. (a)Seebeck measurements for Mg substituted NCO sample, (b) after subtracting the $K_{0.61}CoO_2$ values

Nominal Mg	ρ(286K) μΩ-cm	α(μV/K)	Curie constant (%Co^{4+})
S1(0)	1.90E+04	79.5	-
S2(1%)	8.34E+03	64.1	0.105 (28)
S3(2%)	9.72E+04	72.6	0.140(37)
S4(4%)	2.09E+04	90.3	-
S5(5%)	6.98E+03	73.8	0.1499(40)

Table 3.2.5. The resistivity and seebeck coefficient values of the samples at 286 K.

According to Heike's formula at high temperature, the spin entropy contribution to the thermopower given as

$$\alpha_{t\to\infty} = -\frac{k_B}{e} \ln\left(\frac{g(Co^{3+})}{g(Co^{4+})}\frac{\rho(Co^{4+})}{1-\rho(Co^{4+})}\right) \qquad 3.2.5$$

Where $g(Co^{3+})$ and $g(Co^{4+})$ represents the degeneracy of Co^{3+} and Co^{4+}, and $\rho(Co^{4+})$ represents the concentration of Co^4. The observed values of seebeck coefficients at high temperature (table 4) are in good agreement with when we consider the deformation of CoO_6 octahedron and the strong correlation effects($e_g^1 - itenerent, and\ a_{1g} - localised$); $g(Co^{4+}) = 2$ and $g(Co^{3+}) = 1$. These approximations results the Co^{4+} contribution in S1, S2, S3, S4, and S5 samples as 0.44, 0.48, 0.46, 0.41, and 0.46. The results much deviates from the magnetic ICP data might be due to several factors like compactness of the pellets as well as the impurity in S4 and S5 samples.

3.3. Conclusions

Till now the layered sodium cobalt oxides which were upcoming materials for thermoelectric applications were synthesised and characterised by solid state as well as rapid-heat up methods. The hydrothermal synthesis for oxide materials is expected to keep the oxygen stoichiometry and to improve the purity of materials as well as the physical properties.

For determination of optimal synthesis conditions of the layered sodium cobalt oxides, we studied all hydrothermal synthesis parameters: temperature, pressure, molaity of the solution, $Co(OH)_2$ concentration, synthesis time.

The literature didn't contain any data for Na_xCoO_2 for the synthesis conditions by hydrothermal method and the first step was to study the system Co-NaOH-H_2O for the temperature region from 150^0C to 250^0C. Stoichiometric quantities of the precursors for $Na_{0.7}CoO_2$ didn't effected the phase of $Co(OH)_2$ until 250^0C and resulting CoO phase for the temperatures 300^0C and 375^0C.

Varying the concentration of $Co(OH)_2$ in accordance with the solubility data gave the formation of different phases with increasing temperature as well as molaity of NaOH solution Increasing the temperature causes formation of different phases at different temperatures with the same ratios of the precursors, effect of temperature studied from 150^0C to 250^0C.

Effect of molaity from 1m to 4m studied for the temperature region from 150^0C to 250^0C. It was observed that the formation of different phases with increasing the molaity.

Effect of synthesis time is expected to change the resultant phases. We observed the effect of synthesis time for 3m of NaOH solution at 180^0C with 24h and 60h of synthesis times.

Thermodynamic parameters for precursors and possible products were calculated and correlated with the experimental phases. Gibbs free energy calculations matched with the experimental results. The required phases Na_xCoO_2 didn't observed for the temperatures region 150^0C to 250^0C, molaity of NaOH from 1m to 4m and the reaction time from 24h to 60h .

Addition of H_2O_2 is studied at 3% and 5% concentrations with 4m of NaOH solutions and changes in the resultant phases were clearly observed. The majority phase of Na_xCoO_2 is obtained at 220^0C,4m of NaOH solution and 5% H_2O_2. [20,21]
To synthesize the layered sodium cobalt oxide β-$Na{\sim}0.6CoO_2$ by hydrothermal synthesis we studied the effect of synthesistime, concentration of $Co(OH)_2$ and the temperature on the resultant phases. As the precursor $Co(OH)_2$ has very less solubility, the final compound obtained is less than 0.2 g. The use of high molaity of NaOH requires cleaning the samples several times to get rid of Na_2O and the other phases of sodium. Hydrogen peroxide is playing an important role as oxidant, the resultant phases by presence and not of hydrogen peroxide were different, and NCO phase is observed only in the presence of hydrogen peroxide. The use of hydrogen peroxide at higher concentrations may destroy the Teflon-liner so we restricted our self at the lower concentration; 5%. Addition of hydrogen peroxide is done by using syringe so that we won't lose much oxygen content during the addition.

The optimal temperature to grow NCO is around 220°C, for the lower and higher temperatures; 180°C and 250°C the resultant phase is Co_3O_4. The phase is identified from the peaks of XRD pattern which were closer to β-$Na{\sim}_{0.6}CoO_2$ we need to do ICP to find the exact composition.

The optimal concentration of $Co(OH)_2$ is found to be around 13 mmol/L, an increase in concentration of $Co(OH)_2$ to 26mmol/L resulting Co_3O_4 , which indicates that the 5% O.A in the system is not sufficient to oxidize the cobalt at higher concentrations than 13 mmol/L.

The synthesis time for obtaining NCO phase using $Co(OH)_2$ is found to be around 60h, a NCO phase is obtained for 60h synthesis time while a result from 24h synthesis time shows CoOOH as minority phases which indicates CoOOH as intermediate phase for the final phase; CoOOH.

The thermal stability of the obtained samples was performed using high temperature XRD chamber and it is found that the obtained NCO is stable until 500^0C in vacuum. After 600^0C the compound is completely decomposed. Unlike solid-state synthesis and other methods we do not have the control over Na content in Na_xCoO_2 by hydrothermal synthesis, as we were using 4 molaity of NaOH solution.

Mg substituted $Na_{0.7}CoO_2$ were successfully obtained using binary oxide as precursor in solid state reactions. It was found that the substitution limit was lower to 4% of Mg. The lattice parameters increase with increasing the Mg substitution rate. The electrical properties show strong correlation, resistivity is varying linearly with temperature above 35K, but bellow it shows T^2 dependence. This approach shows the importance of precursor; no report existed with Mg substitution in $Na_{0.7}CoO_2$. The use of binary oxide makes the possibility of higher substitution rates of divalent ions in solid state reactions

Chapter 4

Synthesis and characterization of layered lithium cobalt oxides

4.1. Synthesis of lithium cobalt oxide by single step soft hydrothermal method

The hydrothermal method for oxide materials shows good stoichiometry, as well as tuneable impurities, one can get rid of by products by optimising the conditions for single phase products. . The subcritical hydrothermal conditions were used to obtain lithium cobalt oxide $LiCoO_2$. The experimental procedure is discussed in 4.1.1.

4.1.1. The experimental procedure

The cobalt hydroxide $Co(OH)_2$ and lithium hydroxide LiOH were used as precursors and NaOH as mineralizer. As the solubility of precursor $Co(OH)_2$ is much lower, we used higher molaity of solution with NaOH and LiOH. The hydrogen peroxide is used as reductant with the concentration of 5%. The solution was prepared with measured amounts of precursors and distilled water. The autoclaves used were Teflon liners with steel covers. The filling percentage kept at 85% with the solution so the pressure expected to be bellow 50 bar. The autoclaves kept in the furnace with 10^0C/Hr as temperature gradient while heating and cooling. The samples were cleaned several times to get rid of by products and the powder is dried at room temperature without any further heating.

4.1.2. Results and discussions

Figure 4.1.1 summarizes the result of varying the NaOH: LiOH mineralizer's ratio in the solution.

Using only LiOH as mineralizer, $LiCoO_2$ crystallizes only from 0.5m as a minority phase in a solution containing mostly Co_3O_4; with the increase of LiOH concentration, $LiCoO_2$ yield increases however with some impurities of CoO for LiOH≤2m; when LiOH≥2m, the only product visible from XRD is $LiCoO_2$. The Inductive Coupled Plasma (ICP) analysis confirmed the close to stoichiometric ratio Li:Co=1:1.

The several steps for the reaction can be written as

$$2\ Co(OH)_2 + H_2O_2 \xrightarrow[LiOH]{220\ deg} 2\ HCoO_2 + 2\ H_2O \qquad 4.1.1$$

$$LiOH \Rightarrow Li^+ + OH^- \qquad 4.1.2$$

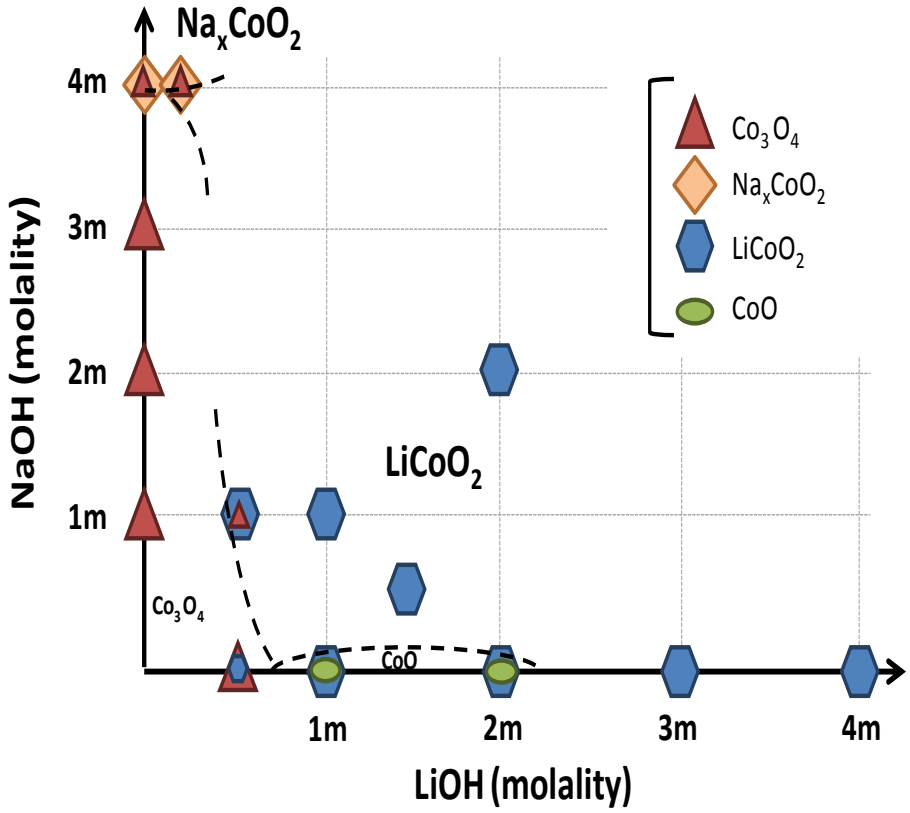

Figure 4.1.1. The effect of ionic mineralizers on resultant phases

$$HCoO_2 + Li^+ + OH^- \Rightarrow LiCoO_2 + H_2O \qquad 4.1.3$$

The total reaction is

$$2\ Co(OH)_2 + 2\ LiOH + H_2O_2 \xrightarrow[5h,15h,24h,60h]{220\ deg} 2\ LiCoO_2 + 4\ H_2O \qquad 4.1.4$$

The role of NaOH is actually multiple: first, just like LiOH, it acts as mineralizer; second, NaOH is slightly more oxidative than LiOH and it might help stabilizing higher valence state of cobalt (CoO traces are disappearing on adding NaOH); third, probably in relationship with point 2, it promotes the crystallization of $LiCoO_2$: the crystallinity of $LiCoO_2$ obtained with 1m LiOH and 1m NaOH is higher than with 4m of LiOH only and the FWHM evolution vs NaOH content clearly evidence a narrowing of the diffraction peaks. It is worth noting that for equimolar

ratios of LiOH and NaOH, only $LiCoO_2$ forms while Na_xCoO_2 could also be expected. Several points can be highlighted that explain this result: i) whatever the conditions used, we were not able to stabilize the stoichiometric compound $NaCoO_2$, meaning that the formed compound always contains a minimum amount of Co^{4+}; as mentioned above, NaOH is more likely to stabilize higher valence state of cobalt however, our phase diagram shows that Co^{4+} might be accessible only for strong excess in NaOH; ii) $HCoO_2$ was shown to be formed at low temperature [ref to the stability diagram of Co-Na-H_2O]; in solution it appears as CoO_2^- which is expected to have a short time life and to fast react with its environment; as lithium has a higher electron affinity than sodium (respectively 0.618eV and 0.548eV), one can expect a faster combination with Li^+ than with Na^+; iii) both compounds are lamellar, however $LiCoO_2$ basically has a more pronounced 3D character (ordered rock salt structure) than Na_xCoO_2 what can favour its growth.

Figure 4.1.2 highlights some typical features in the crystal shapes depending on the mineralizer's concentration and the reaction time. For the lowest concentrations of mineralisers and with 24h of synthesis duration, only desert-rose shape could be observed (Fig. 4.1.2a). Keeping constant the overall mineralizer concentration but increasing the LiOH to NaOH ratio results in the growth of small spherical particles (Fig. 4.1.2b). Further increasing the reaction time leads to the growth of concave cuboctahedrons (Fig. 4.1.2c).

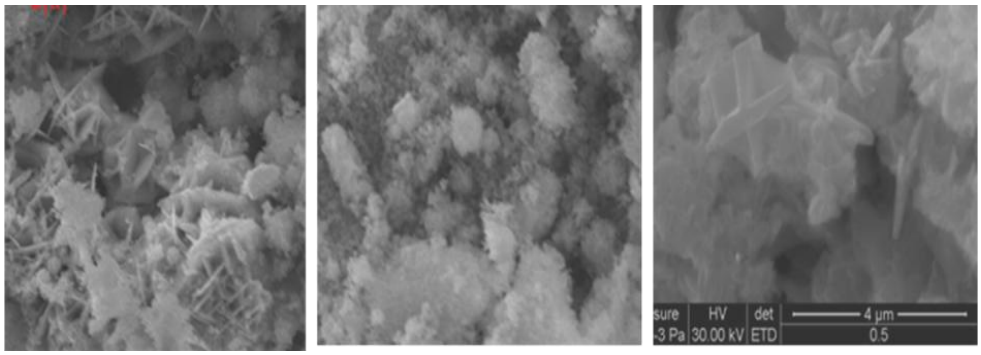

Figure 4.1.2. SEM images of $LiCoO_2$ obtained with (a) LiOH-1m, NaOH-1m, 24h; (b) LiOH-1.5m, NaOH-0.5m, 24h; (c) LiOH-1.5m, NaOH-0.5m, 48h.

The only available report on synthesis of concave cuboctohedrons mentions the use of nanosize precursors and CoO seeds as well as high concentrations of ionic mineralizing agents. Here, we were able to grow such cuboctohedrons only using standard micro size $Co(OH)_2$, precursor and without CoO seed; furthermore we were not able to detect any presence of this latter at the centre of the particles. This suggests show that an alternative mechanism for the growth of these particles should be considered.

In order to analyze the influence of the concentration of $Co(OH)_2$ on the formation of $LiCoO_2$ and to optimize it, the temperature (220 °C), the reaction time (24 h) and the ratio between NaOH: LiOH (2m: 2m) were kept constant while the concentration of $Co(OH)_2$ was varied from 13 mmol/l to 130 mmol/l. The results are shown in figure 4.1.3.

At 130 mmol/l only $Co(OH)_2$ could be identified from XRD. On decreasing the concentration, $LiCoO_2$ slowly appears at *ca.* 65 mmol/l however with CoO impurities. Only when the initial concentration is lower or equal to 50 mmol/l a pure $LiCoO_2$ compound can be obtained.

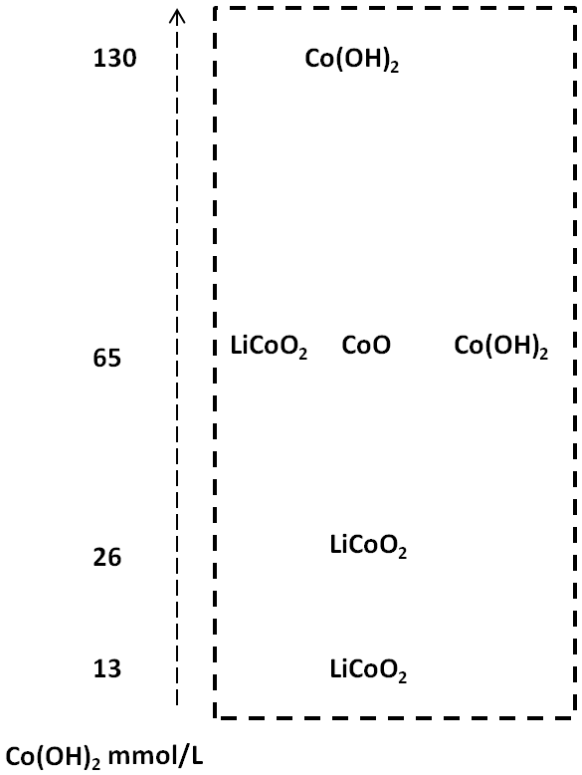

Figure 4.1.3. Dissolution and oxidation of $Co(OH)_2$ at different concentrations. Operating conditions: LiOH-2m, NaOH-2m, 5% H_2O_2, 85% filled autoclave, T=220 °C, t=24 h

These results suggest that i) the solubility limit of $Co(OH)_2$ is close to 50 mmol/l and that, as compared to $Co(OH)_2$ ii) the seeding of $LiCoO_2$ is energetically favoured iii) while its growth is energetically unfavoured. Indeed as the $Co(OH)_2$ concentration increases some undissolved traces remain and serve as seeds for the re-crystallization; conversely, for low initial precursor concentration, as the seeding of $LiCoO_2$ compound is much favoured, no trace of $Co(OH)_2$ is visible in the final product.

The X-ray diffraction pattern for the product resulting from the synthesis with 26 mmol/l concentration in $Co(OH)_2$ is shown in Figure 4.1.4. The refinement with R-3m space group leads to lattice parameters a=b=2.81547 Å and c= 14.0635 Å which are in good agreement with **previous reports.** Some SEM micrographs for the samples synthesized from $[Co(OH)_2]$=13 mmol/l and equimolar LiOH and NaOH mineralizers amount (2m) are shown in Fig. 4.1.5 for several reaction time. Particles size is regularly increasing with the reaction time however their shape is evolving throughout the process. For low reaction time (15 h) only desert-rose shape particles are obtained.

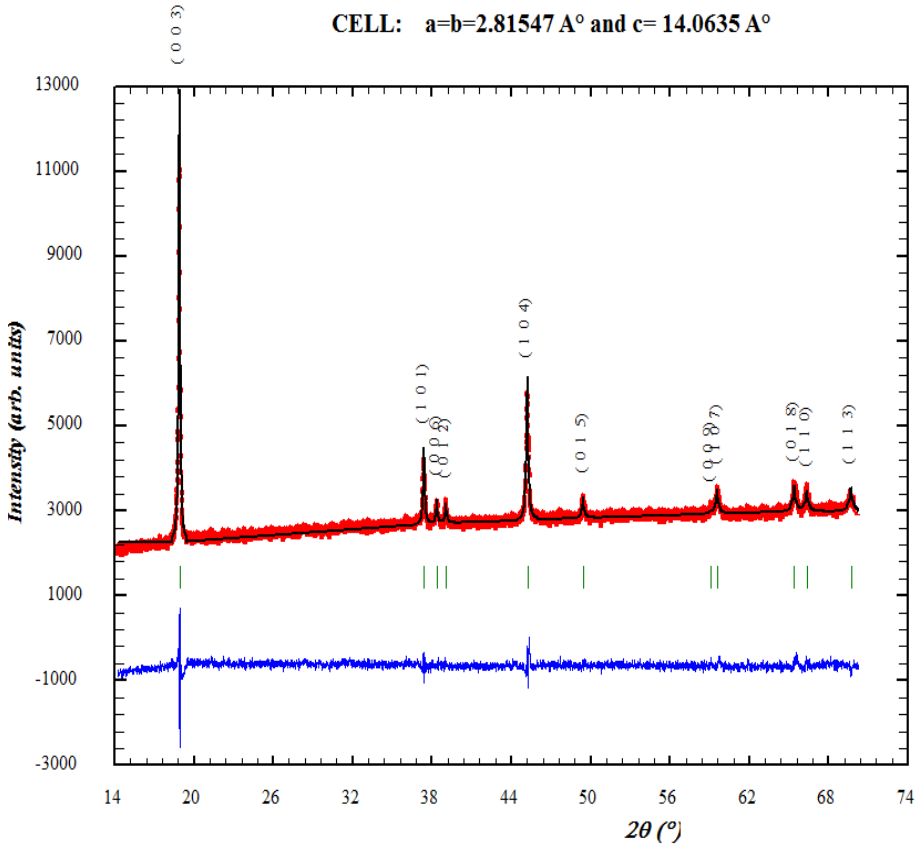

Figure 4.1.4. The XRD pattern of $LiCoO_2$.

With 24 h reaction time a mixture of concave cuboctohedrons and small spheroidal particles are present. With 48 and 60 h reaction time mainly concave cuboctohedrons are visible with few spheroidal particles. With 80 h reaction time the concave cuboctohedron shape looks fully destroyed and mostly classical hexagonal platelets like particles are obtained.

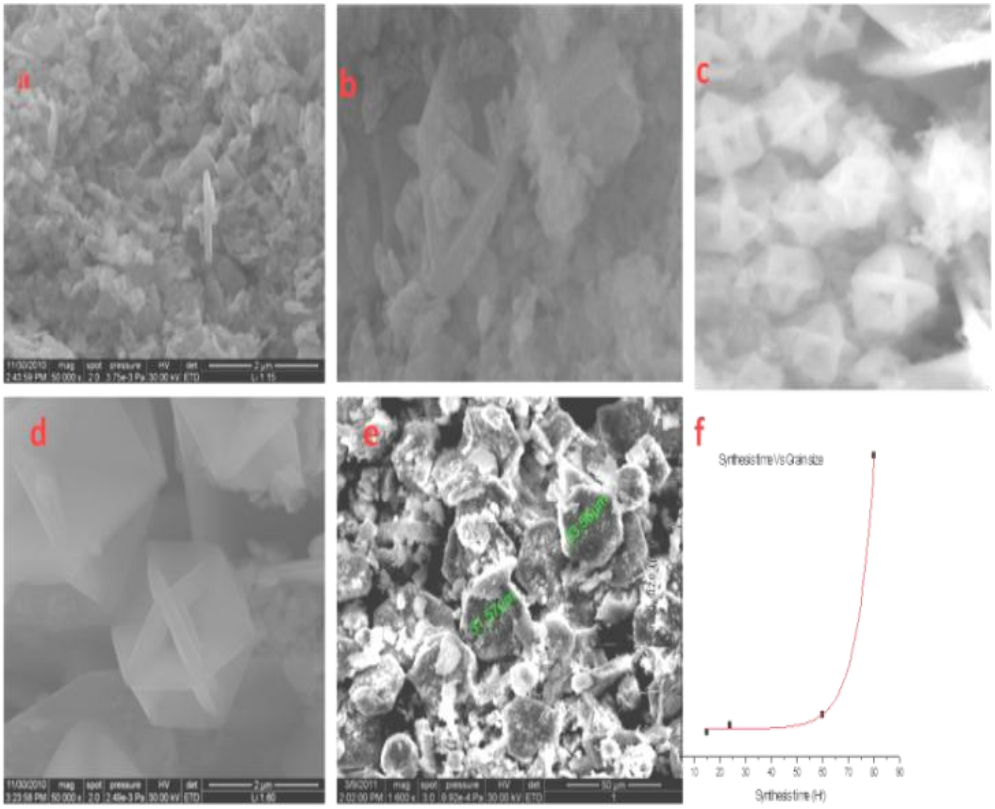

Figure 4.1.5 . SEM images of the samples synthesized with (a)-15h, (b)-24h, (c)-48h, (d)-60h, (e)-80h reaction times, and (f) - growth of particle size with synthesis duration. Synthesis conditions: $Co(OH)_2$- 13 mml/L, LiOH-2m, NaOH-2m, H_2O_2-5% and fill% of autoclave -85%

.

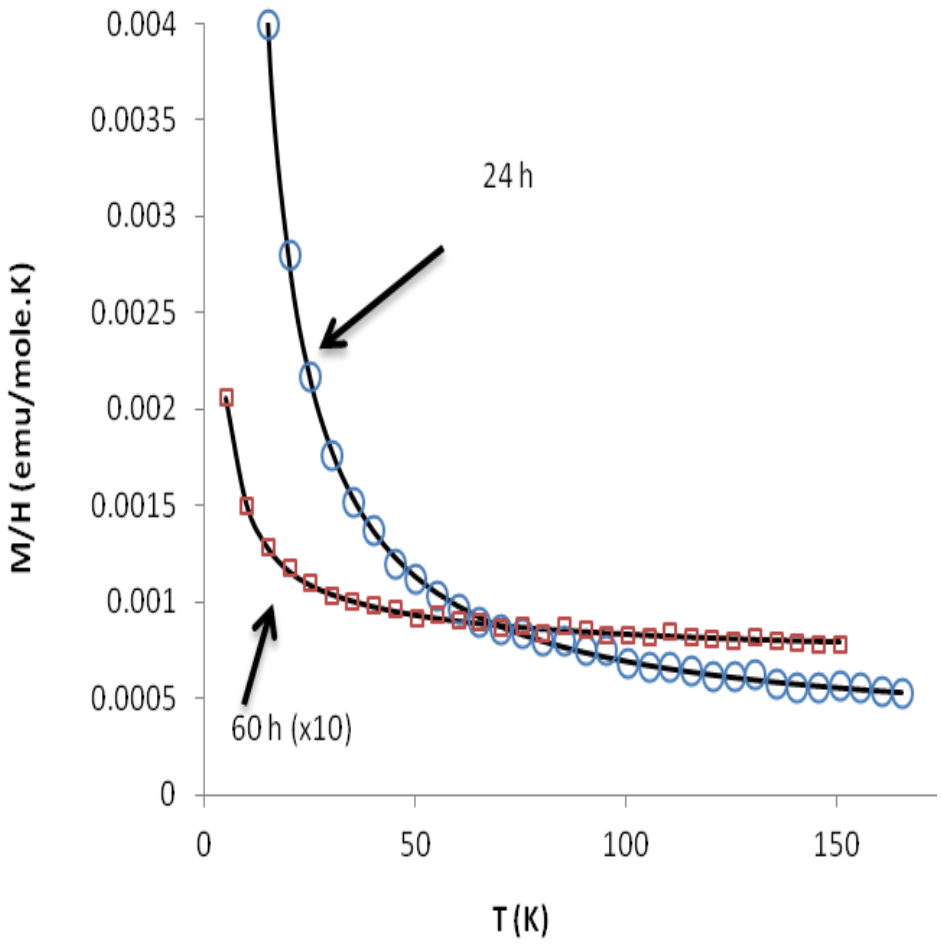

Figure 4.1.6. Magnetization of the samples prepared with 24 (circle) and 60 h synthesis time (square) measured using H=100 Oe (the signal for the 60 h synthesis time sample is multiplied per 10); black lines are the fit to the data.

Magnetization data *vs.* temperature are shown in Fig.4.1.6 for samples prepared using 24 and 60 h reaction time. They evidence a marked decrease in the signal when the synthesis time increases. Pure $LiCoO_2$ compound is only expected to contribute a temperature independent second order Zeeman component while the temperature dependant part of the magnetization is expected to arise from secondary phases and structural defects or impurities. Both data sets could be fitted using the raw data for pure Co_3O_4 and CoO compounds, a temperature independent second order Zeeman contribution and an additional Curie component

$$(\tilde{M}/H)_{total} = (\tilde{M}/H)_{Co_3O_4} + (\tilde{M}/H)_{CoO} + \chi_0 + {}^{C}/_{T}. \qquad 4.1.5$$

In both cases $\chi_0 \approx 65 \times 10^{-6}$. With 24 h reaction time, the total secondary phase amount is about 4% and it is less than 0.1% after 60 h reaction time. Similarly, C decreases from 0.036 to 0.0009 with reaction time. Assuming the last term of the model function to originate in defects in $LiCoO_2$, such a high difference in the Curie constant can be related to the size and shape of the particles (Fig. 4.1.5): for 24 h reaction time the particles size is much lower (and their number much higher) and a large number of surface defects can be expected resulting in a high Curie constant; conversely, with 60 h reaction time mainly nicely shaped and big concave cuboctohedrons are obtained and the defects amount should be largely reduced supporting the low calculated Curie constant.

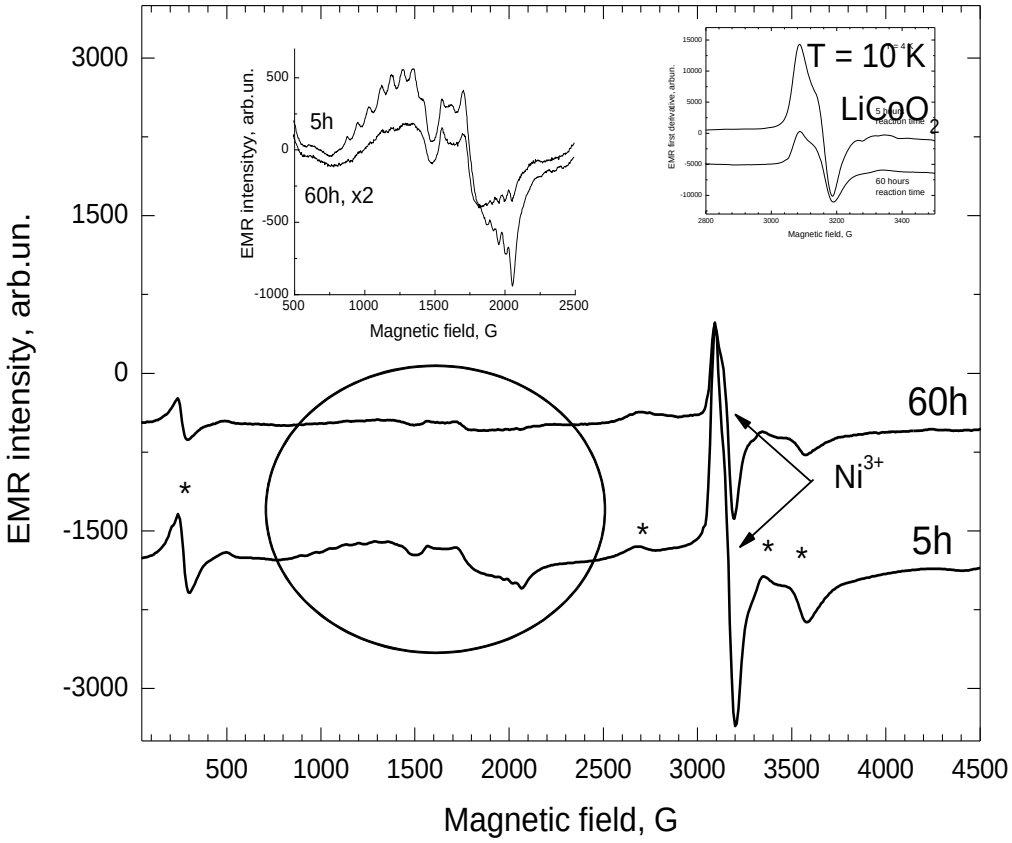

Figure 4.1.7. EMR spectra observed at T = 10 K for $LiCoO_2$ samples with 5 h and 60 h synthesis durations. Resonances originating from the Co_3O_4 are marked with asterisks. Left inset: zoom in the region 500-2500 G highlighting resonances ascribed to the cobalt ions in distorted octahedral site of $LiCoO_2$ (spectra are shifted for readability and the intensity of the spectrum of the 60 h reaction time sample is multiplied per 2). Right inset: zoom in the region 2800-3500 G highlighting resonances from unavoidable Ni^{3+} impurity (g = 2.14) and from Li^+-O^- center (g=2.16)

EMR studies were performed for the samples prepared with 5, 24 and 60h synthesis durations. Data were collected in a wide temperature range (4-300 K) in order to study the stability of the charged defects, intrinsic and/or impurity. The detailed analysis of EMR spectra is out of scope of this article and we just present here some results supporting the observations made with macroscopic magnetic measurements. Fig.8 shows the plots for EMR spectra recorded at 10 K for the samples prepared with 5 and 60h synthesis durations. It is worth noting, as observed from magnetic measurements, that the intensity of the signal sharply decreases when the reaction time increases. A part of the spectra is similar to the spectra observed with $LiCoO_2$ powder prepared by conventional solid state chemistry [22]. This allows identifying for all the samples resonances arising from Co_3O_4, from unavoidable Ni^{3+} impurity and from Li^+-O^- surface centres. As compared to previous work additional resonances are visible in the magnetic field region 800-2400 G up to *ca.* 80 K. The existence of 8 hyperfine lines in this spectrum allows identifying it unambiguously as originating from cobalt ion (^{59}Co) which has 100% natural abundance nuclear spin I = 7/2. Several Co-related defects can however give such resonances. High symmetry Co^{4+} ($3d^5$; S=1/2 or S=5/2) related center due for instance to some cation deficiency in the structure have to be discarded: the g-factor value should be close to the free electron one (g=2.0023) and the spin-lattice relaxation time is large enough to make it visible at room temperature. Similarly the presence of Co^{2+} ($3d^7$ ion with S=1/2 LS or S=3/2 HS configuration) to compensate for some oxygen-related defects should be discarded: these defects are strongly influencing the crystal field strength and symmetry and lead to the formation of defects with axial symmetry (Co^{2+} -V(O) or/and Co^{2+} - $V(O)^-$); such defects were already observed for cobalt ions in the vicinity of the surface of $LiCoO_2$ samples prepared by solid state chemistry [2] and their hallmark (S, g, A) is not matching with present results.

The three visible resonances are characterized with g_1 = 5.712(2), $10^4|A_1|$ = 70(4) cm^{-1}, g_2 = 4.105(2) and $10^4|A_2|$ = 22(2) cm^{-1}, g_3 = 3.518(2) and $10^4|A_3|$ = 45(2) cm^{-1}. For all the reasons listed above, the only possible defect matching both with the crystal symmetry and such parameters has to have an effective spin S_{eff}=1 and has to sit in a slightly distorted octahedral environment. The three resonances are then due to two allowed by spin transitions with Δm_s=1 and one forbidden transition with Δm_s=2. Such effective spin could arise from an intermediate spin Co^{3+}, or as revealed in the case of $LaCoO_3$ (and consistently with $LiCoO_2$ structure) from a low-lying triplet subterm of the $^5T_{2g}$ manifold in the trigonally distorted environment [28,29]. The decrease in the amount of such centres with increasing reaction time from 5 h to 60 h as well as their fast decay with temperature suggest that they are located close to the surface of $LiCoO_2$ particles (just like Li^+-O^- centres) which is decreasing as the shape evolves from desert-rose to cuboctahedrons (Fig.4.1.5).

4.2. Conclusions

Layered lithium cobalt double oxide was synthesized by soft hydrothermal synthesis method at 220^0C using $Co(OH)_2$ and LiOH as precursors, LiOH/NaOH as mineralizers and $5\%H_2O_2$ as oxidant. The effect of ionic mineralizers and the concentration of precursor were studied to optimize the synthesis conditions of $LiCoO_2$: i) for low mineralizers concentration, only cobalt oxides form; ii) as the concentration increases, pure $LiCoO_2$ grows; iii) the crystallinity of the compound increases as the ratio NaOH/LiOH increases; iv) the $Co(OH)_2$ concentration threshold is *ca.* 50 mmol/l; bellow this limit a single phase $LiCoO_2$ grows and above, $Co(OH)_2$ re-crystallizes

The layered lithium cobalt oxide $LiCoO_2$ is synthesized by hydrothermal method using LiOH and $Co(OH)_2$ as precursors and hydrogen peroxide as oxidant agent. The effect of various dominant parameters; concentration of $Co(OH)_2$, molaity of LiOH and NaOH and the synthesis time is studied.It is observed that increasing the concentration of $Co(OH)_2$ to 65 mmol/L results impurity phases of precursor and CoO phase. For 130 mmol/L of concentration only the precursor itself remains. The pure phases of $LiCoO_2$ were observed for 13mmol/L as well as 26-mmol/L. We did not continue to find out the exact optimal concentration of precursor to get pure phase of $LiCoO_2$.
The synthesis time plays an important role on the grain size of the $LiCoO_2$ particles. We studied the effect of synthesis time on the grain size with various synthesis times; 5h, 15h, 24h, 60h and 80h while keeping the rest of the parameters same. For the 60h of synthesis time we obtained the shape of concaved cuboctahedrons. For the 80h of synthesis time the shape of the particle changed to hexagonal shaped plates.

It can be interesting to lower the synthesis time to evidence an intermediate phase of CoOOH.

It is observed that either using 4m of LiOH solution or taking 2m of LiOH and 2m of NaOH resulting the pure phases for 13 and 26 mmol/L concentrations of $Co(OH)_2$. The pure phase of $LiCoO_2$ is obtained even for 5h synthesis time. The synthesis time is lower in comparison with NCO, it may be from the difference in the reactance of Li and Na ions. The magnetic measurements shows impurity for the samples synthesised with lower synthesis times, while the samples obtained for 60h synthesis duration shown magnetic impurity free phase of $LiCoO_2$

. In the reaction time window 24-60 h we were able to stabilize CoO free concave cuboctahedrons particles suggesting that an alternative mechanism for the growth of these particles should be considered. Magnetic measurements (local and macroscopic) highlight the presence of cobalt oxides impurities which amount is decreasing (and nearly vanishes) with reaction time; they also reveal, as already observed, the presence of several kind of close to surface centres.

Chapter 5

High level Mg substitution in $ACoO_2$ (A-Pt and Pd) single crystals
An alternate approach for divalent substitutions in ABO_2 compounds

As discussed in chapter 2.7 and 2.8, Thermopower in $PtCoO_2$ can be enhanced either by increasing the spin entropy or by increasing the thermal resistivity in c-axis direction; substitution of divalent element at Co-site. In this regard, magnesium can be a suitable element due to its ionic radii Mg^{2+} (0.72Å) which is close to Co^{3+}(LS-0.53Å). The substitutions using metathetical reactions are a difficult task in traditional chemical approach; usage of individual precursors for the each cation. The usage of carbonate or the nitrate precursors ($MgCO_3$ or $Mg(NO_3)_2$ will destroy the vacuum and results no metathetical reactions, while the chloride precursor ($MgCl_2$) can be useful for the lower level substitutions. This problem can be solved by taking the solid solutions of B-cationic substitute and substitutions as the precursor. We used solid solution of substitute and substitution elements (binary oxide (CoMg)O) as the precursor and succeeded to higher level Mg substitution.

$$Co_3O_4 + MgO \rightarrow CoMgO, \qquad 5.1.1$$

The complete solid solution of CoO-MgO is available.

5.1. Synthesis and characterization of $Pt(CoMg)O_2$ crystals

5.1.1. Experimental conditions

The $Pt(CoMg)O_2$ crystals were grown in metathetical reactions using $PtCl_2$, and $Co_{1-x}Mg_xO$ were the precursors. The stoichiometric amounts of the precursors were well grinded and the mixture was vacuum sealed in a quartz tube and then heat treatment was carried out at 700^0C for 40h with heating rate of 1.5^0C/min and the cooling rate at 1^0C/min. The expected reaction is

$$PtCl_2 + 2\ Co_{1-x}Mg_xO \rightarrow PtCo_{1-x}Mg_xO_2 + (1-x)\ CoCl_2 + x\ MgCl_2 \qquad 5.1.2$$

Figure 5.1.1. Photo graph of the vacuum sealed quartz tube after the thermal treatment

X-ray diffraction (XRD) patterns were recorded using PANalytical X'Pert Pro powder diffractometer using Cu-Kα radiation, and the data were collected using X'Celerator detector and analyzed with FULLPROF program. The morphology of the crystals was studied by using a Scanning Electron Microscopy (SEM) Hitachi S-4500 field emission microscope, EPMA (Electron Probe Micro Analysis) was performed for the elemental analysis using microprobe analyzer CAMECA X100, and temperature depended susceptibility, Zero Field Cooled (ZFC) and Field Cooled (FC) DC-magnetization data were recorded using Superconducting Quantum Interface Device (SQUID) magnetometer at an applied field of 10 kOe in the temperature region from 5K to 300K.

5.1.2. Results and discussions

5.1.2.1. Structural and morphological properties of $Pt(CoMg)O_2$ crystals

The synthesized $Pt(CoMg)O_2$ crystals shows plate like shaped with surface along c-axis orientation. The resultant product in general was about 50% of the nominal amount aimed. The profile matching with FULL PROOF program (Figure 5.1.2)

represents that the crystals obtained were with 3R polytype (R-3m). The lattice parameters show an increment with respect to the Mg substitution rate due to higher radius of Mg^{2+} compared to Co^{3+}. Figure 5.1.4 shows the variation of lattice parameters with Mg substitution rate. A slight variation from linearity of the lattice parameters with Mg substitution rate might be due to the fact that platinum cobalt oxide can exists several range of stoichiometry, particularly in metathetical reactions which was revealed by R.D.Shannon et al, which can cause irregularity in the Pt content in the obtained crystals. As the nominal Mg rate increases the reaction won't results single phase product, when the nominal Mg rate exceeds 20%, Mg_2PtO_4 spinal appears as the secondary phase. The limit of Mg substitution rate might be coming from the slightly larger radius of Mg^{2+} (0.72Å) while the Co^{3+} (LS in octahedral site) is 0.54Å.

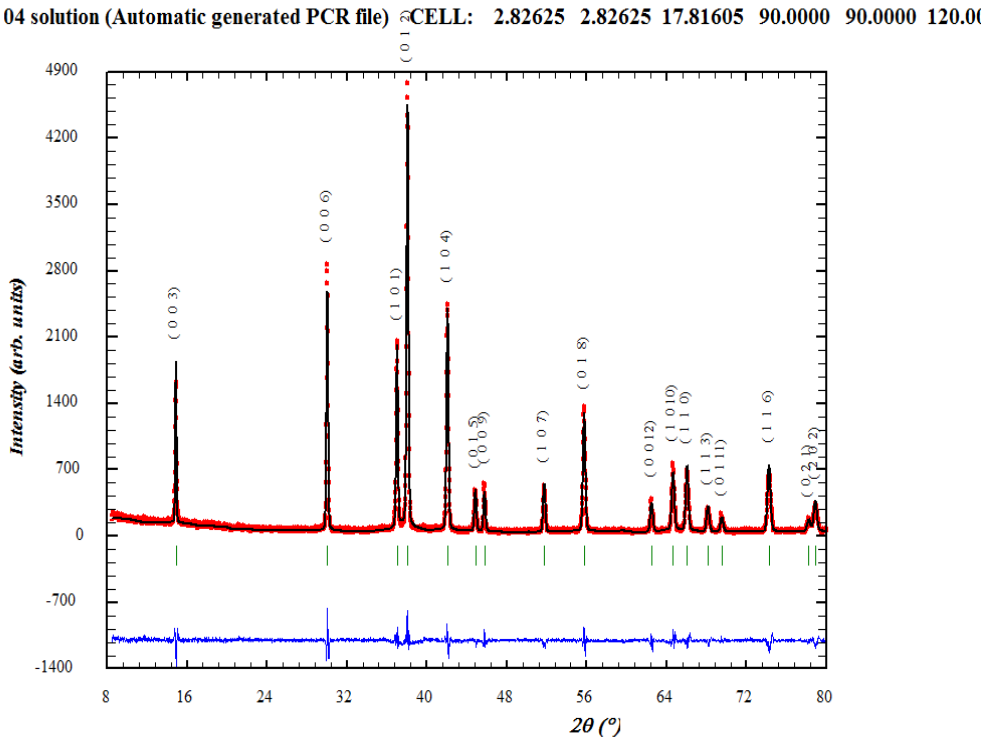

Figure 5.1.2 (a)

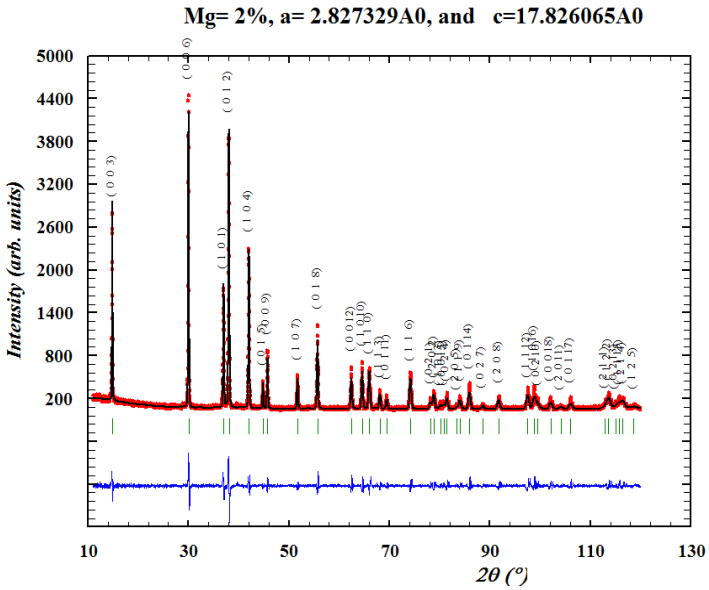

Figure 5.1.2 (b)

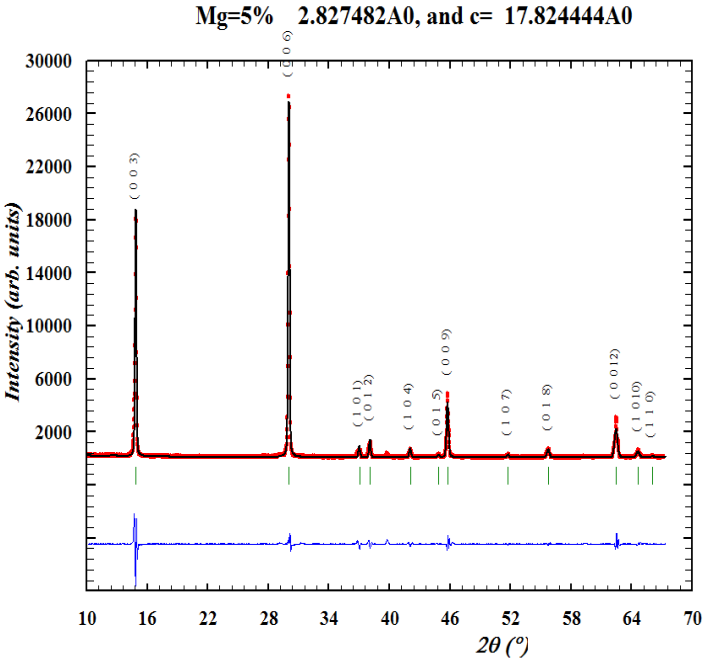

Figure 5.1.2 (c)

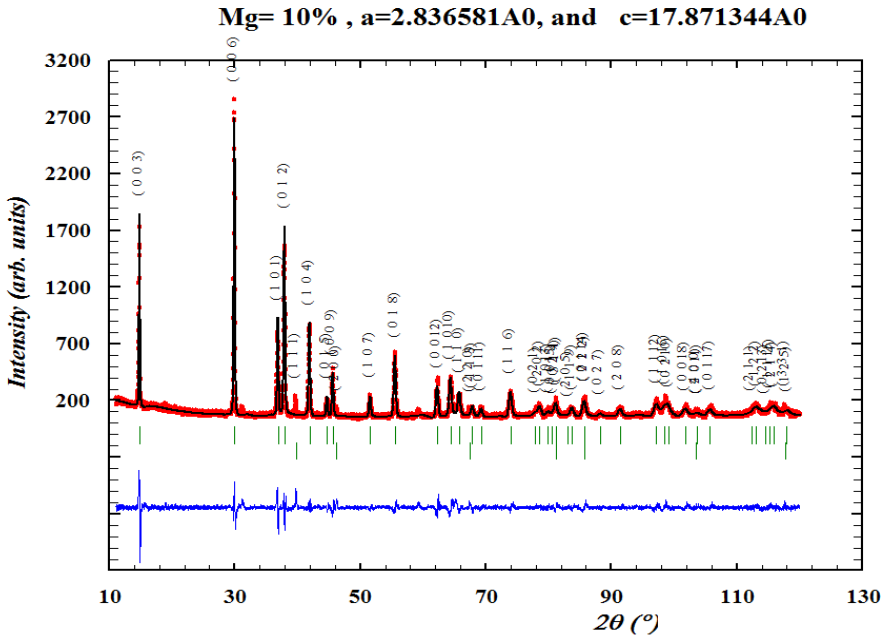

Figure 5.1.2 (d)

Figure 5.1.2. X-ray diffraction patterns of $PtCo_{1-x}Mg_xO_2$ crystals a, b, c and represents 0, 2, 5 and 10% of nominal Mg substitution rate.

Fig.5.1.3, the SEM images of non-substituted and Mg substituted $PtCoO_2$, shows crystals were with hexagonal plate shaped, has the dimensions of 70μm*40μm, 150μm*150μm, 300μm*150μm and 100μm*40μm respectively for the 0% (Fig 2a), 2%(Fig.2b), 5% (Fig.2c) and 10% (Fig.2d) of nominal Mg substitutions rates.

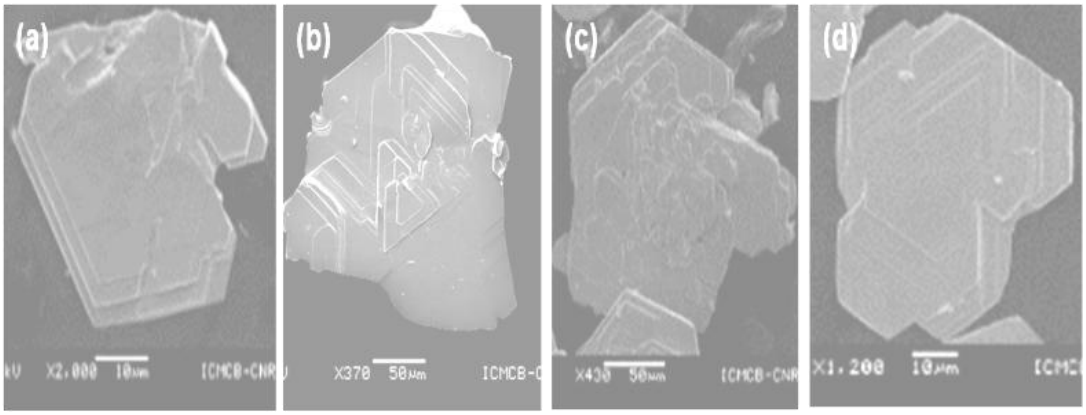

Fig.5.1.3. SEM images of $Pt(CoMg)O_2$ crystals; Mg =0 (a) ,2(b), 5(c) and 10% (d) of nominal rates

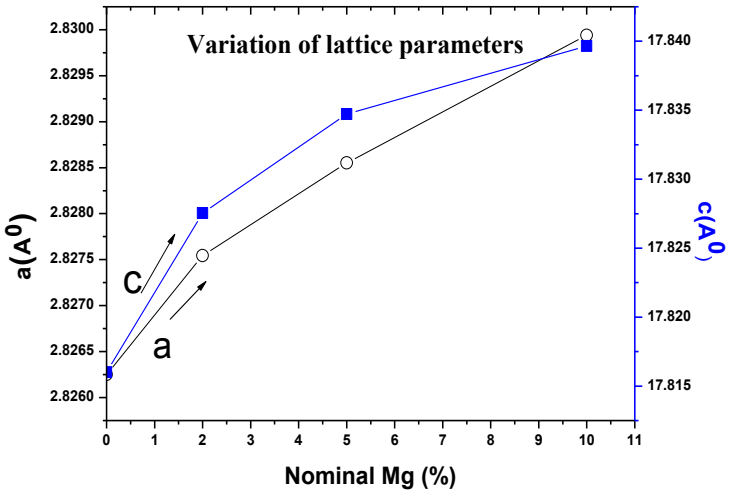

Figure 5.1.4. Variation of lattice parameters with nominal Mg substitution rate in $PtCoO_2$

The chemical composition analysis using EMPA shows non-stoichiometry (Pt/(Co+Mg) ≠1) in all the compounds. The Mg content for 2% of nominal Mg shows just 1% in EPMA analysis; it might be due to the lower values to detect exactly. But for 5% substitution, the results were close to the expected value, and for 10% (starting) show 7.5% Mg content.

EPMA analysis: The EMPA analysis of the $PtCoMgO_2$ crystals is shown in table 1.

Nominal Mg(%)	Pt(At%)	Co (At%)	Mg(At%)	Pt:CoMg	Co:CoMg	Mg:CoMg
0	21.2375	22.9982	-	0.923442: 1	-	-
2	22.5038	21.8172	0.2247	1.020956: 1	0.989806: 1	0.010194
5	22.8166	20.8012	1.1819	1.037915: 1	0.946236:1	0.053764
10	26.4461	22.6259	1.883	1.079041:1	0.923171	0.076829

Table 5.1.1. EPMA analysis of the $PtCoMgO_2$ crystals

5.1.2.2. Magnetic measurements

The temperature dependence of susceptibilities of the $Pt(CoMg)O_2$ crystals at an applied field of 10 kOe in the temperature region from 5 K to 300 K are shown in Figure 4. The inverse susceptibility (insert fig 3) shows liner variation with temperature. The physical parameters; Curie-constant (c), temperature independent susceptibility (χ_0), and Curie temperature (θ) were derived by fitting into the equation

$$\chi_{total} = \chi_{0(dia)} + c / (T-\theta) \qquad 5.1.3$$

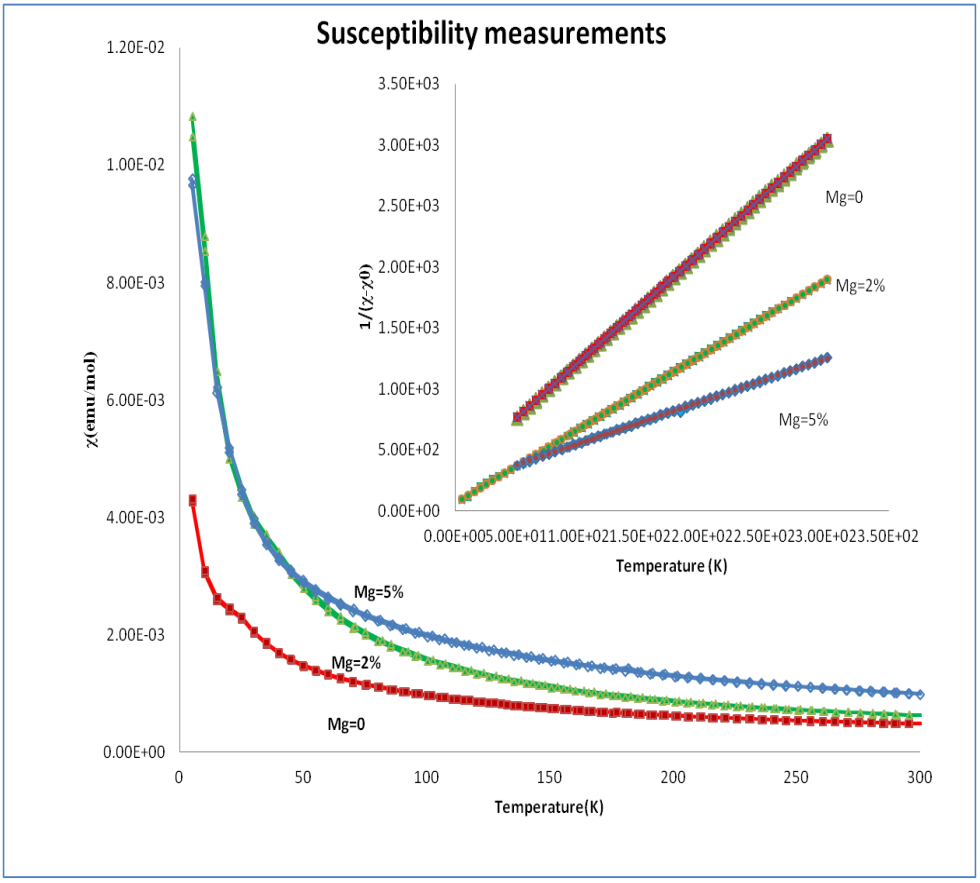

Figure 5.1.5. The susceptibility measurements for $Pt(CoMg)O_2$ crystals

	χ0 (emu/mol)	*C (free spns%)*	*Θ(K)*
0	*0.000158*	*0.10927 (29%)*	*-26.5814*
2%	*0.000103*	*0.167219 (45%)*	*-10.572*
5%	*0.000198*	*0.285857 (76%)*	*-58.4203*

Table 5.1.2. Derived values from Curie-Weiss fit for the $Pt(CoMg)O_2$ crystals

The Curie constant for non-substituted $PtCoO_2$ shows the value of 0.109 (s ½ = 29%), which represents non stoichiometry in $PtCoO_2$. The contribution of (CoMg)O was ignored as there were no traces of it either from X-ray diffraction patterns, SEM images or from the magnetic measurements, where the Anti-Ferromagnetic transition has to be observed bellow 300 K [19]. The possibility of $PtCo_2O_4$ wasn't considered, according to which the materials should have much higher values of Curie constant in accordance with fig 5b, and also an unmatched EPMA results.

The only possible contributions are either merely from Pt^{2+} or from the combination of Pt^{2+} and Co^{4+}. If we consider that the entire contribution is coming from Co^{4+} (LS), according to the observed value of Curie constant, the material should have 29% deficiency in Pt-layer (0.29066*0.375 (Co^{4+}LS) =0.109) which cannot be possible in delafossite compounds and didn't obey the observed values from EPMA analysis. While the consideration of merely contribution from Pt^{2+} shows an approximate values (0.027*3.90625= 2.8% of Pt^{2+}) they were observed from our susceptibility measurements (table 2). Bellow figure 5a represents the variation of Curie constant with respect to deficient in $Pt_{1-x}CoO_2$ by assuming that the overall contribution is coming from only Pt^{2+} ($5d^8$; c =125/32).

These results suggest that the excess contribution to Curie-constant originates from the fractional alteration of Pt^{1+} to Pt^{2+}. The privileged stable ionized state of Pt; Pt^{2+}, and the lower ionization energy of Pt (from $Pt^{1+} \rightarrow Pt^{2+}$) compared to Cobalt ($Co^{3+} \rightarrow Co^{4+}$) might be the reason for establishment of hole in Pt-layer favorable than that of CoO_2 layer. The EPMA as well as the magnetic measurements supports the cationic deficiency in $PtCoO_2$ crystals; the chemical composition of non-substituted compound was established as $Pt^{1+}_{0.948}$ $Pt^{2+}_{0.026}$ $Co^{3+}O^{2-}_2$. The crystals that were obtained using 2% and 5% of nominal Mg substitution rates shows the curie constants values of 0.167 and 0.2858 respectively. The contributions to the Curie constant are from the combination of Pt^{2+} and Co^{4+} (figure 5.1.7).

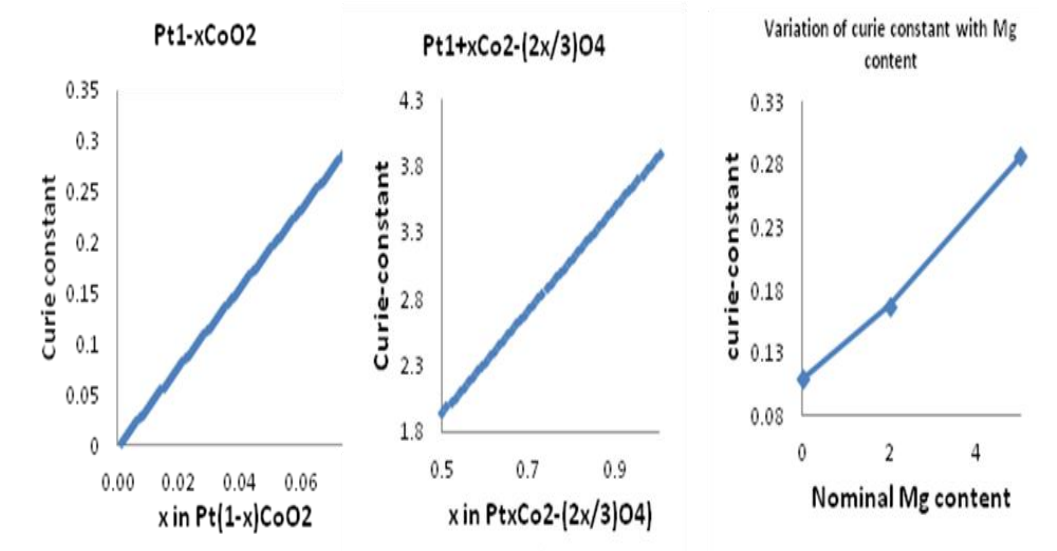

Figure 5.1.6. a, b, and c represents variation of Curie constant in Pt_xCoO_2, $Pt_{1+x}Co_{2-(2x/3)}O_4$, and the experimental results corresponds to Fig 5.1.5

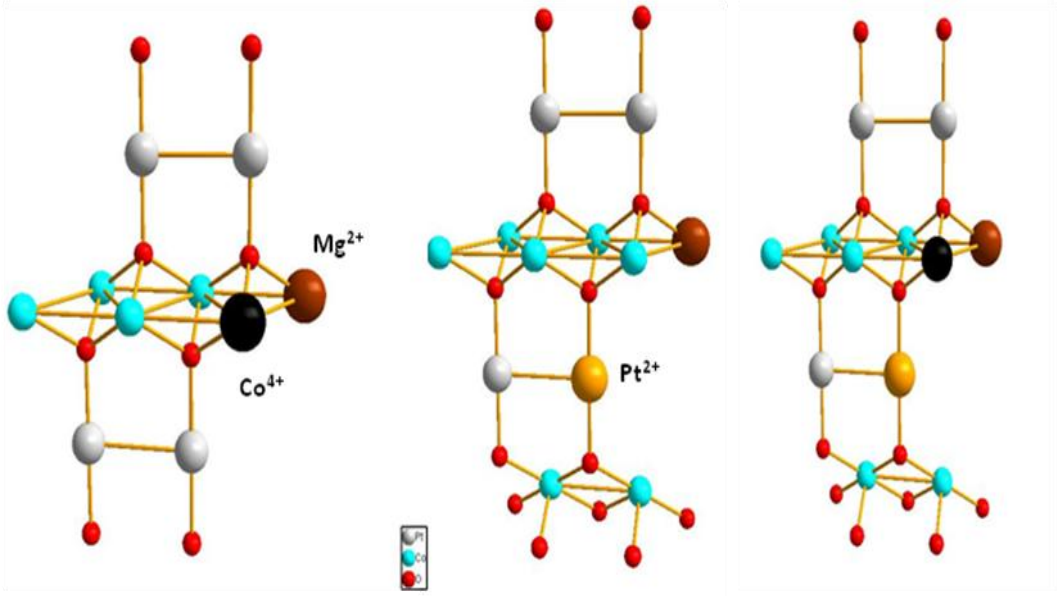

Figure 5.1.7. Possible creation of HOLE with Mg^{2+} substitution at Co-site in $PtCoO_2$

Nominal Mg	Compound	Pt^{2+}	Pt^{1+}	Co^{3+}	Co^{4+}	Mg^{2+}
0	$Pt_{0.972}CoO_2$	0.028	0.944	1	-	-
2	$Pt_{0.977}Co_{0.98}Mg_{0.02}O_2$	0.043	0.934	0.98	-	0.02
5	$Pt_{0.977}Co_{0.95}\ Mg_{0.05}O_2$	0.073	0.904	0.95	-	0.05

Table 5.1.3. The table shows the possible stoichiometry of the obtained $PtCoMgO_2$ crystals.

It should be noted that the observed ratios Pt:Co from EPMA analysis and the Curie-constant analysis obey that the crystals that are started with 2% and 5% nominal composition are $Pt_{0.977}Co_{0.98}Mg_{0.02}O_2$, and $Pt_{0.977}Co_{0.95}\ Mg_{0.05}O_2$ respectively, the cationic ratios Pt:Co shows that the hole was substituted in Pt-layer.

5.1.3. Conclusions

The Mg substituted $PtCoO_2$ crystals were successfully obtained by means of $PtCl_2$ and *binary oxide* (CoMg)O were precursors in metathetical reactions. Both, Mg substituted and non-substituted $PtCoO_2$ crystals show cationic deficiency. The obtained crystals were crystallized with 3R-poly type (R-3m), and the lattice parameters increased with an increase of Mg substitution rate. The variation of susceptibility with temperature shows Curie-Weiss behaviour. The Curie constant, Curie temperature and temperature dependent susceptibility were determined by means of Curie-Weiss law.In general divalent substitutions in delafossite compounds were shown to be limited at low rates, where the individual precursors for each cation were taken. The present study reveals the higher level substitutions; Mg substitution rate exceeds 5% which is much higher compared to divalent substitution in any delafossite compounds in the available literature.

The future work will be to focus on the study of transport properties of $Pt(CoMg)O_2$ series. The size of the crystals are too small for transport measurements, the future work will be to obtain the larger crystals in order to make transport measurements.

5.2. Synthesis and characterization of $Pd(CoMg)O_2$ single crystals

As discussed in chapter 2.7 and 2.8, the enhancement of thermopower can be achieved by substituting Mg at Co-site. However its high rate hole doping using low valence ion substitution is unexplored yet. In this report, we focus on the synthesis and growth of hole-doped $PdCo_{1-x}Mg_xO_2$ single crystals ($x \leq 2\%$) and some preliminary characterizations. Here we propose to use the solid solution $Co_{1-x}Mg_xO$ as a precursor as it exists on the whole range of the solution and as it offers the opportunity to introduce the substituent homogeneously and directly as reactant what should result in an higher substitution rate.

5.2.1. Experimental conditions

The precursors for the metathetical reactions were $PdCl_2$, CoO or alternatively $Co_{1-x}Mg_xO$ for the substituted samples. The expected reaction is

$$PdCl_2 + 2\ Co_{1-x}Mg_xO \rightarrow PdCo_{1-x}Mg_xO_2 + (1-x)\ CoCl_2 + x\ MgCl_2 \qquad 5.2.1$$

Samples corresponding to nominal x=0, 10, 20 and 50% were prepared. Two methods were used for the growth, either a direct one (*Method 1*) in which stoichiometric amounts of the precursors were mixed and then heated at 700 ^{0}C for 40 h (heating and cooling rates at 1.5 K/min) or a multiple steps one (*Method 2*) in which stoichiometric quantities of the precursors were first vacuum sealed and then heated following a more complex thermal path [18] (heating to 930 °C in 2 h, then 1000 °C in 6 h; fast cooling to 580 °C in 1-2 h; heating to 700 °C in 2 h with a dwell of 40 h; final cooling to RT at the rate of 40 K/h). The single crystals were finally cleaned with ethanol and distilled water to get rid of by products.

Phase quality checking: $PdCoO_2$ crystallizes with space group R-3m [11]. As depicted in Fig. 5.2.1, it consists of alternating stacks of a triangular lattice of palladium and a triangular lattice of edge-shared CoO_6 octahedra connected by the O–Pd–O dumbbells. The RT lattice parameters are a= 2.830 Å and c=17:743 Å.

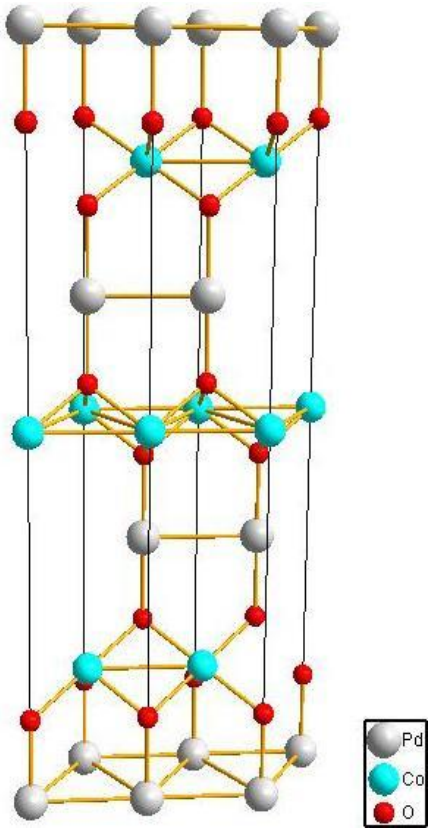

Figure 5.2.1. Crystal structure of $PdCoO_2$ (R-3m)

Powder x-ray diffraction (XRD) was performed on a PANalytical X'Pert Pro diffractometer with monochromatized Cu Kα1 radiation at RT. The FULLPROF package was used to fit the x-ray diffraction profiles and check the quality of the products. The Scanning Electron Microscopy (SEM) was performed using Hitachi S-4500 field emission microscope. EPMA (Electron Probe Micro Analysis) was used for the chemical compositional analysis, and temperature depended magnetization Zero Field Cooled (ZFC) and Field Cooled (FC) DC-magnetization data was collected using Superconducting Quantum Interface Device (SQUID) magnetometer at an applied field of 10 kOe in the temperature region from 5K to 300K. The direct current resistivity measurements were carried out using four-point probe method in 4-300K range in both ab-plane, and c-axis directions.

5.2.2. Results and discussions

5.2.2.1 Structural properties

The $PdCoO_2$ reference was prepared following the two methods described above. In both cases, flakes like single crystals were obtained, however with different sizes. The XRD profiles in Fig.5.2.2.1 reveals the only presence of $PdCoO_2$ in both cases without any trace of impurity and the calculated profile agrees with a strong preferential orientation as expected from the preferred in-plane growth for such structure and the available literature data . With the first method, the dimensions of the single crystals were limited to about 400 x 150 x 10µm^3 (Fig. 5.2.2.1.2). With *Method 2*, the single crystals were significantly larger reaching *c.a.* 2 x 1.5 x 0.1 mm^3. (Fig 5.2.3)

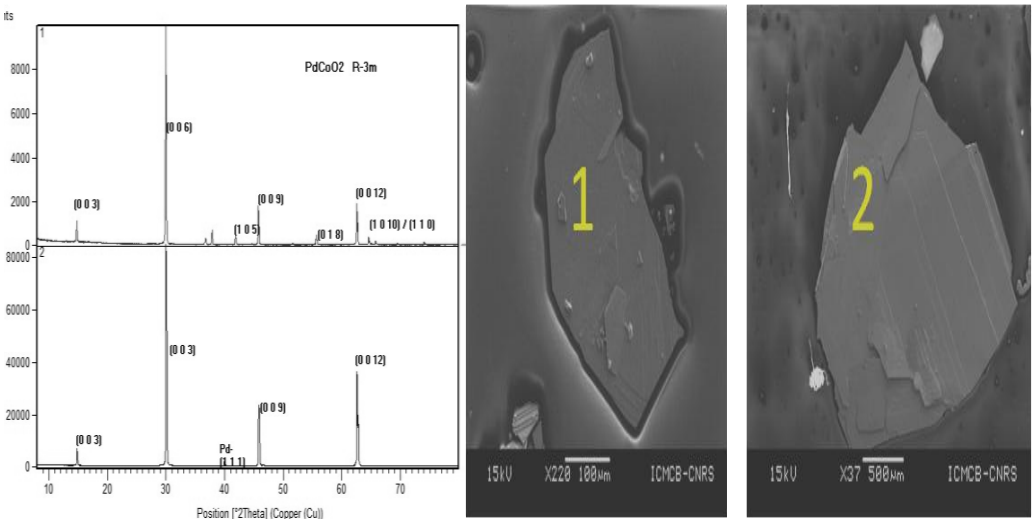

Figure 5.2.2. The X-ray diffraction patterns and SEM images of the $PdCoO_2$ crystals grown with either method 1 or 2.

Following this result, only *Method 2* was used to grow the Mg^{2+} substituted single crystals in order to optimize their dimension for further characterizations. The fractional yield is c.a. 20wt%. The resulting crystals are still all flakes like with the same preferred orientation and their larger dimension is increasing nearly linearly with Mg content. The largest crystals observed are much arger in dimensions compared literature data, where they obtained about 2mm*1mm size using metathetical reactions.

(Fig.5.2.3); the largest crystals were obtained from the nominal 50% Mg substituted batch with maximum dimension of about 6 x 3 x 0.5 mm^3; while the size is roughly multiplied per 3 in the preferred directions, it is increased by a factor 5 along the c-axis, suggesting a strengthening of the links between layers.

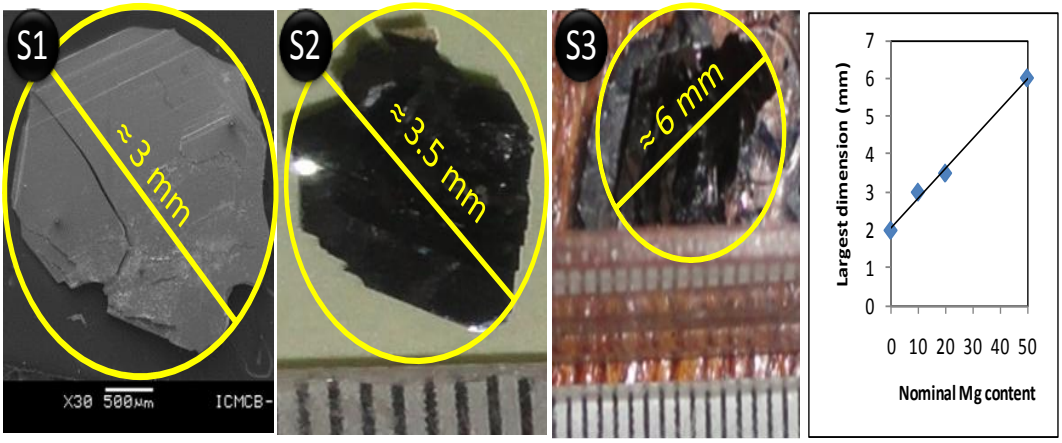

Figure 5.2.3. (S1).SEM image of the sample prepared from $Co_{0.9}Mg_{0.1}O$, (S2) and (S3) Photographs of single crystals obtained respectively from $Co_{0.8}Mg_{0.2}O$ and from $Co_{0.5}Mg_{0.5}O$.

The X-ray diffraction patterns were shown in Figure 5.2.4. The lattice parameters show an increase of lattice parameters with Mg substitution, which were derived from FullProf profile matching for sample S1 and single crystal X-ray diffraction for S2 and S3. The reflections observed from c-axis planes, which represents that the surface of the crystals are oriented along c-axis direction. The single crystal X-ray diffraction was performed on S2 an S3 samples. All the samples show crystallization in 3R(*R-3m*) polytype, the lattice parameters were shown in table 5.2.1.

	a(Å)	c(Å)
S1	2.8300	17.6824
S2	2.83100	17.7584
S3	2.8313	17.813

Table 5.2.1. Lattice parameters of $Pd(CoMg)O_2$ crystals

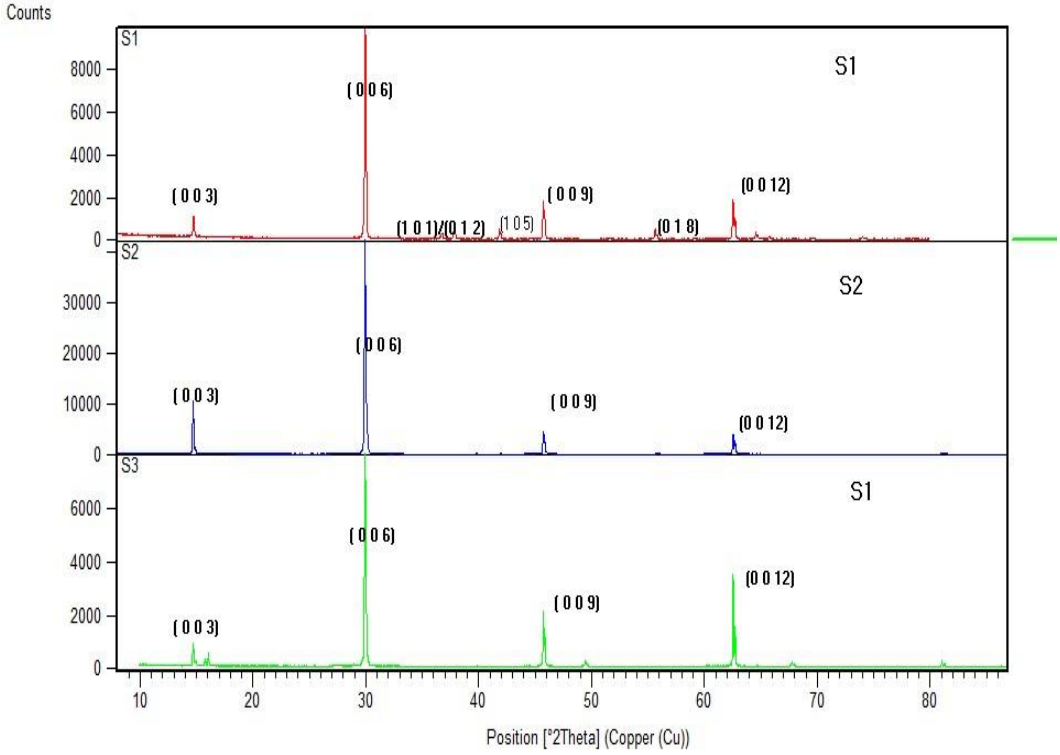

Figure 5.2.4. X-ray diffraction patterns of the crystals correspond to images in Figure 5.2.3

EPMA: The EMPA results show larger deviation of Mg content, might be due to metallic Pd-layer on the surface of the crystals. Etching the sample results the decomposition of the sample.

Single crystal X-ray diffraction data

	S2	S3
Identification code	Shelxl	Shelxl
Empirical formula	Co O2 Pd	Co O2 Pd
Formula weight	197.33	197.33
Temperature	293(2) K	293(2) K
Wavelength Å	0.71073	0.71073 Å
Crystal system	Hexagonal	Hexagonal
Space group	R-3m	R-3m
Unit cell dimensions	a = 2.8313(2) Å□= 90°. b = 2.8313(2) Å□= 90°. c = 17.813(2) Å□ = 120°.	a = 2.83100(10) Å= 90°. b = 2.83100(10) Å= 90°. c = 17.75840(10) Å = 120°
Volume z	123.661(19) $Å^3$	123.258(6) $Å^3$
Density (calculated)	7.949 Mg/m^3	7.978 Mg/m^3
Absorption coefficient	20.463 mm^{-1}	20.537 mm^{-1}
F(000)	267	267
Crystal size	0.085 x 0.075 x 0.010 mm^3	0.050 x 0.025 x 0.002 mm^3
Theta range for data collection	3.43 to 34.52°.	3.44 to 34.55°.
Index ranges	-4<=h<=4, -4<=k<=4, -27<=l<=27	-4<=h<=4, -4<=k<=4, -27<=l<=27
Reflections collected		

Table.5.2.2. Single crystal X-ray diffraction data of S2 and S3 single crystals

5.2.2.2. Magnetic properties

The magnetic measurements were employed using MPMS at an applied field of 1T in the temperature region from 5K to 300K (Figure 5.2.5). The sample S1 (without substitution) , the size of the crystals are very small and contains some magnetic impurity, Co_3O_4 which can be seen around 30K in figure 5.2.5 (S1). While the other crystals didn't represents any impurity ; either precursor CoMgO or Co_3O_4, where the AFM transition was expected bellow 45K for Co_3O_4 impurity and bellow 300K for CoMgO.

All the crystals show curie-Weiss behaviour. The percentage of Mg in $Pd(CoMg)O_2$ was estimated by considering that total Mg content was substituted at Cobalt site; Co^{4+} low spin state; Pd $(Co_{1-2x}^{3+}\ Co_x^{4+}Mg_x^{2+})O_2$. The inverse susceptibility with temperature shows linear variation.

The values of Curie constant, Curie temperature and temperature independent susceptibility values were derived by applying Curie-Weiss law; $\chi = \chi_0 + (C/(T-\theta))$. The curie-constant of the Mg substituted samples S1(10%), S2(20%) and S3(50%) (In the bracket represents the initial Mg% taken) shows the values of 0.0045, 0.0461 and 0.0406 successively, which represents the 1.23%, 12.3% and 11% of free spins. This contribution might be either from Co^{4+} or Pd^{2+} or presence of both.

The curie temperature of the $Pd(CoMg)O_2$ single crystals shifts towards negative with Mg content; -4.3K (S1), -14K(S2),and -28K(S3) which indicates an increase of anti-ferromagnetic interactions with substitutions.

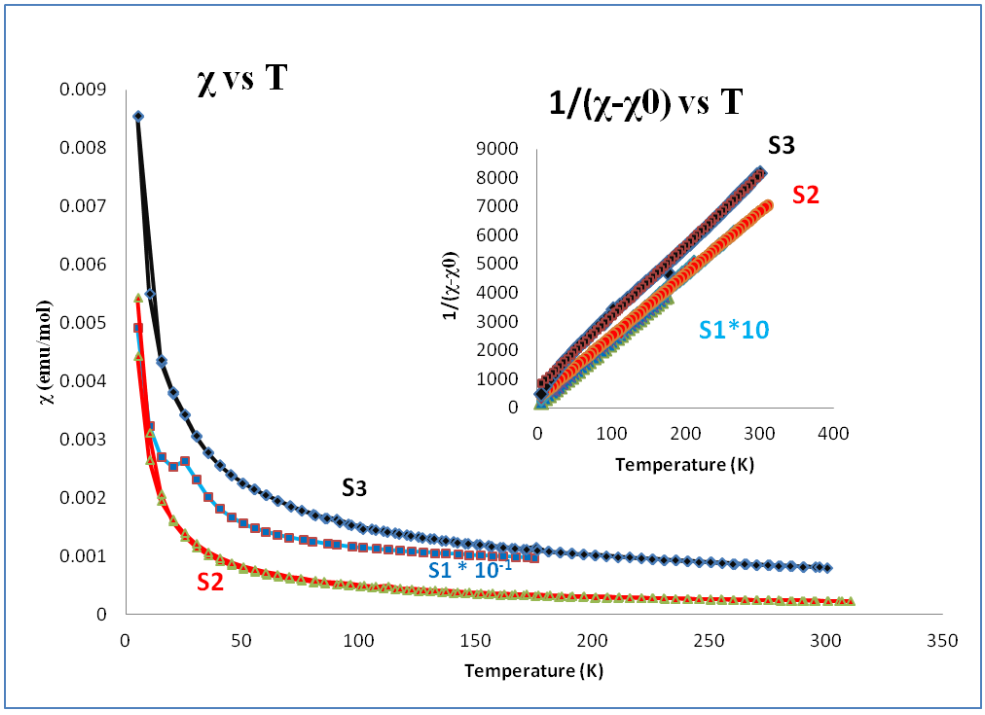

Figure 5.2.5. Susceptibility measurements for the Mg doped $PdCoO_2$ single crystals. Inset show fitting in Curie-Weiss law.

	Θ	X_0 (emu/mol)	C	S ½ %
S2	-14 K	$8.6189*10^{-05}$	0.0461158	12.30
S3	-28	$8.71*10^{-05}$	0.04062	11

Table 5.2.3. The Curie-constant (c), Curie temperature (Θ), diamagnetic susceptibility (X_0) and the percentage of half-spins of the Pd(CoMg)O_2 single crystals.

5.2.2.3. Electrical properties

Resistivity measurements were carried out in the temperature region from 0K to 300K along ab-plane and c-axis directions. The residual resistivity ratios ρ(288)/ρ(4.6) of S2 shows 336 and 2.75 successively along ab-plane and c-axis directions. The anisotropy in resistivities at 4.4K and 286K are about 34205 and 280 respectively. The average anisotropy from 41K to 307K shows the value of 1.28 $*10^3$. The temperature coeffiecients of resistivity ($\frac{1}{T_1-T_2}\frac{\rho_{T_1}-\rho_{T_2}}{\rho_{T_2}}$) in both directions show the values in the order of 10^{-3}/K which represents the high metallic bahviour. For S3 sample, the residual resistivity ratio ρ(288)/ρ(4.6) =16.8 along ab-plane and ρ(250)/ρ(4.26) =1.5 along c-axis directions. The anisotropy at 4.14K was about 5 orders in magnitude ($2.26*10^5$) and four orders in magnitude ($2.3*10^4$) at 250K. The calculated temperature coefficients of resistivity are in the order of 10^{-3}/K. The average anisotropy between 50K and 250K is found to be 4 fold order; 10^4. The experimental results are shown in figure 5.2.6.

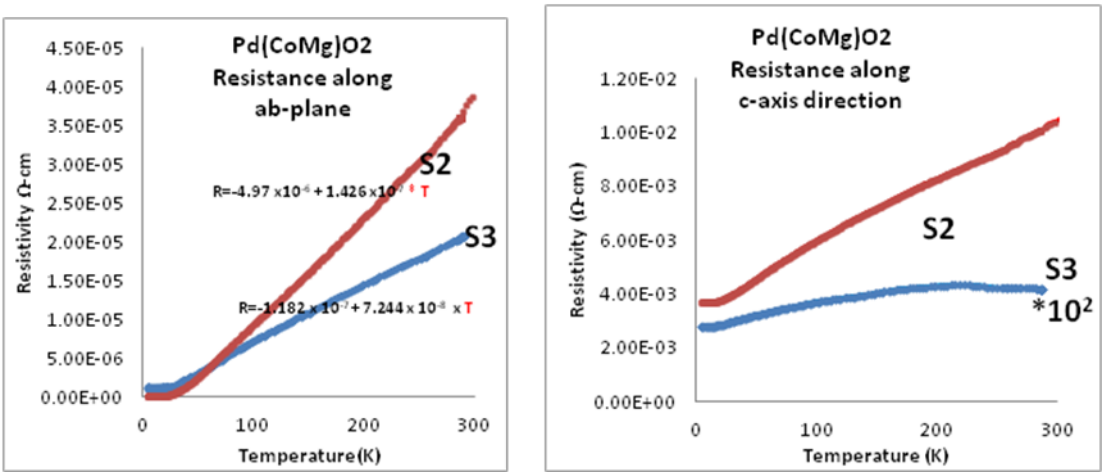

5.2.6.(a) 12(b)

Figure 5.2.6. (a). Resistivity along ab-plane 7(b) along c-axis for the crystals S2 and S3

	ρ(288)/ρ(4.6) ab-plane	ρ(86)/ρ(4.26) c-axis	$\alpha = \left(\frac{1}{T_1-T_2}\frac{\rho_{T_1}-\rho_{T_2}}{\rho_{T_2}}\right)$	
			ab-plane	c-axis
S2	336	2.75	3.53 *10^{-3} /K	2.26 *10^{-3} /K

Table 5.2.4. Characteristic values of resistivity for S2 single crystal

	ρ(288)/ρ(4.6) ab-plane	ρ(250)/ρ(4.26) c-axis	$\alpha = \left(\frac{1}{T_1-T_2}\frac{\rho_{T_1}-\rho_{T_2}}{\rho_{T_2}}\right)$	
			ab-plane	c-axis
S3	16.8	1.51	1.38 *10^{-3} /K	3.32 *10^{-3} /K

Table 5.2.5. Characteristic values of resistivity for S3 single crystal

The observed resistivity values for both the samples S2 and S3 show increase of conductivity by one order in magnitude compared to the pure $PdCoO_2$ and huge anisotropy in resistivity along both ab-plane and c-axis directions.

5.2.2.4. XPS measurements

If the Mg ion completely occupies the Co-site; Co^{4+} in CoO_2 plane can cause increase in conductivity along ab-plane, If the Mg creates a hole in Pd-plane; Pd^{2+} should give higher resistivity values than Pd^{1+}. The observed resistivity values for both the samples S2 and S3 show increase of conductivity by one order in magnitude compared to the pure $PdCoO_2$. The X-ray Photo emission Spectra show the appearance of Pd^{2+} in both the samples. It was clear from the XPS measurements that the creation of hole in Pd-layer with Mg substitution at Co-site.

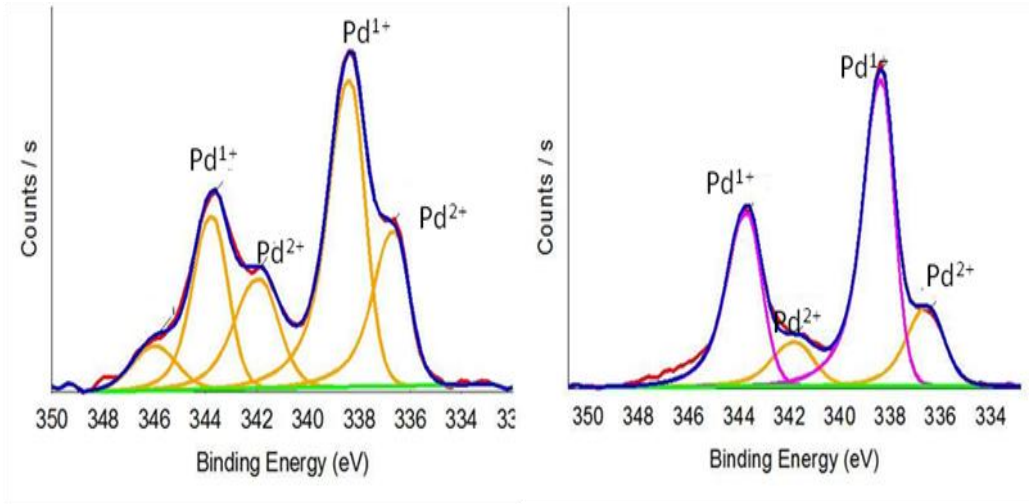

Figure 5.2.7.a, b. X-ray Photoemission Spectra of S2 and S3 samples.

5.3. Conclusions

The Mg substituted $PdCoO_2$ single crystals were grown successfully using $PdCl_2$ and binary oxide CoMgO were the precursors in metathetical reactions. The lattice parameters show slight increment with Mg substitution. All the crystals show Curie-Weiss behaviour in susceptibility measurements; inverse of susceptibility varies liner to temperature. The single crystals show metallic behaviour, and the resistivity was changed by one order in magnitude with Mg substitution. The crystals show huge anisotropy in resistivity measured along ab-plane and c-axis directions. The residual resistivity is about 405 (ρ(300K)/ ρ(4K)) and 2.8 for 20% of Mg substituted samples along ab-plane and c-axis directions respectively.

5.4. Comparing Mg substituted $PdCoO_2$ and $PtCoO_2$ system

$Pd(CoMg)O_2$ and $Pt(CoMg)O_2$ systems show 3R-polytype (*R-3m*) and increase of the lattice parameters with Mg substitution due to divalent ionic radii Mg^{2+} (0.72Å) is slightly larger than Co^{3+}(LS-0.54Å). Both the systems show Curie-Weiss behaviour in susceptibility measurements. The physical parameters; Curie-constant (c), temperature independent susceptibility (χ_0), and Curie temperature (θ) were derived by fitting into the equation;

$$\chi_{total} = \chi_{0(dia)} + c / (T-\theta) \qquad 5.4$$

Because of the size of the $Pt(CoMg)O_2$ are much smaller compared to $Pd(CoMg)O_2$ crystals; the transport properties were measured only for $Pd(CoMg)O_2$ crystals. The resistivity measurements show one order change in the magnitude of resistivity and increase of anisotropy with Mg substitution in $PdCoO_2$. The future work is to obtain the larger crystals of $Pt(CoMg)O_2$ and to measure the transport properties.
The XPS spectra for $Pd(CoMg)O_2$ shows contribution of Pd^{2+} , which represents the transformation due to Mg substitution. Also XPS measurements for $Pt(CoMg)O_2$ crystals are under progress. The magnetic measurements for $Pt(CoMg)O_2$ have revealed that the contribution of Pt^{2+} to the Curie-constant; A-cationic deficiency as well as the partial transformation of Pt^{1+} to Pt^{2+} due to Mg substitution.

Conclusions

In this thesis the alkaline cobalt oxide $Na_{0.6}CoO_2$ and $LiCoO_2$ were synthesized using *hydrothermal method*, Mg substituted metallic delafossite oxides $PtCoO_2$ and $PdCoO_2$ were obtained using *metathetical reactions*, and Mg substituted $Na_{0.7}CoO_2$ using *solid state reactions* to study their physical properties towards thermoelectric applications.

The main results are

$Co(OH)_2$ and NaOH were used as precursors for obtaining the Na_xCoO_2 using hydrothermal method. Phase diagram of Na-Co-H_2O was studied in soft hydrothermal conditions (Fig.3.1.1) by varying the temperature from150^0C to 250^0C, synthesis time from 24-60h, and molaity of hydrogen peroxide from 1-4m. This shows the possibility of obtaining $NaxCoO_2$ using hydrothermal method. Based on this phase diagram as well as the usage of H_2O_2, the single phase of $Na_{0.6}CoO_2$ has been stabilized (Fig.3.1.7). The evolution of phases with cleaning process was observed (Fig.3.1.4-5) might be due to unstable state of Co^{4+}. The structural refinement of the powder X-ray diffraction shows *R3m* space group with lattice parameters as a= 2.8312 Å, and c= 16.5915 Å (Fig.3.1.8). The phase transformation from *R3m* to *R-3m* was observed (Fig.3.1.10-3.1.11) above 450^0C. The surface morphology shows hexagonal plate like micro particles (Fig.3.1.12).

Polycrystalline samples of Mg substituted $Na_{0.7}CoO_2$ were obtained using CoMgO and Na_2CO_3 as precursors in solid state method with continuous flow of oxygen at 900^0C. The secondary phase of CoMgO was observed above 4% of nominal Mg substitution rate (Fig.3.2.1). The powder X-ray diffraction of the samples show P2 poly type phase with *P63/mmc* space group. The lattice parameters increase with increasing the nominal Mg rate of substitution (Table.3.2.1). The susceptibility measurements show Curie-Weiss behaviour; the inverse of susceptibility was linear with temperature (Fig.3.2.2). The $\%s_{1/2}$ was estimated by considering Co^{4+} is in Low Spin state (spin =1/2) (Table.2.2.2). The resistivity measurements show metallic behaviour (Fig.3.2.4). The T^2 dependence of resistivity at low temperature (Fig.3.2.5) represents electron-electron scattering. The usage of binary oxide for substitutions was introduced by synthesizing the $Na_x(CoMg)O_2$ compounds using CoMgO as the precursor having benefit of tuneable magnetic and transport properties, the substituted Na_xCoO_2 as well as $LiCoO_2$ also can also be used as precursors in ion exchange reactions to stabilize several compounds like $AgCoO_2$, $CuCoO_2$, and Ca_xCoO_2 where the direct synthesis as well as substitutions in these materials is much complex. This alternate approach might affect the rate of degree of substitution. Besides.

Polycrystalline $LiCoO_2$ was synthesized using $Co(OH)_2$ and LiOH were the precursors, NaOH as ionic mineralizer and 5% H_2O_2 as oxidizing agent in soft hydrothermal conditions. The effect of ionic mineralizer was studied by varying the NaOH/LiOH ratio by keeping rest of the parameters fixed (Fig.4.1.1). The structural refinement for powder X-ray diffraction pattern *shows* R-3m space group with lattice parameters a=b=2.81547 Å and c= 14.0635 Å (Fig.4.1.4). The morphology of the samples differ for different synthesis conditions, it varies from desert rose to concaved cuboctahedrons either with higher synthesis times or with specific ratios of ionic mineralizers used (Fig.4.1.2 and 4.1.5). The susceptibility measurements of the samples show Curie-Weiss behaviour (Fig.4.1.6). And then the EPR measurements show a very small impurity from nickel that might be from the precursor. The effect of ionic mineralizers and the concentration of precursor were studied to optimize the synthesis conditions of $LiCoO_2$: i) for low mineralizers concentration, only cobalt oxides form; ii) as the concentration increases., pure $LiCoO_2$ grows; iii) the crystallinity of the compound increases as the ratio NaOH/LiOH increases; iv) the $Co(OH)_2$ concentration threshold is *ca.* 50mmol/l; bellow this limit a single phase $LiCoO_2$ grows and above, $Co(OH)_2$ re-crystallizes (Fig.4.1.3). In the reaction time window 24-60 h was able to stabilize CoO free concave cuboctahedrons particles suggesting that an alternative mechanism for the growth of these particles should be considered. Magnetic measurements (local and macroscopic) highlight the presence of cobalt oxides impurities which amount is decreasing (and nearly vanishes) with reaction time; they also reveal, as already observed, the presence of several kind of close to surface centres (Fig.4.1.7). $LiCoO_2$ was obtained at lower synthesis parameters compared to the available literature, the structural, morphological, and magnetic properties were studied.

The crystals of $Pt(CoMg)O_2$ were grown using $PtCl_2$, CoO or alternatively $Co_{1-x}Mg_xO$ for the substituted samples in metathetical reactions in vacuum sealed quartz tubes (Fig.5.1.1) at 700^0C for 40h with heating rate keeping at 1.5^0C/min and the cooling rate at 1^0C/min. The profile matching with FULL PROOF program for the power X-ray diffraction patterns (Fig.5.1.2) represents that the crystals obtained were with 3R polytype (*R-3m*). The lattice parameters show an increment with respect to the Mg substitution rate due to higher radius of Mg^{2+} compared to Co^{3+} (Figure 5.1.4) . The morphology of the crystals shows plate like 2D hexagonal shape (Fig.5.1.3). The EPMA analysis shows the approximate Co:Mg for lower Mg substitution rate and the optimal value was found around 7.5 (Table.5.1.1). The variation of susceptibility with temperature shows Curie-Weiss behaviour. The Curie constant, Curie temperature and temperature dependent susceptibility were determined by means of Curie-Weiss law (Fig.5.1.5). The $\%s_{1/2}$ was calculated with the assumption that the Co^{4+} is in LS state (spin=1/2). The deviation of these values shows the deficiency in Pt-layer (Table.5.1.3). In general divalent substitutions in delafossite compounds were shown to be limited at low rates, where the individual precursors for each cation were taken. The present study reveals the higher level substitutions; Mg substitution rate exceeds 5% which is much higher compared to divalent substitution in any delafossite compounds in the available literature.

The crystals of $Pd(CoMg)O_2$ were grown using $PdCl_2$, CoO or alternatively $Co_{1-x}Mg_xO$ for the substituted samples in metathetical reactions in vacuum sealed quartz tubes. The larger crystals were obtained by the following thermal treatment; heating the vacuum sealed quartz tube to 930 °C in 2 h, then 1000 °C in 6 h; fast cooling to 580 °C in 1-2 h; heating to 700 °C in 2 h with a dwell of 40 h; final cooling to RT at the rate of 40 K/h). The single crystals were finally cleaned with ethanol and distilled water to get rid of by products. The crystals show 3R-polytype (R-3m) (Fig.5.2.4) and the lattice parameters increases with increasing Mg substitution rate (Table.5.2.1). The single crystal X-ray diffraction confirms that the crystals obtained were single crystals (Fig.5.2.2). The obtained single crystals were larger in dimensions (Fig.5.2.3) with 2D growth.

The susceptibility measurements show Curie-Weiss behaviour (Fig.5.2.5). The $\%s_{1/2}$ was calculated with the assumption that the Co^{4+} is in LS state (spin=1/2) (Table.5.2.3). These results show the high-level Mg substitution at Co-site. The single crystals show metallic behaviour, and the resistivity was changed by one order in magnitude with Mg substitution. The crystals show huge anisotropy in resistivity measured along ab-plane and c-axis directions. The residual resistivity is about 405 (ρ(300K)/ ρ(4K)) and 2.8 (Table.5.2.4) for 20% of Mg substituted samples along ab-plane and c-axis directions respectively (Fig.5.2.6-7). The XPS spectra shows the existence of Pd^{2+} with Mg substitution, it can be concluded that the substitution of Mg creates hole in Pd-layer instead of Co-site. These results suggest the enhancement of Mg substitution rate using binary oxide as precursor. This approach might impact several divalent substitutions in ABO_2 compounds.

As an outlook over ongoing research on $ACoO_2$ compounds towards thermoelectric applications in this thesis can be summarized as

- Synthesis of oxide materials by hydrothermal method gives good oxygen stoichiometry, this regard several oxides were synthesized and impurity free phases with oxygen stoichiometry were obtained. This study achieved the synthesis of $NaxCoO_2$ using hydrothermal method for the first time in this method and with lower synthesis parameters to stabilize concaved cuboctahedron $LiCoO_2$.
- The divalent substitution at Co-site in $ACoO_2$ enhances the spin entropy thus improves the thermoelectric properties. The high level Mg substitutions at Co-site were limited to low level in traditional chemical approach. The present study enhances the substitution rate by using binary oxide CoMgO as precursor. This alternate chemical approach was successful for obtaining $Na_{0.7}(CoMg)O_2$ (polycrystalline), $Pt(CoMg)O_2$ (micro crystals) , $Pd(CoMg)O_2$(single crystals). The high level Mg substitution in metallic delafossite compounds were successfully obtained in this approach which a challenge in traditional chemical approach methods.

/

Work under progress:

- Polycrystalline samples of Mg substituted $LiCoO_2$ were obtained using CoMgO and Li_2CO_3 were the precursors in solid-state method. The transport properties are in the progress.
- The XPS measurements for $Pt(CoMg)O_2$ crystals which can reveals the oxidation state of Pt (1+/2+) are on the process.
- Mg substitution in $LiCoO_2$ using hydrothermal method is one of the ongoing work
- The study of electrochemical properties of $LiCoO_2$ obtained using hydrothermal method is on process.

Challenges to overcome and future work:

- Control of Na content in Na_xCoO_2 is a challenge in hydrothermal method as the entire reaction is taking place in heavier atmosphere of Na^+, the future work to find the possible conditions to control it.
- The future work regarding alkaline cobaltites will be to obtain Mg substituted $Na_{0.6}CoO_2$ and $LiCoO_2$ using hydrothermal method and to compare the physical properties of these materials obtained using two different synthesis methods.
- The obtained crystals of $Pt(CoMg)O_2$ were too small for transport measurements. The future work will be to optimize the conditions to obtain the larger crystals and to study the physical and transport properties

Publications:

1. 1. **Kiran K Bokinala**, M.Miclau, I. Grozescu and M.Pollet „" Synthesis of lithium cobalt oxide by single step soft hydrothermal method" (DOI10.1016/jssc.2012.09.028)
2. **Kiran Kumar Bokinala,** M.Miclau " A preliminary study on the hydrothermal synthesis of layered cobalt oxides" (JOAM-Accepted)
3. **Kiran Kumar Bokinala**, M.Miclau and I. Grozescu "The stability diagram of Na-Co-H2O system at 150-250ºC for obtaining layered sodium cobalt oxides by hydrothermal method" (communicated to Applied Physics A)
4. M.Miclau,Kiran **Kumar Bokinala** "Low temperature synthesis of the three-layered sodium cobaltite P3-NaxCoO2 (x ~ 0.60) by hydrothermal synthesis" (communicated to Crystal Growth and Design)

National patent with title: "Hydrothermal synthesis of LiCoO2", no2011 00087 / 02.02.2011
Inventors: M. Miclau, **Kiran.K. Bokinala**, D. Ursu and I. Grozescu

Manuscript preparation:

5. **Kiran Kumar Bokinala**, M.Miclau, and M.Pollet " Structural and magnetic properties of Mg substituted PtCoO2 single crystals "
6. **Kiran Kumar Bokinala**, M.Miclau, and M.Pollet "Properties of high level Mg substituted PdCoO2 single crystals""
7. **Kiran Kumar Bokinala**, M.Miclau, and M.Pollet „"Synthesis and characterization of Nax(CoMg) O2 ""
8. **Kiran Kumar Bokinala**, M.Miclau, and M.Pollet "Synthesis and characterizations of Li(CoMg) O2 "
9. **Kiran Kumar Bokinala**, M.Miclau, and M.Pollet "Physical properties of (CoMg)O Solid solutions "

Conferences:

1. **Kiran Kumar Bokinala**, R.Decourt, I. Grozescu, M.Miclau2, M.Pollet „"Newapproach forhigh level Mg substitution in lamellar cobalt oxides,A(CoMg)O2; Investigation of structural and transport properties SPSSM4, Bordeaux, France, June, 2012.
2. **K.K. Bokinala**, M. Miclau, I Grozescu. Hydrothermal study of Cobalt Oxidation State in NaOH Solution for Obtaining Layered Sodium Cobalt Oxides, Inorganic Materials Conference, Biarritz, France 12 - 14 September (2010).
3. **K.K. Bokinala**, M Miclau, Daniel Ursu, I Grozescu, Layered sodium cobalt oxides by hydrothermal synthesis and Study Of the system Co-NaOH-H_2O ,Physics conference TIM- 10, 25 - 27 Timisoara, Romania, November (2010).

Workshop: Complementary Skills Workshop in IPDIA, Caen-France 22-23rd July 2011

References

[1]. C. Delmas, J.-J. Braconnier, and P. Hagenmuller, Mater. Res. Bull., 17,117 (1982)
[2]. R. Berthelot et al. Electrochemical and Solid-State Letters, 12 -11- A207 A210 (2009)
[3]. G. Amatucci, J. Tarascon, L. Klein. J. Electrochem. Soc., 143(3), 1114(1996)
[4]. A. Mendiboure, C. Delmas, P. Hagenmuller. Mater Res Bull, 19(10), 1383(1984)
[5]. J. Paulsen, J. Mueller-Neuhaus, and J. Dahn, J. Electrochem. Soc., 147, 508 (2000)
[6]. I.Terasaki, Y.Sasago and K.Uchinokura, Phys.Rev.B56,R12 685 (1997)
[7]. Yayu Wang, N.S.Rogado,R.J.Cava and N.P.Ong, Nature 423,425 (2003)
[8]. K. Takada, H. Sakurai, E. Takayama -M, R. Dilanian, and T. Sasaki, Nature 422, 53 (2003)
[9]. L. Viciu, J. W. G. Bos, et al. Physical Review B 73, 174104 (2006)
[10]. Q. Huang, M. L. Foo, R. A. Pascal, et,all. Phys. Rev. B 70, 184110 (2004)
[11]. R. Jin et.al. PHYSICAL REVIEW B 72, 060512,R(2005)
[12]. Mizushima et al.Mater. Res. Bull. 15, 783–789 (1980).
[13]. G. Amatucci, J. Tarascon, L. Klein. J. Electrochem. Soc., 143(3), 1114 (1996)
[14]. Y. Ono, R. Ishikawa, Y. Miyazaki, Y. Ishii, Y. Morii, and T.Kajitani, J. Solid State Chem. 166, 177 (2002).
[15]. Q. Huang, M. L. Foo, J. W. Lynn, H. W. Zandbergen, G. Lawes,Y. Wang, B. H. Toby, A. P. Ramirez, N. P. Ong, and R. J. Cava,J. Phys.: Condens. Matter 16, 5803 (2004)
[16]. R.J. Balsys, R.L. Davis, Solid State Ionics 69 (1994)
[17]. Q. Haung, M.L. Foo, R. A. Pascal Jr and R. JCava et al. Phys. Rev B 70, 184110(2004)
[18]. Q.Haung et al, Condens.Matter 16 5808(2004).
[19]. H.W.Zandbergen, M.Foo, Q.Xu,V.Kumar, and R.J.Cava, Phys.Rev.B70, 024101(2004).
[20]. Yasuhiko Takahashi.et. all Journal of Solid State Chemistry 22-26, 172 (2002)
[21]. A. Van Der Ven, M.K. Aydinol, G. Ceder, G. Kresse, J. Hafner, Phys. Rev.B 58 2975 (1998).
[22]. J.N. Reimers, J.R. Dahn, J. Electrochem. Soc. 139, 2091(1992)
[23]. H. Gabrisch, R. Yazami, B.S Fultz, in: K. Striebel (Ed.), Proceedings of the 204th Meeting of the Electrochemical Society, Symposium Lithium/Lithium-Ion Batteries, Orlando, FL, October, (2003)
[24]. J. M. Paulsen et al., J. Electrochem. Soc. 147, 508 (2000).
[25]. M. Ménétrier et al., J. Mater. Chem. 9, 1135 (1999).
[26]. Mizushima, K et al.Mater. Res. Bull. 15, 783–789 (1980).
[27]. C. Delmas, C. Fouassier, and P. Hagenmuller, Physica B & C, 99, 81 (1980)
[28]. Ohzuku, T. et al. J. Electrochem. Soc. 141, 2972–2977 (1994).
[29]. H. Gabrisch et al Electrochemical and Solid-State Letters, 5 (6) A111-A114 (2002)
[30]. Yuzuru Miyazaki. Solid State Ionics 172 , 463–467, (2004).
[31]. T. Motohashi et a, Physical Review B 80, 165114 (2009)

[32]. J Meena devi. Et, al.Bull. Mater. Sci., Vol. 30, No. 4, , pp. 345–348, August 2007
[33]. L. Wang. et al. Journal of Alloys and Compounds 471, 519–523, (2009).
[34]. Y.Ando, N.Miyamoto K.Segawa, T.Kawata and Terasaki, Phys.Rev.B 60 10580(1999)
[35]. M.M. Thackeray, J.O. Thomas, M.S. Whittingham, MRS Bull 39 (2000)
[36]. W.Y.Zang, H.C.Yu, Y.G.Zaho,X.P.Zhang,and J.Q.Li, Phys.Condens.Matter 16, 4935(2004)
[37]. L.B.Luo, Y.G.Zaho,G.M.ZHAng and L.Chi.Phys.Rev.B 73, 245113(2006)
[38]. Lencka, M. M. and Riman, R. E. Chem. Mater., 7:18–25 (1995)
[39]. Lencka, M. M., Andreko, A., and Riman, R. E J. Am. Ceram, Soc., 78:2609–2618 (1995)
[40]. R. Gupta and A. Manthiram, J. Solid State. Chem, 121, 483(1996)
[41]. A .R. Wizansky, P. E Rauch and F .J. Disalvo, J. Solid State Chem , 81,203 (1989)
[42]. T. Wu, D. F. Fang, G. Y Wang, L. Zaho Phys.Rev B 76,024403 (2007)
[43]. C.Delmas, C.Fouassier, and P.Hagenmuller, PhysicsB&C 99,81(1980)
[44]. J.Molenda,C.Delmas,P.Dordor, Solid state ionics 12, 473 (1989)
[45]. M.Karppinen, I.Asako, E.Motohashi, and H.Yamauchi, Phys.Rev B 71, 092105(2005)
[46]. C.Delmas.J-J.Braconnier, C.Fouassier, and P.Hagenmuller, Solid State Ionics, 165 (1981)
[47]. Liu, C.-J.; Liao, J.-Y.; Wu, T.-W.; Jen, B.-Y. J. Mater. Sci. 2004, 39, 4569
[48]. Y. Shao-Horn, S. A. Hackney, A. J. Kahaian and M. M. Thackeray, Journal of Solid State Chemistry 168, 60–68 (2002)
[49]. Artemenko et al. J. Appl. Phys. **106**, 064914 (2009)
[50]. Handbook of hydrothermal technology for Crystal Growth and Materials Processing.
[51]. Kutty,T. R. N. and Balachandran, R., Mat. Res. Bull., 19:1479–1488(1984)
[52]. L. Predoană 1, A. Barău, Proceedings of the International Workshop "Advanced Techniques for Energy Sources Investigation and testing", Sofia, Bulgaria-9 Sept (2004)
[53]. E.C.Gonzalo, E.Moran, Materials chemistry and physics 121-3, 484-488 (2010)
[54]. Hailong Chen et al. J. am. chem. soc. 133, 262–270 (2011)
[55]. Y. Ono, et al, J. Solid State Chem. 166, 177 (2002).
[56]. William C. Sheets. Chem. Mater. 18, 7-20 (2006)
[57]. Shigeyuki somiya Bull. Mater Sci., Vol. 23, No. 6, December 453–460,(2000)
[58]. http://skuld.bmsc.washington.edu/~merritt/bc530/bragg
[59]. http://ipc.iisc.ernet.in/~magsquid/contents.html
[60]. J.Chivot et al.Corrosion Science 50 , 62-69 (2008)
[61]. Alexey A. Alexandrov14th International Conference on the Properties of Water and Steam in Kyoto (2003)
[62]. Zhenhua Zhou and Ctirad Uher REVIEW OF SCIENTIFIC INSTRUMENTS 76, 023901 (2005)
[63]. http://www-inst.eecs.berkeley.edu/~ee143/fa10/lab/four_point_probe
[64]. Rodriguez-Carvajal, J., Physica B 192, 55(1993)
[65]. M.C. Friedel, C. R. Hebd. Acad. Sci. 77 ,211 (1873)
[66]. R.D. Shannon, D.B. Rogers, C.T. Prewitt, Inorg. Chem10 713 (1971)

[67]. C.T. Prewitt, R.D. Shannon, D.B. Rogers, Inorg. Chem. 10, 719 (1971)
[68]. D.B. Rogers, R.D. Shannon, C.T. Prewitt, J.L. Gillson, Inorg. Chem. 10, 723(1971)
[69]. Gordon RG. MRS Bull; 25:52 (2000)
[70]. Thomas G. Nature; 389:907 (1997)
[71]. B.U. Kohler, M. Jansen, Z. Anorg. Allg. Chem. 543, 73(1986)
[72]. R. Berthelot, M. Pollet, J.-P. Doumerc, and C. Delmas, Inorg. Chem., 50, 4529–4536 (2011)
[73]. H. Kawazoe, M. Yasukawa, H. Hyodo, M. Kurita, H. Yanagi, H. Hosono, Nature 389, 939 (1997)
[74]. Takuya Otabe, K.Ueda, A.Kudoh, H.Hosono, and H. Kawazoe A .P.L.,72, 92(1998)
[75]. M.Tanaka et al. Journal of the Physical Society of Japan. Vol.65, No.12, 3973-3977(1996)
[76]. Meagen A. Marquardt, Nathan A. Ashmore, David P. Cann Thin Solid Films 496146 – 156 , (2006)
[77]. H. Hahn, C.Z. Lorent, Z. Anorg. Allg. Chem. 279, 281 (1955)
[78]. F.A. Benko, F.P. Koffyberg, J. Phys. Chem. Solids 45, 57 (1984)
[79]. H. Kawazoe, M. Yasukawa, H. Hyodo, M. Kurita, H. Yanagi, H. Hosono, Nature 389, 939 (1997)
[80]. T. Ishiguro, A. Kitazawa, N. Mizutani, M. Kato, J. Solid State Chem. 40, 170 (1981)
[81]. T. Ishiguro, N. Ishizawa, N. Mizutani, M. Kato, J. Solid State Chem. 41,132 (1982)
[82]. T. Ishiguro, N. Ishizawa, N. Mizutani, M. Kato, Acta Cryst. B 39, 564 (1983)
[83]. K. Ueda, T. Hase, H. Yanagi, H. Kawazoe, H. Hosono, H. Ohta, M. Orita, M. Hirano, J. Appl. Phys. 89, 1790 (2001)
[84]. H. Yanagi, T. Hase, S. Ibuki, K. Ueda, H. Hosono, Appl. Phys. Lett. 78, 1583 (2001)
[85]. H. Yanagi, K. Ueda, H. Ohta, M. Orita, M. Hirano, H. Hosono, Solid State Commun. 121, 15 (2001)
[86]. B.V. Kohler, M. Jansen, Z. Anorg. Allg. Chem. 543, 73 (1986)
[87]. M. Shimode, M. Sasaki, K. Mukaida, J. Solid State Chem. 151, 16 (2000)
[88]. Nagarajan R, Draeseke A D, Sleight A W and Tate J , J. Appl. Phys. 89 8022 (2001)
[89]. Nagarajan R, Duan N, Jayaraj M K, Li J, Vanaja K A, Yokochi A, Draeseke.A, Tate J and Sleight A W , Int. J. Inorg.Mater. 3 265–70(2001)
[90]. Scanlon D O, Godinho K G, Morgan B J andWatson G W J. Chem. Phys. 132 024707 (2010)
[91]. Benko F A and Koffyberg F P, J. Phys. Chem. Solids 48 431–43(1987)
[92]. Snure M and Tiwari A, Appl. Phys. Lett. 91 092123 (2007)
[93]. Marquardt M A, Ashmore N A and Cann D P, Thin Solid Films 496 , 146–56 (2006)
[94]. Shi L J, Fang Z J and Li J J. Appl. Phys. 104 073527 (2008)
[95]. Scanlon D O and Watson G W J. Phys. Chem. Lett. 1 3195–9(2010)
[96]. Scanlon D O and Watson G W, J. Mater. Chem. 21 3655–63 (2011)
[97]. K G Godinho, B J Morgan, J P Allen, D O Scanlon and G.Watson, J.phys.: Condens. Matter 23 , 334201(2011)
[98]. Kadowaki H, Kikuchi H and Ajiro Y J. Phys.: Condens. Matter 2, 4485 (1990)

[1]. William C. Sheets, Evan S. Stampler,Mariana I. Bertoni, Makoto Sasaki,Tobin J. Marks,Thomas O. Mason, and Kenneth R. Poeppelmeier Inorg Chem. Vol. 47, No. 7(2008)
[2]. K A VANAJA, UMANANDA M BHATTA†, R S AJIMSHA, S JAYALEKSHMI and M K JAYARAJ Bull. Mater. Sci., Vol. 31, 5, 753–758(2008)
[3]. Berthelot R, Pollet M, Doumerc JP, Delmas C.*Inorg. Chem.*, 50 (10), pp 4529–4536 (2011)
[4]. Nagarajan R, Duan N, Jayaraj M K, Li J, Vanaja K A, Yokochi A, Draeseke A, Tate J and Sleight A W 2001 Int. J. Inorg.Mater. 3 265–70
[5]. R.D. Shannon, D.B. Rogers, C.T. Prewitt, Inorg. Chem. 10 (1971) 713
[6]. H.H. Emons, E. Beger, Z. Chem. 7 , 200(1967)
[7]. P. Porta, R. Dragone, G. Fierro, M. Inversi, M.L. Jacono, G. Moretti, J. Chem. Soc. Faraday Trans. 88 , 311(1992)
[8]. M. Beekman, J. Salvador, X. Shic, G.S. Nolas, J. Yang, Journal of Alloys and Compounds 489 336–338 (2010)
[9]. Masayuki Tanaka et al. Journal of the physical society of Japan..65, 12, 3973-3977 (1996)
[10]. Masayuki Tanaka et al Journal of crystal growth 173 440-445 (1997)
[11]. Mayasuki Tanaka et al. Physica B 245 157-163 (1998)
[12]. T.Higuchi et al. Journal of Electron Spectroscopy and Related Phenomena 92 71–75(1998)
[13]. Mashaashi Hasegava et al. Solid State Communications 121203-205 (2002)
[14]. Hirotakaa Okabe et al. Physica B 329–333, 948–949(2003)
[15]. Kyoo Kim et al. PHYSICAL REVIEW B 80, 035116 (2009)
[16]. Han-Jin Noh et al. PHYSICAL REVIEW B 80, 073104 (2009)
[17]. Han-Jin Noh et al. PHYSICAL REVIEW LETTERS 102, 256404 (2009)
[18]. Masashi Hasegawa et al Journal of Crystal Growth 226 277–280 (2001)
[19]. Khuong P. Ong et al, PRL 104, 176601 (2010)
[20]. M. Hasegawa et al, Solid State Communications 109 477–482 (1999)
[21]. Hiroshi TAKATSU et al Journal of the Physical Society of Japan Vol. 76, 10, 104701 (2007)
[22]. D. P. Chen, et, Phys. Rev. B 70, 024506 (2004)
[23]. Akimoto J.; Gotoh Y.; Honig Y.J.M. Journal of Solid State Chemistry, 141, pp. 298-302(5) (1998),
[24]. M Frontzek et al J. Phys.: Condens. Matter 24 016004 (2012)
[25]. Meagen A. Marquardt et al mat letters 81–85 (2006)